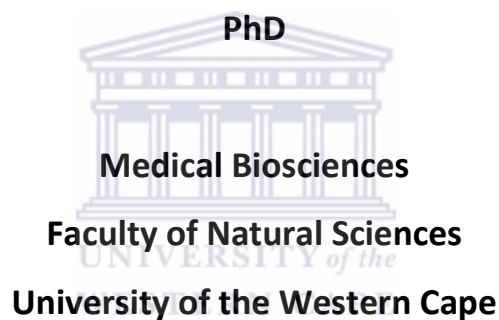


# **Structural and Functional Characterization of Human DDX5 and Its Interaction with NS5B of Hepatitis C Virus**

by

**Yook-Wah Choi**

**Thesis Submitted in Fulfillment of the Requirements for the Degree**



**Supervisor: Professor BC Fielding**

Department of Medical Biosciences  
University of the Western Cape

**Co-Supervisor: Prof YJ Tan**

Department of Microbiology  
Yong Loo Lin School of Medicine  
National University of Singapore

**November 2011**

# DECLARATION

I, Yook-Wah Choi, declare that this thesis, "*Structural and Functional Characterization of Human DDX5 and Its Interaction with NS5B of Hepatitis C Virus*" hereby submitted to the University of the Western Cape for the degree of *Philosophiae Doctor* (PhD) has not previously been tendered by me for a degree at this or any other university or institution, that it is my own work in design and in execution, and that all materials contained herein have been duly acknowledged.

Yook-Wah Choi : .....

Date Signed : .....



# DEDICATION

This study is dedicated to my parents for their unconditional love and patience.



## ACKNOWLEDGEMENTS

- I would like to express my gratitude to Professor Burtram C. Fielding and Professor Tan Yee-Joo for their patience and guidance.
- I would like to thank Dr Sujit Dutta for my induction into the amazing world of crystallography and his help in data collection and solving of the crystal structure.
- I sincerely thank the members of SHW lab for help rendered, sharing of equipment and reagents and the interesting discussions about crystallography work.
- To the staff of the IMCB sequencing facility, thank you for getting my sequences back to me so promptly.
- To all the wonderful, co-operative lab members that were in CAVR, I thank you for your friendship and encouragement.
- To my parents, sister, brother-in-law and friends, near and far, a heart-felt thank you for your encouragement and support!



## ABSTRACT

Hepatitis C was first recognized as a transfusion-associated liver disease not caused by hepatitis A or hepatitis B virus after serological tests were developed to screen for their presence in the blood. The infectious agent was finally identified with the cloning of the cDNA of hepatitis C virus (HCV) using random polymerase chain reaction (PCR) screening of nucleic acids extracted from plasma of a large pool of chimpanzee infected with non-A non-B hepatitis.

NS5B, a membrane-associated RNA-dependent RNA polymerase essential in the replication of HCV, initiates the synthesis of a complementary negative-strand RNA from the genomic positive-strand RNA so that more positive-strand HCV RNA can then be generated from the newly synthesised negative-strand template. The crystal structure of NS5B presented typical fingers, palm and thumb sub-domains encircling the GDD active site, which is also seen in other RNA-dependent RNA polymerases, and is similar to the structure of reverse transcriptase of HIV-1 and murine Moloney leukaemia virus. The last 21 amino acids in the C-terminus of NS5B anchor the protein to the endoplasmic reticulum (ER)-derived membranous web. NS5B has been shown to interact with the core, NS3/NS4A, NS4B and NS5A proteins, either directly or indirectly. Numerous interactions with cellular proteins have also been reported. These proteins are mainly associated with genome replication, vesicular transport, protein kinase C-related kinase 2, P68 (DDX5),  $\alpha$ -actinin, nucleolin, human eukaryotic initiation factor 4All, and human VAMP-associated protein.

Previous studies have confirmed that NS5B binds to full-length DDX5. By constructing deletion mutants of DDX5, we proceeded to characterize this interaction between DDX5 and HCV NS5B. We report here the identification of two exclusive HCV NS5B binding sites in DDX5, one in the N-terminal region of amino acids 1 to 384 and the other in the C-terminal region of amino acids 387 to 614. Proteins spanning different regions of DDX5 were expressed and purified for crystallization trials. The N-terminal region of DDX5 from amino acids 1 to 305 which contains the conserved domain I of the DEAD-box helicase was also cloned and

expressed in *Escherichia coli*. The cloning, expression, purification and crystallization conditions are presented in this work.

Subsequently, the crystal structure of DDX5 1-305 was solved and the high resolution three-dimensional structure shows that in front of domain I is the highly variable and disordered N terminal region (NTR) of which amino acids 51-78 is observable, but whose function is unknown. This region forms an extensive loop and supplements the core with an additional  $\alpha$ -helix. Co-immunoprecipitation experiments demonstrated that the NTR of DDX5 1-305 auto-inhibit its interaction with NS5B. Interestingly, the  $\alpha$ -helix in NTR is essential for this auto-inhibition and seems to mediate the interaction between the highly flexible 1-60 residues in NTR and NS5B binding site in DDX5 1-305, presumably located within residues 79-305. Furthermore, co-immunoprecipitation experiments revealed that DDX5 can also interact with other HCV proteins, besides NS5B.



## KEY WORDS

Hepatitis C virus (HCV), NS5B, DEAD box polypeptide 5 (DDX5, a human RNA helicase), DDX5 1-305, crystallization trials, DEAD-box helicases, transfection and co-immunoprecipitation, GST fusion protein, sequence alignment, fast protein liquid chromatography, protein crystallisation screens, drug and vaccine development.



# TABLE OF CONTENTS

<b>TITLE PAGE</b>	i
<b>DECLARATION</b>	ii
<b>DEDICATION</b>	iii
<b>ACKNOWLEDGEMENTS</b>	iv
<b>ABSTRACT</b>	v
<b>KEYWORDS</b>	vii
<b>TABLE OF CONTENTS</b>	viii
<b>LIST OF ABBREVIATIONS</b>	xiii
<b>LIST OF TABLES</b>	xvii
<b>LIST OF FIGURES</b>	xvii
<b>LIST OF APPENDIXES</b>	xx
<b>LIST OF RESEARCH PUBLICATIONS</b>	xxi
<b>CHAPTER 1: Literature Review</b>	<b>1</b>
1.1 Introduction	2
1.2 Hepatitis C Virus Genome	3
1.3 Hepatitis C Virus Proteins	3
1.3.1 The Core Protein	3
1.3.2 Envelope Glycoproteins E1 and E2	5
1.3.3 Ion Channel p7	5
1.3.4 Zinc Metalloproteinase NS2	6
1.3.5 Serine Protease NS3	6
1.3.6 Modulating Cofactor NS4A	6
1.3.7 Integral ER Membrane Protein NS4B	7
1.3.8 Phosphoprotein NS5A	7
1.3.9 Membrane-Associated RNA-Dependent RNA Polymerase NS5B	7
1.4 Animal Models	8
1.5 HCV Replicons	9





1.6	Production of Infectious Hepatitis C Virions in Tissue Culture	10
1.7	Helicases	10
1.7.1	Transcription	11
1.7.2	Pre-mRNA Splicing	12
1.7.3	Ribosome Biogenesis	12
1.7.4	Nuclear Export	13
1.7.5	Translation	13
1.7.6	Degradation	13
1.7.7	Conserved Motifs of Helicases	14
1.7.8	The DEAD-Box Helicases	14
1.7.8.1	Significance of Conserved Motives in DEAD-Box Proteins	15
1.7.8.2	Q Motif	16
1.7.8.3	Motif I	16
1.7.8.4	Motif Ia and Motif Ib	16
1.7.8.5	Motif II	17
1.7.8.6	Motif III	18
1.7.8.7	Motif IV	18
1.7.8.8	Motif V	18
1.7.8.9	Motif VI	19
1.8	Aim of this Study	19
 <b>CHAPTER 2: Expression, Purification and Preliminary Crystallographic Analysis of Recombinant Human Dead-Box Polypeptide 5</b>		<b>20</b>
2.1	Abstract	21
2.2	Introduction	21
2.3	Materials and Methods	23
2.3.1	Molecular Cloning	23
2.3.1.1	DDX5 Constructs for GST Fusion Protein Expression	23
2.3.1.2	Polymerase Chain Reaction (PCR)	24
2.3.1.3	Agarose Gel Electrophoresis	25
2.3.1.4	DNA Extraction and Gel Purification	25



2.3.1.5	Restriction Enzyme Digest and Ligation	25
2.3.1.6	Bacterial Transformation	26
2.3.1.7	Plasmid DNA Isolation and Purification from <i>Escherichia coli</i> Cells	26
2.3.1.8	DNA Sequencing	26
2.3.1.9	Constructs for Expression and Co-Immunoprecipitation Studies in Mammalian Cells	27
2.3.2	Cell Culture and Protein Analysis	27
2.3.2.1	Cell Lines and Maintenance	27
2.3.2.2	Cell Harvesting	27
2.3.2.3	Quantitation of Mammalian Cell Lysate Protein Concentration	28
2.3.2.4	Co-Immunoprecipitation	28
2.3.2.5	SDS-PAGE	28
2.3.2.6	Western Blot Analysis	29
2.3.3	GST Fusion Protein Expression and Purification	29
2.3.3.1	Small-Scale GST Fusion Protein Expression	29
2.3.3.2	Large-Scale GST Fusion Protein Expression and Purification for Crystallisation	31
2.3.3.3	Coomassie Blue Staining	32
2.3.3.4	Direct Spectrophotometric Protein Concentration Determination	32
2.3.4	Protein Crystallisation Screens	32
2.3.4.1	Sitting Drop	33
2.3.4.2	Hanging Drop	33
2.4	Results and Discussion	33
2.4.1	Mapping the Domain of Interaction of DDX5 with HCV NS5B	33
2.4.1.1	HCV NS5B Interacted with DDX5 and DDX5 Deletion Mutants	34
2.4.1.2	NS5B Interacted Independently with Two Sites on DDX5	34
2.4.2	Cloning of DDX5 Plasmids for GST Fusion Protein Expression in <i>E. coli</i>	34
2.4.3	Expression and Purification of Fusion Protein in a Bacterial System	35
2.4.3.1	Expression of GST-DDX5 61-434, GST-DDX5 163-411 GST-DDX5 204-319 and GST-DDX5132-434 at 30°C Induction	35
2.4.3.2	Expression of GST-DDX5 61-434, and GST-DDX5132- 434 at 16°C Induction	35
2.4.3.3	Expression of GST-DDX5 43-487 and GST-DDX5 at 30° C Induction	37
2.4.3.4	Expression of GST-DDX5 43-487 and GST-DDX5 at 16°C Induction	38

2.4.3.5	Expression and Purification of GST-DDX5 Deletion Mutants Induced at 18°C and Lysed in Buffer with High Salt Concentration	38
2.4.3.6	Expression and Purification of HCV GST-NS5BdelC21 and GST-NS5B 282-570	45
2.4.4	Large-Scale Protein Purification	46
2.4.4.1	Purification of DDX5	46
2.4.4.2	Purification of DDX5 43-487	47
2.4.4.3	Purification of DDX5 1-305	47
2.4.4.4	Purification of DDX5 1-480	47
2.4.4.5	Purification of DDX5 1-80	48
2.4.4.6	Purification of DDX5 61-305	49
2.4.4.7	Purification of HCV NS5BdelC21	50
2.4.4.8	Purification of HCV NS5B 282-570	50
2.4.5	Crystal Screens	50
2.4.5.1	Co-Crystallisation	51
2.4.5.2	Refinement of Crystal Screens	51
2.4.5.3	Refinement of DDX5 Screens	51
2.4.5.4	Refinement of DDX5 43-487 Screen	54
2.4.5.5	Refinement of DDX5 1-305 Screen	55
2.4.5.6	Refinement of DDX5 1-480 Screen	56
2.5	Conclusion	56
 <b>CHAPTER 3: Structural and Functional Characterization of Human DDX5 and Its Interaction with NS5B of Hepatitis C Virus</b>		<b>57</b>
3.1	Abstract	58
3.2	Introduction	58
3.3	Experimental Procedures	60
3.3.1	Cloning of Plasmids	60
3.3.1.1	Mammalian Expression Constructs	60
3.3.1.2	Glutathione S-Transferase (GST) Fusion Protein Expression Constructs	61
3.3.2	Cell Lines and Maintenance	61
3.3.3	Transfection and Co-Immunoprecipitation	61
3.3.3.1	Co-Immunoprecipitation Using Unconjugated Protein A-Agarose Beads	62



3.3.3.2	Co-Immunoprecipitation Using Preconjugated ANTI-FLAG® M2 Affinity Gel	63
3.3.4	Quantitation of Mammalian Cell Lysate Protein Concentration	63
3.3.5	SDS-PAGE	63
3.3.6	Western Blotting	64
3.3.7	Expression and Purification for Crystallisation	64
3.3.8	Crystallisation and Data Collection	65
3.3.9	Structure Determination and Refinement	65
3.3.10	GST Fusion Protein Expression and Purification for Use in GST Pull-Down Assay	65
3.3.11	In Vitro Translation	65
3.3.12	GST Pull-Down Assay	67
3.3.13	Antibodies	67
3.4	Results and Discussion	68
3.4.1	DDX5 Contains Two Sites That Can Interact with NS5B Independently	68
3.4.2	Amino Acids 61-80 in DDX5 Were Sufficient for Interaction with NS5B	68
3.4.3	Domain I of DDX5 is Similar to That of Other DEAD-Box RNA Helicases	72
3.4.4	The ATP Binding Property of DDX5 61-305 Is Not Essential for the Interaction with NS5B	73
3.4.5	Flexible Region in the N-terminal of DDX5 1-305 Auto-Inhibits Its Interaction with NS5B	75
3.4.6	DDX5 1-80 Is Able to Interact with DDX5	81
3.4.7	GST Pull-Down of DDX5 61-305 with GST-DDX5 1-80	81
3.4.8	Unspecific Binding of DDX5 61-305 to GST-H5N1 NS1 1-75 and GST-BLR	81
3.4.9	Amino Acids 1-80 of DDX5 Are Able to Interact with the Rest of DDX5	82
3.4.10	DDX5 Also Interacts with Core and NS3	88
3.5	Conclusion	91
<b>CHAPTER 4: Summary</b>		<b>94</b>
<b>REFERENCES</b>		<b>97</b>
<b>APPENDIX 1: List of Primers Used in the Generation of DDX5 Constructs</b>		<b>114</b>

## LIST OF ABBREVIATIONS

aa	Amino acid
ADP/ATP	Adenosine diphosphate/ Adenosine triphosphate
cDNA	Ccomplementary deoxyribonucleic acid
cAMP	Cyclic adenosine monophosphate
Co-IP	Co-immunoprecipitation
DDX3	DEAD box polypeptide 3, RNA helicase
DDX3X	DEAD box polypeptide 3, RNA helicase, X-linked isoform
DDX5	DEAD box polypeptide 5, RNA helicase
DEAD	Aspartic acid-Glutamic acid-Alanine-Aspartic acid (Asp-Glu-Ala-Asp)
DNA	Deoxyribonucleic acid
DTT	Dithiothreitol
<i>E. coli</i>	<i>Escherichia coli</i>
EDTA	Ethylenediamine tetraacetic acid
Erg2	Ets related gene 2
eIF	Eukaryotic initiation factor
EMCV	Encephalocaditis virus
ER	Endoplasmic reticulum
FPLC	Fast-performance liquid chromatography

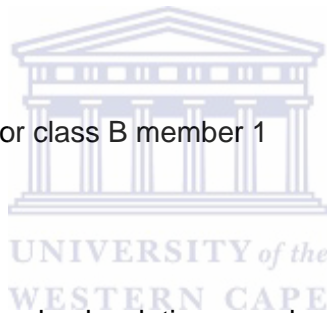
GDD	Glycine-Aspartic acid-Aspartic acid (Gly-Asp-Asp)
GSH	Glutathione
GST	Glutathione S-transferase
HCl	Hydrochloric acid
HCV	Hepatitis C virus
HEPES	4-(2-hydroxyethyl)-1-piperazineethanesulfonic acid
HIV	Human immunodeficiency virus
HVR	Hypervariable region
IFN- $\alpha$	Interferon alpha
IgG	Immunoglobulin G
IP	Immunoprecipitation
IPTG	Isopropyl-1-thio- $\beta$ -D-galactopyranoside
IRES	Internal ribosomal entry site
ISDR	Interferon sensitivity determining region
JFH	Japanese fulminant hepatitis
KCl	Potassium chloride
kDa	Kilodalton
LB	Luria Bertani
LiCl	Lithium chloride



LMP	Low molecular weight protein
LDLR	Low-density lipoprotein receptor
mRNA	Messenger ribonucleic acid
Mg	Magnesium
MyoD	Mysogenic differentiation 1 protein
NaCl	Sodium chloride
NS	Non-structural protein
nt	Nucleotide
NTPase	Nucleoside triphosphatase
NTR	Non-translated region
NTR	N-terminal region
OD	Optical density (absorbance)
ORF	Open reading frame
PBS	Phosphate-buffered saline
PCR	Polymerase chain reaction
PEG	Polyethylene glycol
PKR	Double-stranded RNA-dependent protein kinase
PMSF	Phenylmethylsulfonyl fluoride
RdRp	RNA-dependent RNA polymerase



RHAU	RNA helicase associated with AU-rich element
RIPA	Radioimmunoprecipitation assay buffer
RNA	Ribonucleic acid
RNP	Ribonucleoprotein
SDS	Sodium dodecyl sulfate
SDS-PAGE	Sodium dodecyl sulfate-polyacrylamide gel electrophoresis
Ski2	RNA helicase of Ski complex, involved in 3' degradation of mRNAs
SF1	Superfamily 1
SF2	Superfamily 2
SR-BI	Scavenger receptor class B member 1
TB	Terrific broth
TRAMP	Trf4p/Air2p/Mtr4p polyadenylation complex
Upf1	Regulator of nonsense transcripts, yeast homolog
UTR	Untranslated region
VAMP	Vesicle-associated membrane protein





## LIST OF TABLES

<b>Table 2.1</b>	Constructs generated and used for protein expression	24
<b>Table 2.2</b>	Constructs generated and used in co-immunoprecipitation studies	27
<b>Table 2.3</b>	Primary and secondary antibodies used in Western blotting	30
<b>Table 2.4</b>	Different lysis buffers used	31
<b>Table 3.1</b>	List of primary and secondary antibodies used	67

## LIST OF FIGURES

<b>Figure 1.1</b>	Schematic representation of the HCV genome and encoded viral proteins	4
<b>Figure 1.2</b>	Schematic representation of the three core protein species	5
<b>Figure 1.3</b>	Structure of full-length eIF4A helicase showing the conserved motifs of domains I and II	15
<b>Figure 1.4</b>	Schematic representation of conserved motifs of yeast eIF4A	17
<b>Figure 2.1</b>	Co-immunoprecipitation of DDX5 deletion mutants with HCV NS5B in co-transfected Huh-7 cells	36
<b>Figure 2.2</b>	Two exclusive DDX5 interaction sites with HCV NS5B	37
<b>Figure 2.3</b>	Map of GST-DDX5 and 19 GST-DDX5 deletions mutants cloned and	

	tested for fusion protein expression	39
<b>Figure 2.4</b>	SDS-PAGE of GST-DDX5 61-434, GST-DDX5 163-411 GST-DDX5 204-319 and GST-DDX5132-434 purification after induction at 30°C	40
<b>Figure 2.5</b>	SDS-PAGE of GST-DDX5 61-434, and GST-DDX5 132-434 purification after induction at 16°C	41
<b>Figure 2.6</b>	SDS-PAGE of GST-DDX5 43-487, and GST-DDX5 purification after induction at 30°C	42
<b>Figure 2.7</b>	SDS-PAGE of GST-DDX5 43-487, and GST-DDX5 purification after induction at 16°C	43
<b>Figure 2.8</b>	SDS-PAGE of GST-DDX5 deletion mutants purified in high salt buffer	44
<b>Figure 2.9</b>	SDS-PAGE of GST-DDX5 480-614, and GST-DDX5 61-614 showing GSH-bound proteins that were smaller than their expected molecular weight	45
<b>Figure 2.10</b>	SDS-PAGE of DDX5 1-305 purification	46
<b>Figure 2.11</b>	SDS-PAGE of DDX5 purification	47
<b>Figure 2.12</b>	SDS-PAGE of DDX5 1-305 purification	48
<b>Figure 2.13</b>	SDS-PAGE of DDX5 1-305 purification	48
<b>Figure 2.14</b>	SDS-PAGE of DDX5 1-80 purification	49
<b>Figure 2.15</b>	SDS-PAGE of DDX5 61-305 purification	49
<b>Figure 2.16</b>	SDS-PAGE of HCV NS5BdelC21 purification	50

<b>Figure 2.17</b>	SDS-PAGE of HCV NS5B 282-570 purification	51
<b>Figure 2.18</b>	Crystals of DDX5 1-305	55
<b>Figure 3.1</b>	Map of myc-DDX5 and its deletion mutants cloned for co-immunoprecipitation with NS5B	62
<b>Figure 3.2</b>	Co-immunoprecipitation of myc-tagged DDX5s and flag- tagged-NS5B	69
<b>Figure 3.3</b>	Co-immunoprecipitation of flag-NS5B with myc-tagged C-terminal DDX5s	70
<b>Figure 3.4</b>	DDX5 GST fusion proteins selected for GST pull-down assay	71
<b>Figure 3.5</b>	GST pull-down of NS5B by DDX5 N-terminal fusion proteins, NS5B pulled down with DDX5 fusion proteins 1-305, 61-305 and 1-80	72
<b>Figure 3.6</b>	Structure of DDX5 1-305	74
<b>Figure 3.7</b>	Sequence alignment of DDX5 61-305 with DDX3X 132-420 and DDX19 49-300 showing conserved motifs of DDX5 61-305	75
<b>Figure 3.8</b>	Structure of DDX5 61-305 and the corresponding domains in DDX3X and DDX19B	76
<b>Figure 3.9</b>	Co-immunoprecipitation of NS5B with DDX5-N with mutated ATP binding site and ATP hydrolysis site	78
<b>Figure 3.10</b>	Map of myc-DDX5 1-305 with modifications in the first 78 amino acids (NTR)	79
<b>Figure 3.11</b>	Co-immunoprecipitation of NS5B with the N-terminal half of DDX5 with modifications in the first 78 amino acids	80

<b>Figure 3.12</b>	Bacterial expression of GST-DDX5 1-80	82
<b>Figure 3.13</b>	GST pull-down of DDX5 61-305 with GST-DDX5 1-80 with GST as control	83
<b>Figure 3.14</b>	GST pull-down of DDX5 61-305 with GST-DDX5 1-80 with NS1 and BLR as controls	84
<b>Figure 3.15</b>	GST pull-down of <sup>35</sup> S-labeled DDX5 1-614 by GST-DDX5 1-80	85
<b>Figure 3.16</b>	GST pull-down of <sup>35</sup> S-labeled DDX5 61-614 by GST-DDX5 1-80	86
<b>Figure 3.17</b>	GST pull-down of <sup>35</sup> S-labeled DDX5 79-614 by GST-DDX5 1-80	87
<b>Figure 3.18</b>	Co-immunoprecipitation of DDX5 with HCV proteins Core 1-151, Core 1-173, NS3, NS4B, NS5A and NS5B	89
<b>Figure 3.19</b>	Co-immunoprecipitation of Core 1-173, NS3, and NS5B with endogenous DDX5	90

## LIST OF APPENDIXES

<b>APPENDIX 1</b>	List of Primers Used in the Generation of DDX5 Constructs
-------------------	---

# LIST OF RESEARCH PUBLICATIONS

## Manuscripts from this Thesis

1. **Choi, Y. W.**, Dutta, S., Fielding, B. C., and Tan, Y. J. (2010) Expression, purification and preliminary crystallographic analysis of recombinant human DEAD-box polypeptide 5, *Acta Crystallogr Sect F Struct Biol Cryst Commun* 66, 192-194.
2. Sujit Dutta, **Yook-Wah Choi**, Masayo Kotaka, Burtram C. Fielding, Yee-Joo Tan. Structural and functional characterization of human DDX5 and its interaction with NS5B of the hepatitis C virus. Submitted to *Journal of Biological Chemistry*.

## Conference Posters and Presentations from this Thesis

1. **Yook-Wah Choi**, Sujit Krishna Dutta, Burtram C Fielding and Yee-Joo Tan, Cellular RNA Helicase p68 re-localization and interaction with HCV (Hepatitis C Virus) NS5B Protein, Virus and Cancer Symposium, Singapore, 9-10 November 2007.

# CHAPTER 1



## 1.1 Introduction

Hepatitis C was first recognized as a transfusion-associated liver disease not caused by hepatitis A or hepatitis B virus after serological tests were developed to screen for hepatitis A and hepatitis B in the blood (Prince, Brotman et al. 1974; Feinstone, Kapikian et al. 1975). The infectious agent was finally identified with the cloning of the cDNA of the hepatitis C virus (HCV), using random polymerase chain reaction (PCR) screening of nucleic acids extracted from plasma of a large pool of chimpanzee infected with non-A non-B hepatitis (Choo, Kuo et al. 1989).

HCV is recognized as a major aetiological agent of liver disease as it infects 3% of the world's population, or more than 170 million people worldwide (Wasley and Alter 2000). In 20-30% of patients, HCV infection is acute and the virus is cleared naturally (Alter and Seeff 2000). However, in the majority of cases, the virus persists, often predisposing infected individuals to fibrosis, cirrhosis and hepatocellular carcinoma (Macdonald and Harris 2004). A recent study proposed that chronic HCV infection increases insulin resistance leading to an increased chance of developing type 2 diabetes (Kasai, Adachi et al. 2009).

The broad genetic diversity amongst HCV genotypes and the high rate of mutations during replication makes it a challenging disease to treat. No effective vaccine has been developed against HCV infection (Lechmann and Liang 2000). The current therapy for HCV infection involves the use of a combination of polyethylene (PEG)-conjugated interferon alpha (IF- $\alpha$ ) and ribavirin. These drugs are expensive and produce severe side effects such as headache, myalgia, fever, depression, arthralgia and haemolytic anaemia (De Franceschi, Fattovich et al. 2000; Hayashi and Takehara 2006). Moreover, this drug treatment is only effective in eradicating the virus in approximately 50% of infected patients and the efficacy varies with different viral genotypes (Hayashi and Takehara 2006; Ghany, Strader et al. 2009).

## 1.2 Hepatitis C Virus Genome

HCV is a member of the *Flaviviridae* family of viruses which includes flavivirus, pestivirus and hepacivirus. Flaviviruses include dengue fever virus, Japanese encephalitis virus, tick-borne encephalitis virus and yellow fever virus. Pestiviruses include bovine viral diarrhoea virus, border disease virus and classical swine fever virus (Tan and National Center for Biotechnology 2006). HCV is a small, enveloped, positive-strand RNA virus and is the only representative of hepacivirus. The 9.6 kb RNA molecule comprises the 5' and 3' untranslated regions (UTR) flanking a single open reading frame (ORF) encoding a polyprotein of approximately 3000 amino acids (Figure 1.1).

## 1.3 Hepatitis C Virus Proteins

HCV viral protein is first translated as a polyprotein precursor via an internal ribosome entry site located in the 5'-UTR. This polyprotein is then cleaved into 10 polypeptides by cellular and viral proteinases. The N- terminus encodes three structural proteins – core, envelope glycoproteins E1 and E2, while the C-terminal two-thirds of the polyprotein comprise the 6 non-structural proteins NS2, NS3, NS4A, NS4B, NS5A, and NS5B (Macdonald and Harris 2004). These proteins encode enzymes or accessory factors that catalyse and regulate the replication of the HCV RNA genome (Tan, Pause et al. 2002). Another protein, called p7, lies at the junction between the structural and non-structural regions of the virus polyprotein.

### 1.3.1 The Core Protein

The core protein interacts with viral RNA and forms the nucleocapsid (Tan, Pause et al. 2002). It has also been shown to be functionally pleiotropic, interacting with many cellular proteins and exerting an array of effects on cells such as apoptosis, lipid metabolism, transcription, cellular transformation and the immune response (Marusawa, Hijikata et al. 1999); (Moriya, Fujie et al. 1998); (Ray, Lagging et al. 1995); (Ray, Lagging et al. 1996); (Large, Kittlesen et al. 1999). When expressed in transfected cells, the protein was found to associate with cellular lipid



storage droplets (Barba, Harper et al. 1997). Depending on the proteolytic processing, the core protein exists as two forms in all HCV strains, known as p21 and p23 according to their molecular weights (Figure 1.2) (Yasui, Wakita et al. 1998). A third core-related protein species, termed p16, has also been detected in studies using HCV-1 (Figure 1.2) (Lo, Masiarz et al. 1995). The functions of these protein species are still unknown, although p21 has been suggested to be the mature form that constitutes the virus capsid (Yasui, Wakita et al. 1998). The core protein was found to self-assemble into virus-like particles in the endoplasmic reticulum (ER) membrane (Ait-Goughoulte, Hourieux et al. 2006).

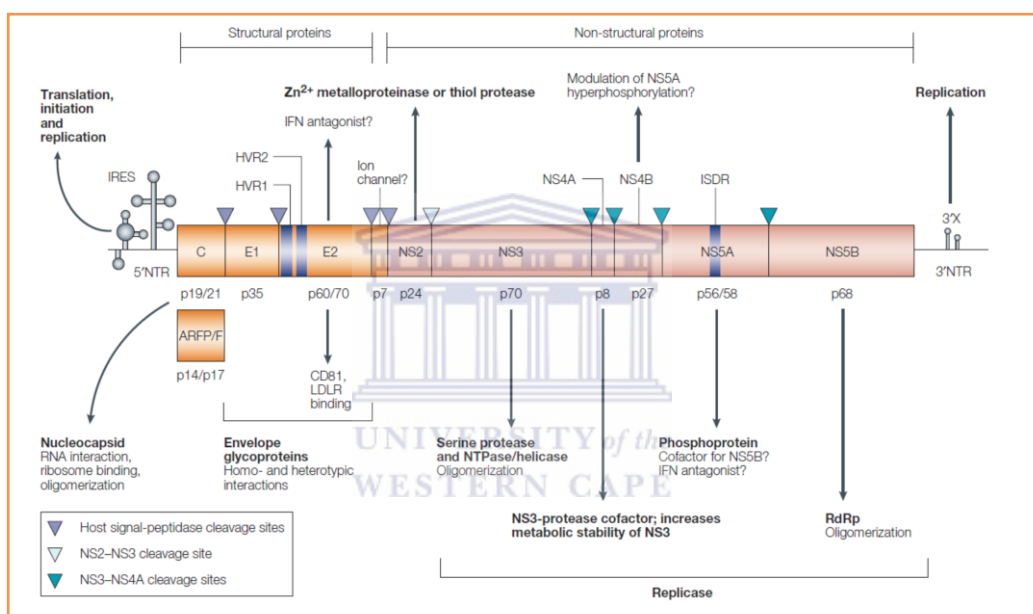


**Figure 1.1: Schematic representation of the HCV genome and encoded viral proteins (Tan, Pause et al. 2002).** The boxed area corresponds to the single ORF of the HCV genome. The stem-loop structures represent the 5' and 3' non-translated (NTR) regions, including the internal ribosome-entry site (IRES) and 3'-X-regions. The function and molecular mass (in kDa) of the gene products after polyprotein processing are shown. Core (C)–E1, E1–E2, E2–p7 and p7–non-structural protein 2 (NS2) junctions are cleaved by cellular signal peptidases to yield structural proteins. The NS2–NS3 metalloproteinase undergoes autocatalytic cleavage, which releases the mature NS3 serine protease. NS3 cleaves the remainder of the NS polypeptide. The two regions that have extreme sequence variability in E2, known as hypervariable regions 1 and 2 (HVR1 and HVR2), are indicated. A region in NS5A, known as the interferon (IFN)-sensitivity-determining region (ISDR), has been linked to the response to IFN- $\alpha$  therapy in some strains of HCV. Both NS5A and E2 have been implicated as antagonists of IFN. ARFP/F: alternative reading-frame protein/frameshift protein; LDLR: low-density lipoprotein receptor; RdRp: RNA-dependent RNA polymerase.

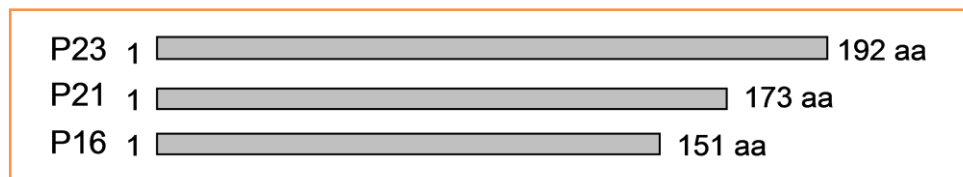


**Figure 1.2: Schematic representation of the three core protein species.** The P23, P21 and P16 core proteins with sizes (number of amino acids) shown.

### 1.3.2 Envelope Glycoproteins E1 and E2

Envelope glycoproteins E1 and E2, together with the core protein, are components of the viral particle (Voisset and Dubuisson 2004). The E2 protein binds CD81, a tetraspan protein expressed on various cell types including hepatocytes and B lymphocytes. E2 binding to human CD81 was mapped to the major extracellular loop of CD81 (Pileri, Uematsu et al. 1998). Both E1 and E2 are important for the binding of HCV to cellular receptor(s) on the surface of host cells such as hepatocytes, and are possibly responsible for the binding to and entry of the virus into target cells (Tan, Pause et al. 2002); (Suzuki, Suzuki et al. 1999). CD81, human scavenger receptor, SR-BI, tight junction claudin-1 and occludin are the most important receptors mediating HCV cell entry (Ploss, Evans et al. 2009).

### 1.3.3 Ion Channel p7

It has been shown that p7 forms an amantadine-sensitive ion channel required for viral replication in chimpanzees, though its precise role in the life cycle of HCV is unknown (Sakai, Claire et al. 2003). However, clinical trials found that the p7 ion channel function is not affected by amantadine (Steinmann, Whitfield et al. 2007). The p7 polypeptide of HCV is critical for infectivity and contains functionally important genotype-specific sequences (Griffin, Harvey et al. 2004).

### **1.3.4 Zinc Metalloproteinase NS2**

The zinc metalloproteinase, NS2-NS3, undergoes autocatalytic cleavage to produce NS2 and NS3. NS2 interacts with other non-structural proteins and forms homodimers with itself (Dimitrova, Imbert et al. 2003). It was found to be an apoptosis inhibitor and interferes with cellular gene expression (Dumoulin, von dem Bussche et al. 2003); (Erdtmann, Franck et al. 2003). A recent study has shown that NS2 plays an essential role in HCV particle assembly by interacting with E1 and E2 glycoproteins as well as NS3-NS4 enzyme complexes (Stapleford and Lindenbach 2011).

### **1.3.5 Serine Protease NS3**

NS3 is a serine protease with nucleoside triphosphatase and RNA helicase activity at its C-terminus (Tan, Pause et al. 2002). NS3 cleaves the remaining nonstructural polyprotein to produce NS4A, NS4B, NS5A and NS5B. When singly expressed, NS3 protein had been shown to be distributed to the cytoplasm and nucleus in an inducible system (Wolk, Sansonno et al. 2000). The NS3 protease, together with its cofactor NS4A, stops the expression of interferon alpha (IF- $\alpha$ ) and interferon beta (IF- $\beta$ ) by cleaving the IF- $\beta$  promoter stimulator-1 and thus evading the innate immune system (Li, Sun et al. 2005).

### **1.3.6 Modulating Cofactor NS4A**

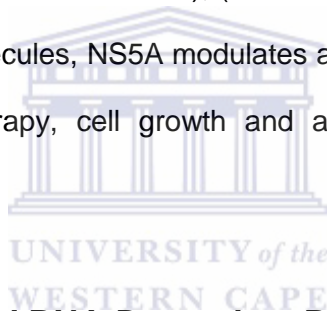
NS4A serves as a cofactor modulating NS3 serine protease and helicase activities, and is responsible for localizing NS3 to the perinuclear ER membrane (De Francesco and Steinkuhler 2000); (Pang, Jankowsky et al. 2002); (Wolk, Sansonno et al. 2000). NS4A also associates with NS5A and contributes to hyperphosphorylation of NS5A (Asabe, Tanji et al. 1997). Expression of NS4A was found to significantly change the intracellular distribution of mitochondria, thus resulting in mitochondrial damage and inducing apoptosis (Nomura-Takigawa, Nagano-Fujii et al. 2006).

### **1.3.7 Integral ER Membrane Protein NS4B**

NS4B is a hydrophobic integral ER membrane protein with four transmembrane (tetraspan) segments (Suzuki, Suzuki et al. 1999); (Hugle, Fehrmann et al. 2001). The protein has been shown to induce a specialized membranous web postulated to be the HCV RNA replication complex (Egger, Wolk et al. 2002).

### **1.3.8 Phosphoprotein NS5A**

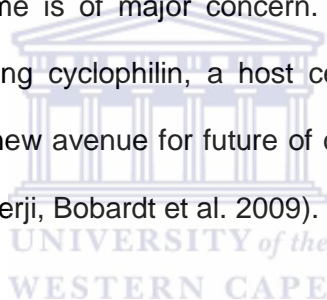
Phosphoprotein NS5A is a pleiotropic protein with key roles in viral RNA replication and modulation of host cell physiology (Macdonald and Harris 2004). It co-localises with the viral RNA and other non-structural proteins in the cytoplasmic membranous web that catalyse viral genome replication (Macdonald and Harris 2004); (Mottola, Cardinali et al. 2002). By binding to a range of cellular signalling molecules, NS5A modulates a range of physiological process such as HCV resistance to IFN therapy, cell growth and apoptosis (Tan, Pause et al. 2002; Macdonald and Harris 2004).



### **1.3.9 Membrane-Associated RNA-Dependent RNA Polymerase NS5B**

NS5B is a membrane-associated RNA-dependent RNA polymerase (Behrens, Tomei et al. 1996; Suzuki, Suzuki et al. 1999). It plays an essential role in the replication of HCV, it initiates the synthesis of a complementary negative-strand RNA from the genomic positive-strand RNA, more positive-strand HCV RNA can then be generated from the newly synthesised negative-strand template. The crystal structure of NS5B presented typical fingers, palm and thumb sub-domains encircling the GDD active site, which is also seen in other RNA-dependent RNA polymerases and is similar to the structure of reverse transcriptase of HIV 1 and murine Moloney leukaemia virus (Bressanelli, Tomei et al. 1999). The last 21 amino acids in the C-terminal of NS5B anchor the protein to the ER-derived membranous web (Schmidt-Mende, Bieck et al. 2001).

NS5B has been shown to interact with the core, NS3/NS4A, NS4B and NS5A proteins either directly or indirectly (Lee, Nam et al. 2006). Numerous interactions with cellular proteins have also been reported. These proteins are mainly proteins associated with genome replication, as well as vesicular transport, such as protein kinase C-related kinase 2, P68 (DDX5),  $\alpha$ -actinin, nucleolin, human eukaryotic initiation factor 4AII, and human VAMP-associated protein (Lee, Nam et al. 2006). NS5B is widely targeted in the development of antiviral therapy due to its essential role in viral replication. Many nucleoside analogues that act as chain terminators target the active site of the polymerase. Non-nucleoside inhibitors that act by binding to one of the four allosteric enzyme sites inhibit polymerase activity (Legrand-Abravanel, Nicot et al. 2010). Due to a lack of proofreading in RNA replication, there is a pre-existence of quasi species in HCV-infected individuals. The selection of species resistant to specific antiviral therapy over time is of major concern. The discovery that cyclosporine A inhibits HCV replication by binding cyclophilin, a host cellular peptidyl-prolyl isomerase that interacts with NS5B, provides a new avenue for future of drug therapy that target a host factor that interacts with the virus (Chatterji, Bobardt et al. 2009).



#### **1.4 Animal Models**

Chimpanzee is the only established animal model for HCV infection, but due to the scarcity of the animal, high cost of maintenance, and ethical and conservation concerns, efforts have been made to establish a small animal model to study HCV infection and liver disease caused by HCV infection. The tree shrew (*Tupaia* sp.) represents the only non-primate small animal model for HCV infection. The tree shrew was successfully infected with HCV after severe immunosuppression (Xie, Riezu-Boj et al. 1998) and more recently, chronic infection were observed in some of the normal adult tree shrews infected with HCV (Xu, Chen et al. 2007). The HCV virus is able to replicate in transgenic mice transplanted with human hepatocytes (Mercer, Schiller et al. 2001). Transgenic mice expressing HCV genes in the liver have been used in the study of hepatocellular carcinoma (Moriya, Fujie et al. 1998).

## 1.5 HCV Replicons

HCV is inefficient in infecting cultured cells and produce very low titers. Efforts to identify cell lines which could produce robust infection and virus production was not successful (Bartenschlager and Lohmann 2001) until the advent of HCV subgenomic replicons (Lohmann, Korner et al. 1999) based on knowledge gained from the development of subgenomic replicons of pestivirus and Kunjin virus (Khromykh and Westaway 1997; Behrens, Grassmann et al. 1998). Using the consensus sequence of HCV genotype 1b termed Con1 as template, the structural protein region was replaced by a neomycin phosphotransferase gene, conferring G418 resistance and the expression of non-structural proteins was controlled by the internal ribosomal entry site (IRES) of encephalomyocarditis virus (EMCV). Transfection of the constructs into human hepatoma Huh 7 cells produced colonies that could autonomously replicate under neomycin selection. The subgenomic replicon helped identify amino acid substitutions (adaptive mutations in cell culture) that increased replication efficiency by several orders of magnitude (Blight, Kolykhalov et al. 2000; Lohmann, Korner et al. 2001).

The development of a full-length HCV genome 1b replicon enabled the study of antiviral agents against HCV structural proteins that were missing in the subgenomic replicon (Blight, McKeating et al. 2002; Ikeda, Yi et al. 2002; Pietschmann, Lohmann et al. 2002). Subsequent development of HCV RNA replicons of genotype 1a (Blight, McKeating et al. 2003) and 2a (Kato, Date et al. 2003) and replicons that were able to replicate in human embryonic kidney cells, non-hepatic epithelial and mouse hepatoma cells provided new insights into genotype-specific replication and the development of quasi species in HCV-infected individuals (Zhu, Guo et al. 2003; Ali, Pellerin et al. 2004). The replicon system enables the efficient study of HCV RNA replication in vitro, shedding light on basic replication processes, structure of the replication complex, virus interactions with the host cell and effects of antiviral agents (Brass, Moradpour et al. 2007; Dustin and Rice 2007).

## 1.6 Production of Infectious Hepatitis C Virions in Tissue Culture

The replicons of genotype 1a, 1b and 2a molecular clones revolutionised the study of basic HCV replication in cell culture, but they did not produce infectious virions. While adaptive mutations were advantageous for replicon replication in cell culture, they could be deleterious for virus production (Lanford, Lee et al. 2001; Lindenbach and Rice 2005). The development of a genotype 2a HCV replicon derived from the consensus sequence of a virus isolated from a Japanese patient with fulminant hepatitis denoted as JFH-1 (Wakita, Pietschmann et al. 2005), overcame the inability to study virus entry and release in a tissue culture. The JFH-1 replicon was able to replicate efficiently in different cell lines and secreted viral particles that were infectious in chimpanzees and could be subcultured to infect naïve Huh 7 cells (Lindenbach and Rice 2005). A chimaeric full-length HCV genomic construct of JFH-1 was cloned by replacing the Core-NS2 region with that of the J6 strain of genotype 2a. The new full-length J6/JFH clone replicated even more efficiently in cell culture producing  $10^5$  infectious units per milliliter within 48 hours in Huh 7.5 cells (Lindenbach, Evans et al. 2005).

Liver cirrhosis and cancer associated with HCV infection are normally caused by genotype 1 HCV. Hence, the development of an infectious HCV of genotype 1 was significant. The first genotype 1a infectious clone boasted 5 cell culture adapted mutations and specificity that were approximately 400-fold lower than that of genotype 2a virus (Yi, Villanueva et al. 2006). Infectious intragenotypic and intergenotypic HCV chimeras of genotype 1a, 1b, 2a and 3a were also developed and characterised (Pietschmann, Kaul et al. 2006). The development of more infectious HCV of different genotypes will broaden the tools available for antiviral and comparative life cycle investigations.

## 1.7 Helicases

Helicases are vital enzymes involved in all aspects of DNA and RNA metabolism. They use energy derived from binding and hydrolysing ATP to unwind double stranded nucleic acids (Lohman 1993; Hall and Matson 1999). DNA helicases are involved in DNA replication,

transcription, conjugation, recombination and repair (Lahue and Matson 1988; Lohman and Bjornson 1996). They are processive in their activity (Lahue and Matson 1988; Roman, Eggleston et al. 1992; Lohman 1993; Sikora, Eoff et al. 2006), binding to regions where breaks in the base pairing form single stranded DNA and double stranded DNA junctions, they proceed to unwind double stranded DNA (Amaratunga and Lohman 1993). Earlier studies proposed that DNA helicases unwound double stranded DNA unidirectionally (3' to 5' or 5' to 3') (Lohman 1993; Yu, Ha et al. 2007), in either an active or passive manner (Lohman 1993). During passive DNA unwinding, helicase bound to single stranded DNA at a single strand double strand DNA-junction translocate stepwise along the single stranded DNA preventing the duplex from reforming when random thermal fluctuations opens up the base pairs. In active DNA unwinding, helicase binds to both single stranded and double stranded DNA at the single strand-double strand DNA junction, unwinding the DNA by destabilising the base-pairing using energy derived from ATP hydrolysis (Lohman 1992; Amaratunga and Lohman 1993; Lohman 1993). More recent theoretical and experimental studies are in favour of a mechanism whereby the energetics involved in helicase activity form a continuum (Betterton and Julicher 2005; Johnson, Bai et al. 2007).

RNA helicases represent a multifunctional group of proteins. Besides their traditional role of using energy derived from binding and hydrolysis of ATP to unwind RNA duplexes, they have been known to function as chaperones that rearrange RNA structures and modify RNA-associated protein complexes (Tanner and Linder 2001; Cordin, Banroques et al. 2006; Bleichert and Baserga 2007). Involved in all aspects of RNA metabolism, they are required during transcription, pre-mRNA splicing, ribosome biogenesis, mRNA nuclear export, translation initiation and RNA degradation (Cordin, Banroques et al. 2006; Linder 2006).

### **1.7.1 Transcription**

RNA helicases facilitate and regulate gene expression. DP103 (Ddx20) was shown to interact and suppress the transcriptional activity of steroidogenic factor 1 (SF-1) and Egr2 (Yan, Mouillet et al. 2003; Gillian and Svaren 2004). RNA helicase A (Dhx9) regulates transcription by acting



as a bridging factor between cAMP-response element-binding protein and RNA polymerase II (Nakajima, Uchida et al. 1997). p68 (Ddx5) and related p72 (Ddx17) interacts with different transcription factors and nuclear receptors as co-repressors or co-activators of transcription (Endoh, Maruyama et al. 1999; Watanabe, Yanagisawa et al. 2001; Wilson, Bates et al. 2004; Cordin, Banroques et al. 2006).

### **1.7.2 Pre-mRNA Splicing**

Spliceosomes are formed by large ribonucleoprotein (RNP) complexes. They assemble and go through modification while the transcribed pre-mRNAs are processed. The removal of introns by two transesterification reactions to form mature mRNAs ready for export, and the subsequent release of the mRNA from the spliceosomes require precise rearrangement of the RNP complexes (Staley and Guthrie 1998; Cordin, Banroques et al. 2006; Linder 2006; Abdelhaleem 2010). RNA helicase p68 is essential in pre-mRNA splicing and is required for the dissociation of U1 small nuclear ribonucleoprotein (snRNP) from the 5' splice site (Liu 2002; Lin, Yang et al. 2005). Prp2 (Kim and Lin 1996) and Prp16 (Schwer and Guthrie 1991) serve as catalysts to the first and second transesterification steps while Prp22 disrupts mRNA/U5 snRNP contacts to release mRNA from the spliceosome (Schwer 2008) and Prp43 catalyses the removal of the lariat-intron (Martin, Schneider et al. 2002).

### **1.7.3 Ribosome Biogenesis**

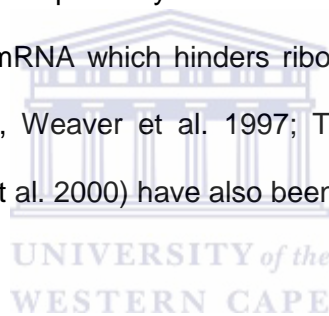
Ribosome biogenesis is a complex process that involves transcription, modification and processing of ribosomal RNA (rRNA) with interactions with ribosomal proteins and a variety of transacting factors. RNA helicases are required during ribosome biogenesis, regulate RNA-protein interactions in the ribosomes (de la Cruz, Kressler et al. 1999; Cordin, Banroques et al. 2006; Linder 2006; Abdelhaleem 2010).

### 1.7.4 Nuclear Export

Mature mRNAs are exported through the nuclear pore into the cytoplasm for translation in eukaryotic cells. Dbp5p was shown to be essential for nuclear export as mutation of Dbp5p resulted in accumulation of poly(A)<sup>+</sup> RNA in the nucleus (Tseng, Weaver et al. 1998). DDX3, a human RNA helicase, acts as a shuttle between the nucleus and cytoplasm and is essential for HIV-1 RNA export (Yedavalli, Neuveut et al. 2004).

### 1.7.5 Translation

Eukaryotic initiation factor 4A (eIF4A) is an RNA helicase with RNA-dependent ATPase activity. It forms part of the cap-binding complex of eIF4F involved in the initiation of translation (Gingras, Raught et al. 1999), and is probably involved in the unwinding of secondary structure in the 5'-untranslated region of mRNA which hinders ribosome binding (Rogers, Komar et al. 2002). Ded1 in yeast (Chuang, Weaver et al. 1997; Tarn and Chang 2009) and Vasa in *Drosophila* (Carrera, Johnstone et al. 2000) have also been shown to be crucial for translation.



### 1.7.6 Degradation

In eukaryotes, different exosomes are responsible for degradation of small regulatory RNAs, defective mRNAs and mRNAs in the nucleus, cytoplasm and mitochondria (Cordin, Banroques et al. 2006). RNA helicase Mtr4p forms part of the Trf4p/Air2p/Mtr4p polyadenylation complex (TRAMP), responsible for polyadenylation and stimulation of exosome degradation of RNA in the nucleus (LaCava, Houseley et al. 2005), while Ski2 is required for cytoplasmic exosomes activity responsible for 3' to 5' mRNA degradation in yeast (Anderson and Parker 1998). Upf1 is critical in the nonsense-mediated mRNA decay pathway whereby mRNA with premature termination codons are recognized and degraded (Cheng, Muhlrud et al. 2007), while RHAU plays a part in the degradation of AU rich elements in mRNA (Tran, Schilling et al. 2004).

### 1.7.7 Conserved Motifs of Helicases

Primary sequence analysis were first used to identify helicases with conserved motifs and categorised them into 3 superfamilies and 2 families (Gorbalenya and Koonin 1993). All the helicases identified carried the Walker A (phosphate-binding loop) and Walker B ( $Mg^{2+}$ -binding aspartic acid) motifs (Walker, Saraste et al. 1982). The majority of helicases identified fell into the superfamily 1 (SF1) and superfamily 2 (SF2) classification (Gorbalenya and Koonin 1993). A classic member of SF2, eIF4A was the first RNA helicase reported to have the ability to change the structure of mRNA using energy supplied from ATP - it was shown that incubation of globin mRNA with eIF4A changed the mRNA sensitivity to nuclease (Ray, Lawson et al. 1985). Alignment studies of yeast eIF4A with its homologues contributed to the identification of the DEAD box family of proteins with the distinct D-E-A-D (Asp-Glu-Ala-Asp) amino-acid sequence at its Walker B motif (Linder, Lasko et al. 1989).

### 1.7.8 The DEAD-Box Helicases

The DEAD-box family of helicases are ubiquitous and play major roles in RNA metabolism (de la Cruz, Kressler et al. 1999; Rocak and Linder 2004; Abdelhaleem 2010). They are distinguished by 9 conserved motifs: the Q-motif, motif I, motif Ia, motif Ib motif II and motif III forms the N-terminal domain I, while motif IV, motif V and motif VI form the C-terminal domain II (Figure 1.3). A conserved sequence of GG is found between Ia and Ib and a conserved sequence QxxR (x is any residue) is found between motifs IV and V. The Q-motif together with a conserved phenylalanine upstream of it sets it apart from the other closely related DEAH, DExH and DExD families of proteins (Tanner, Cordin et al. 2003; Cordin, Banroques et al. 2006; Bleichert and Baserga 2007). The conserved motifs are involved in the regulation of helicase and ATPase activities (Tanner, Cordin et al. 2003).

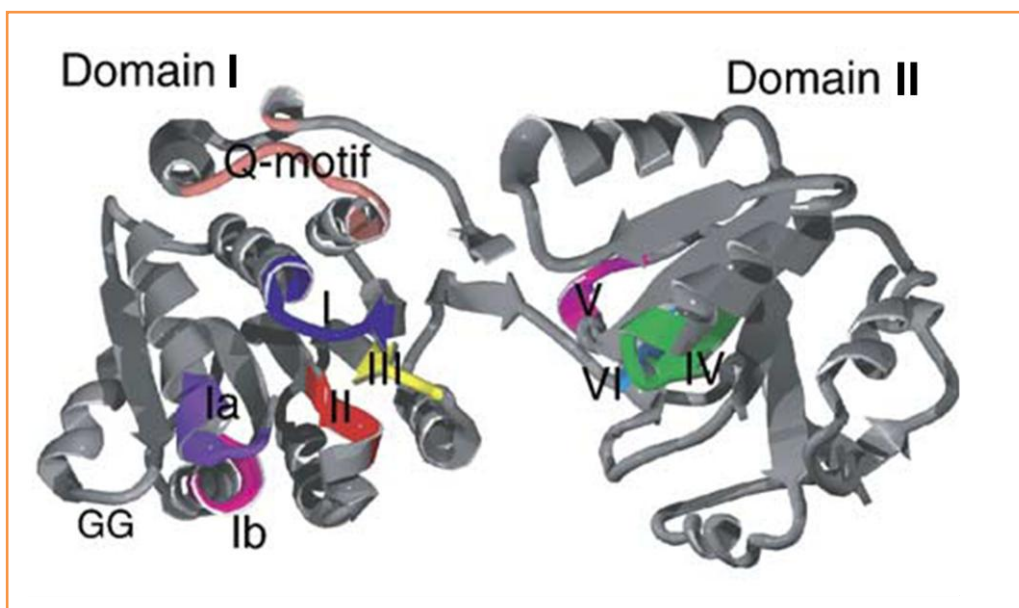


**Figure 1.3: Structure of full-length eIF4A helicase showing the conserved motifs of domains I and II (Caruthers et al., 2000; PDB accession number: 1FUU).** Domain I on the left contains the conserved Q-motif, motif I, motif Ia, the conserved GG sequence, motif Ib, motif II and motif III. Domain II on the right holds conserved motifs IV, V and VI.



### 1.7.8.1 Significance of Conserved Motives in DEAD-Box Proteins

Solved crystal structures of MjDEAD the DEAD-box protein of *Methanococcus jannashii* (Story, Li et al. 2001), UAP56 - a human splicing and export factor (Shi, Cordin et al. 2004), yeast mRNA translation and degradation factor Dhh1p (Cheng, Collier et al. 2005), human elongation factor 4AIII (eIF4AIII) (Andersen, Ballut et al. 2006; Bono, Ebert et al. 2006), and human DEAD-box helicase DDX3X (Hogbom, Collins et al. 2007) show that domains I and II are connected via a short flexible linker. Each globular domain consists of at least 5  $\alpha$ -helices flanking 5  $\beta$ -strands, corresponding to the core structure of Rec A (Story and Steitz 1992; Caruthers and McKay 2002; Cordin, Banroques et al. 2006).

### 1.7.8.2 Q Motif

Sequence alignment analysis of yeast eIF4A with other related DEAD box proteins resulted in the identification of a 9 amino acid motif and a highly conserved aromatic residue phenylalanine (F) upstream of motif I. The consensus sequence defined for this motif was GaccPohlQ, where a represents an aromatic residue, c: a charged group, o: an alcohol, h: a hydrophobic group and l: an aliphatic residue. The Q motif was thus named after the glutamine residue that was conserved in 99% of the sequences. In solved structures of DEAD-box proteins, the Q motif and the aromatic residue 17 amino acids upstream of it shows up as an extra  $\beta$ -strand and 2  $\alpha$ -helices forming a cap-like structure on domain I (Figure 1.4) (Tanner, Cordin et al. 2003; Cordin, Tanner et al. 2004; Cordin, Banroques et al. 2006). The Q motif is a conserved adenine recognition motif needed for adenine binding - it interacts with motif I during ATP and RNA binding and regulates ATPase activity (Tanner 2003; Cordin, Tanner et al. 2004).

### 1.7.8.3 Motif I

Motif I (AxTGoGKT) was first described as the Walker A motif, which was found in all helicases and many NTPases (Walker, Saraste et al. 1982). It forms the phosphate-binding P-loop responsible for nucleotide binding and is essential for ATPase and helicase activity. In nucleotide-bound structures of eIF4A and UAP56, the helix formed by motif I was found in an unwound "open" conformation (Benz, Trachsel et al. 1999; Story, Li et al. 2001; Shi, Cordin et al. 2004; Zhao, Shen et al. 2004). In eIF4A, UAP56 and BstDEAD crystallised without a ligand, the P-loop was found in a "closed" conformation (Johnson and McKay 1999; Carmel and Matthews 2004; Shi, Cordin et al. 2004).

### 1.7.8.4 Motif Ia and Motif Ib

Motifs Ia (PTRELA) and Ib (TPGR) form part of domain I, but they have not been observed to participate directly in ATP binding or hydrolysis. They have, however, been shown to be crucial for RNA binding, acting in conjunction with motifs IV and V (Rogers, Komar et al. 2002). Motif Ia

has also been found to be essential for formation of an exon-junction complex and nonsense mediated mRNA decay (Shibuya, Tange et al. 2006).

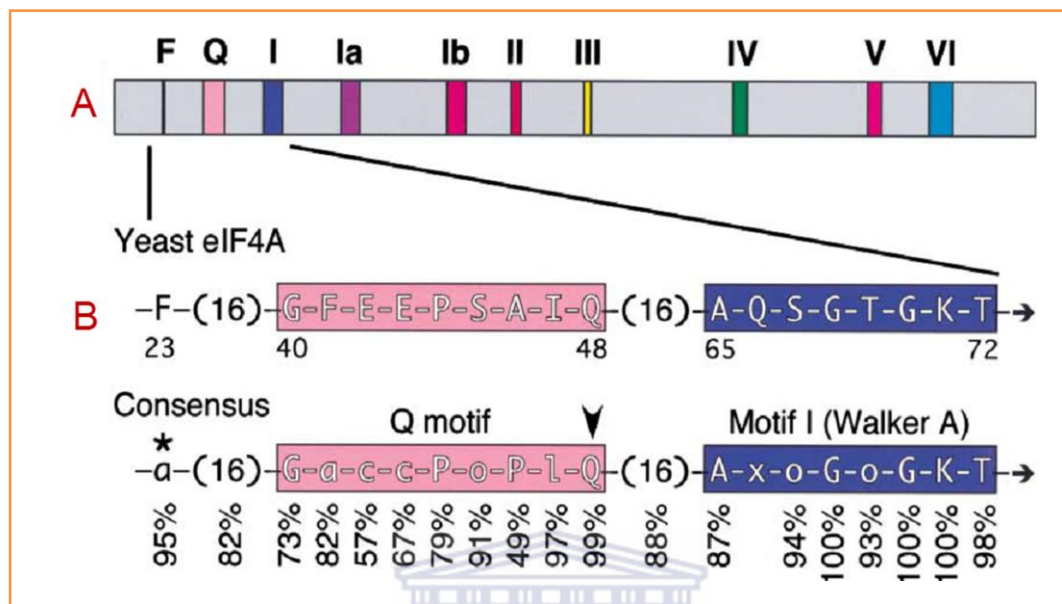


**Figure 1.4: Schematic representation of conserved motifs of yeast eIF4A (adapted from Cordin, Tanner et al. 2004).** **A.** The positions of the conserved motifs are shown (Tanner and Linder, 2001). **B.** Enlargement of the region containing the upstream phenylalanine, the Q motif, and the previously characterized motif I. The numbers below refer to the positions of the amino acids in eIF4A. The consensus is based on the same alignment as in (A), but the conservation of amino acids (uppercase) and functional groups (lowercase) are shown (a: F, W, Y; c: D, E, H, K, R; l: I, L, V; o: S, T; x: any amino acid). The glutamine is 17 aa upstream of motif I 88% of the time (range 14–32 aa), and the isolated aromatic group is 17 aa upstream of the Q motif 82% of the time (range 12–20 aa).

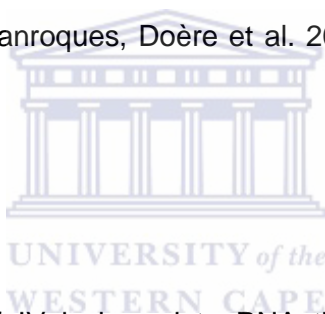
### 1.7.8.5 Motif II

Motif II (also known as Walker B motif) is necessary for ATPase activity. The majority of DEAD-box proteins carry the signature sequence of DEAD in this motif (Tanner and Linder 2001), while the consensus sequence of DExx is found in other SF1 and SF2 proteins (Gorbalenya and Koonin 1993). Mutations in this region have been shown to decrease or abolish NTPase and

helicase activity without affecting RNA binding (Pause and Sonenberg 1992; Iost, Dreyfus et al. 1999). The glutamine residue of motif II forms interaction with the  $\beta$  and  $\gamma$  phosphates of bound ATP through a coordinated magnesium ion and may be involved in hydrolysis (Story, Li et al. 2001; Shi, Cordin et al. 2004; Cordin, Banroques et al. 2006).

#### **1.7.8.6 Motif III**

Motif III (SAT) is highly conserved in SF2 helicases. It was proposed to link ATP binding and helicase activities. Earlier studies showed that mutations in this motif affected substrate unwinding, but not ATP binding and hydrolysis (Pause and Sonenberg 1992; Schwer and Meszaros 2000). A recent study of Ded1 reviewed that mutations in Motif III affected RNA dependent hydrolysis of ATP and reduced its binding affinity of single-stranded RNA, but the affinity for ATP is not affected (Banroques, Doère et al. 2010). The role of motif III may differ amongst helicases.



#### **1.7.8.7 Motif IV**

It has been proposed that motif IV is bound to RNA through interactions with the ribose-phosphate backbone (Caruthers and McKay 2002). Located at the bottom of domain II, the consensus sequence of motif IV is 2 aliphatic groups, a phenylalanine and a hydrophobic group followed by 5 polar and charged groups. The phenylalanine is the only residue that is conserved at 98% in this motif, and plays a crucial role in linking ATP binding and hydrolysis with RNA binding (Banroques, Cordin et al. 2008).

#### **1.7.8.8 Motif V**

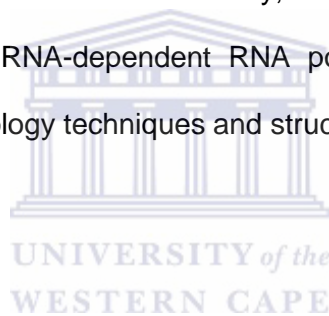
Motif V is involved in RNA binding and unwinding and stimulates ATPase activity (Caruthers, Johnson et al. 2000; Schneider, Campodonico et al. 2004). Situated between Domain I and II, motif V is crucial in conformational change that closes the inter-domain cleft which affects ATP binding, hydrolysis and RNA unwinding (Karow and Klostermeier 2009).

### 1.7.8.9 Motif VI

Situated at the interface between domain I and domain II, motif VI (HRIGRTGR) of the DEAD-box proteins was shown to be critical for RNA binding and ATP hydrolysis (Pause, Methot et al. 1993; Rogers, Komar et al. 2002). It was proposed that the first and second arginines in motif VI bound to the  $\gamma$ -phosphate of ATP and the second arginine was essential to ATP binding and hydrolysis (Caruthers, Johnson et al. 2000).


## 1.8 Aim of this Study

To ensure productive infections, viruses need to manipulate and/or alter the host cell's biological mechanisms. Interaction between virus and host proteins is a critical event through which the virus can exploit host cellular processes. In this study, the interaction between host DEAD-box RNA helicase (**DDX5**) and an RNA-dependent RNA polymerase of HCV (**NS5B**), will be characterized using molecular biology techniques and structural analysis.





# CHAPTER 2<sup>1</sup>



**Expression, Purification and Preliminary  
Crystallographic Analysis of Recombinant  
Human DEAD-Box Polypeptide 5**

---

<sup>1</sup>This chapter is an expanded version of the manuscript published as Choi, Y. W., Dutta, S., Fielding, B. C., and Tan, Y. J. (2010) Expression, purification and preliminary crystallographic analysis of recombinant human DEAD-box polypeptide 5, *Acta Crystallogr Sect F Struct Biol Cryst Commun* 66, 192-194.

## 2.1 Abstract

The DEAD-box RNA helicase, DDX5, is involved in many aspects of RNA processing and has been implicated in a number of cellular processes involving alteration of RNA secondary structure. DDX5 was shown to bind NS5B of Hepatitis C virus (HCV), an RNA-dependent RNA polymerase. We proceeded to characterize this interaction between DDX5 and HCV NS5B by constructing deletion mutants of DDX5 for interaction, expression and crystallisation studies. Using over-expressed protein in mammalian cells, two interaction sites with NS5B have been identified in DDX5 through co-immunoprecipitation, one in the N-terminal region of amino acids 1 to 384 and the other in the C-terminal region of amino acids 387 to 614. Full-length and different fragments of DDX5 were expressed in bacterial cells and purified under different lysis buffer conditions. DDX5 was found to be less soluble when purified in low salt buffer and low induction temperature improved protein yield. In general, fragments encompassing the C-terminal end of DDX5 showed signs of degradation after purification. The N-terminal region of DDX5 which contains the conserved domain 1 of the DEAD-box helicases was cloned and successfully expressed in *Escherichia coli*. In this chapter, the purification and crystallisation conditions are presented.

## 2.2 Introduction

RNA helicases are involved in all aspects of RNA metabolism. They are ATPases with RNA binding and unwinding activities, are involved in transcription, pre-mRNA splicing, ribosome biogenesis, mRNA nuclear export, translation initiation and degradation of mRNA (Cordin, Banroques et al. 2006; Linder 2006). DDX5 (also known as p68) was first discovered due to its cross-reactivity with a monoclonal antibody of the large T antigen of simian virus 40 (Lane and Hoeffler 1980). Subsequent analysis of the DNA sequence of DDX5 revealed an extensive homology with translation initiation factor eIF-4A. The molecular similarity of DDX5 with both the large T antigen and eIF-4A, an ATP-dependent DNA helicase and an ATP-dependent RNA helicase, respectively, implied that DDX5 may function as an RNA or DNA helicase (Ford, Anton et al. 1988). DDX5 belongs to the DEAD-box family of proteins named after their conserved

amino acid sequence Asp-Glu-Ala-Asp (D-E-A-D) (Linder, Lasko et al. 1989). Based on their conserved sequence motifs, they are classified under superfamily 2 (SF2) of the helicases (Gorbalenya and Koonin 1993). The DEAD-box family of helicases is characterized by the unique Q motif as well as 8 other conserved motifs (Tanner, Cordin et al. 2003). The motifs Q, I (Walker A, phosphate-bind P-loop), Ia, Ib, II (Walker B, DExD-box) and III form Domain 1 while motifs IV, V and VI form domain 2 (Tanner, Cordin et al. 2003; Cordin, Banroques et al. 2006).

DDX5 is implicated in a wide range of biological processes, with early studies reporting its possible involvement in the regulation of differentiation/maturation of different animal and human cells (Abdelhaleem 2005). Later, it was shown to bind, unwind and rearrange RNA secondary structures (Rossler, Straka et al. 2001) and it was also found to be crucial in the processing, alternate splicing and degradation of mRNA (Abdelhaleem 2005; Fuller-Pace 2006). DDX5 acts as a transcriptional co-regulator to hormone receptors and transcription factors of differentiation, transcriptional initiation and mRNA decay (Abdelhaleem 2005; Fuller-Pace and Ali 2008). DDX5 is also a transcriptional co-activator of estrogen receptor (Endoh, Maruyama et al. 1999), tumour suppressor p53 (Bates, Nicol et al. 2005),  $\beta$ -catenin (Shin, Rossow et al. 2007), MyoD (Caretto, Schiltz et al. 2006) and androgen receptor (Clark, Coulson et al. 2008).

HCV NS5B protein, an RNA-dependent RNA-polymerase crucial to virus replication, was found to interact with DDX5, implicating it as a cellular factor involved in HCV replication (Goh, Tan et al. 2004). Overexpression of NS5B results in the redistribution of endogenous p68 from the nucleus to the cytoplasm, which may be important for enhancement of viral replication, depletion of endogenous DDX5 and associated reduction in the transcription of negative-strand HCV RNA (Goh, Tan et al. 2004). Using co-immunoprecipitation and immunofluorescence techniques, we also found that HCV core and its helicase NS3 protein also interacted with DDX5 (unpublished data).

The role of DDX5 in viral replication is not well understood, but other DEAD box RNA helicases have been shown to play crucial roles in viral replication. HCV core protein has also been found to interact with DEAD box proteins DBX (Mamiya and Worman 1999), DDX3

(Owsianka and Patel 1999) and DDX1 (Tingting, Caiyun et al. 2006). RNA helicases DDX1 and DDX3 have both been implicated in the replication of human immunodeficiency virus type 1 (HIV-1) through interaction with HIV-1 Rev, they enhance Rev-dependent HIV-1RNA nuclear export (Fang, Kubota et al. 2004; Yedavalli, Neuveut et al. 2004). DDX3 is required for HCV RNA replication since its core protein expression level was lower in DDX3 knockdown cells and JFH1 RNA production was reduced by up to 90% when DDX3 knockdown cells were infected (Ariumi, Kuroki et al. 2007). DDX1 was also reported to enhance viral replication through interaction with non-structural protein 14 of coronavirus (Xu, Khadijah et al. 2010).

The research undertaken by us identified two independent sites of interaction between DDX5 and HCV NS5B and herein we report the cloning, expression, purification and preliminary X-ray diffraction analysis of the N-terminal of DDX5 from amino acids 1 to 305, spanning domain I of the DEAD-box helicase.

## 2.3 Materials and Methods

### 2.3.1 Molecular Cloning

#### 2.3.1.1 DDX5 Constructs for GST Fusion Protein Expression

DDX5 and its deletion mutants were cloned for fusion protein expression in *E. coli* (Table 2.1). The open reading frame encoding human DDX5 was amplified from a spleen cDNA expression library (Goh, Tan et al. 2004). It was cloned into pGEX6p1 (GE Healthcare, USA), an expression plasmid with an amino-terminal glutathione S-transferase (GST) fusion partner. Subsequent deletion mutants were amplified from this plasmid. Sequence identity was confirmed by DNA sequencing (DNA Core Facility, IMCB, Singapore). The constructs were first transformed into DH5 $\alpha$  bacterial cells before plasmid DNAs were extracted and then retransformed into BL21-CodonPlus competent cells (Stratagene) for use in protein expression studies.



**Table 2.1: Constructs generated and used for protein expression.** DDX5 and its deletion mutants were cloned into the pGEX-6p1 vector for fusion protein expression in *E. coli*.

Designation	Vector	Insert
pGEX6p1-DDX5 1-614	pGEX6p1	DDX5 1-614aa
pGEX6p1-DDX5 1-480	pGEX6p1	DDX5 1-480aa
pGEX6p1-DDX5 1-305	pGEX6p1	DDX5 1-305aa
pGEX6p1-DDX5 1-80	pGEX6p1	DDX5 1-80aa
pGEX6p1-DDX5 43-487	pGEX6p1	DDX5 43-487aa
pGEX6p1-DDX5 61-614	pGEX6p1	DDX5 61-614aa
pGEX6p1-DDX5 61-480	pGEX6p1	DDX5 61-480aa
pGEX6p1-DDX5 61-434	pGEX6p1	DDX5 61-434aa
pGEX6p1-DDX5 61-305	pGEX6p1	DDX5 61-305aa
pGEX6p1-DDX5 72-409	pGEX6p1	DDX5 72-409aa
pGEX6p1-DDX5 80-614	pGEX6p1	DDX5 80-614aa
pGEX6p1-DDX5 80-480	pGEX6p1	DDX5 80-480aa
pGEX6p1-DDX5 80-305	pGEX6p1	DDX5 80-305aa
pGEX6p1-DDX5 132-434	pGEX6p1	DDX5 132-434aa
pGEX6p1-DDX5 163-411	pGEX6p1	DDX5 163-411aa
pGEX6p1-DDX5 204-391	pGEX6p1	DDX5 204-391aa
pGEX6p1-DDX5 306-614	pGEX6p1	DDX5 306-614aa
pGEX6p1-DDX5 306-480	pGEX6p1	DDX5 306-480aa
pGEX6p1-DDX5 406-574	pGEX6p1	DDX5 406-574aa
pGEX6p1-DDX5 480-614	pGEX6p1	DDX5 480-614aa
pGEX6p1-NS5B delC21	pGEX6p1	NS5B deleted C-terminal 21aa
pGEX6p1-NS5B 282-570	pGEX6p1	NS5B 282-570aa

### 2.3.1.2 Polymerase Chain Reaction (PCR)

Amplification of specific gene fragments was performed using the respective primers flanking the 3' and 5' ends of constructs (APPENDIX 1) in a T3000 Thermocycler (Biometra, USA). DNA template (1 µl) was used in a 50 µl PCR mix containing 1xPCR buffer (Promega, USA), 1 µl 10

mM dNTP (New England Biolabs, USA), 1  $\mu$ l of 10  $\mu$ M forward and reverse primer and 1.0 U Taq DNA polymerase (Roche Diagnostic, USA). PCR reactions were cycled under the following conditions: initial denaturation at 94°C for 2 minutes (min), followed by 30-35 cycles of (i) 94°C for 30 seconds (s), (ii) annealing for 20-30 s with annealing temperature determined by the primer sets used (APPENDIX 1), (iii) elongation at 72°C for 60 s per 1000 bps and a final elongation step at 72°C for 5 min.

### **2.3.1.3 Agarose Gel Electrophoresis**

5X DNA loading dye (25% glycerol, Invitrogen, USA) and 0.1% bromophenol blue (Sigma-Aldrich, USA) was added to DNA samples before being resolved on a 1.25% agarose gel (UltraPure™ Agarose, Invitrogen, USA) with 200 ng/ml of ethidium bromide (Bio-Rad) added. 0.5X TBE buffer (44.5 mM Tris, 44.5 mM boric acid and 1 mM EDTA) was used in a Hoefer HE 33 mini horizontal submarine unit (Pharmacia Biotech, USA, GE Healthcare) for electrophoresis. Electrophoresis was carried out at 120 volts using power supply EPS 500/400 (Pharmacia Biotech, USA). DNA bands were visualised under UV light using GeneFlash (Syngene Bio Imaging, UK). 0.5  $\mu$ g of either 100 bp or 1 kb DNA ladder (New England Biolabs, USA) was loaded with the sample for size reference.

### **2.3.1.4 DNA Extraction and Gel Purification**

DNA bands corresponding to the expected size was excised from the agarose gel with a sterile surgical blade. DNA was extracted and purified using Qiagen's Gel Extraction Kit (Qiagen, Germany), adhering to the manufacturer's protocol. The purified DNA was stored at -20°C.

### **2.3.1.5 Restriction Enzyme Digest and Ligation**

*Bam*HI and *Xho*I restriction endonucleases (New England Biolabs, USA) were used for cloning. 0.5  $\mu$ l of each restriction endonuclease was added to a mixture containing 15  $\mu$ l of DNA sample, 2  $\mu$ l of 10X BSA and 2  $\mu$ l of 10x *Bam*HI buffer. Digestion was carried out for 3 hours at 37°C in a T3000 Thermocycler. 7.5  $\mu$ l of the digested DNA insert was added to 1  $\mu$ l of the plasmid

vector, 1  $\mu$ l of 10x T4 DNA ligation buffer (New England Biolabs, USA), and 0.5  $\mu$ l of T4 DNA ligase (New England Biolabs, USA). Ligation was carried out overnight at 16°C using T3000 Thermocycler.

### **2.3.1.6 Bacterial Transformation**

Ligated DNA products were transformed into 100  $\mu$ l of chemical competent *E. coli* strain DH5 $\alpha$  for plasmid isolation. Purified and sequence-verified plasmid DNA for protein expression was transformed into chemical competent BL21-CodonPlus RIL (Stratagene, USA). Briefly, DNA was added to the bacterial cells and incubated on ice for 30 min before heat shock treatment in a 42°C water bath for 45 s. The transformed cells were recovered with 500  $\mu$ l LB broth at 37°C for 45 min in a water bath (Grant, UK). The cells were then plated onto LB plates containing 100  $\mu$ g/ml ampicillin and incubated at 37°C overnight for selection of clones.

### **2.3.1.7 Plasmid DNA Isolation and Purification from *Escherichia coli* Cells**

Single colonies were picked and inoculated into LB broth containing 100  $\mu$ g/ml of ampicillin and incubated at 37°C overnight with shaking. QIAprep Spin Miniprep Kit and QIAGEN Plasmid Midi Kit (Qiagen, Germany) were used for the isolation of plasmid DNA, following the manufacturer's protocol. The isolated plasmids were stored at -20°C.

### **2.3.1.8 DNA Sequencing**

ABI PRISM BigDye™ Terminator Cycle Sequencing Ready Reaction Kit (Applied Biosystem, USA) was used for sequencing according to the manufacturer's protocol, with the appropriate primers. The extension products were then sequenced (Sequence Facility, Institute of Molecular and Cell Biology, Singapore). The published DDX5 and DDX1 sequences were obtained from National Center for Biotechnology Information (NCBI) database and analysis of the sequences were done using SeqMan II expert sequence analysis software (DNASTAR, USA).

### 2.3.1.9 Constructs for Expression and Co-Immunoprecipitation Studies in Mammalian Cells

DDX5 and selected deletion mutants constructed for fusion protein expression were sub-cloned into plasmids derived from pXJ40 (Xiao, Davidson et al. 1991) using *Bam*HI and *Xho*I (New England Biolabs, USA) restriction endonuclease.

**Table 2.2: Constructs generated and used in co-immunoprecipitation studies.** DDX5 and its deletion mutants were cloned into the pXJ40myc and NS5B was cloned into pXJ40flag vectors used for protein expression in mammalian cells.

Designation	Vector	Insert
pXJmyc-DDX5	pXJ40myc	DDX5
pXJmyc-DDX5 1-384	pXJ40myc	DDX5 1-384aa
pXJmyc-DDX5 1-507	pXJ40myc	DDX5 1-507aa
pXJmyc-DDX5 206-614	pXJ40myc	DDX5 206-614aa
pXJmyc-DDX5 206-507	pXJ40myc	DDX5 206-507aa
pXJmyc-GST	pXJ40myc	GST
pXJflag-NS5B	pXJ40flag	NS5B

## 2.3.2 Cell Culture and Protein Analysis

### 2.3.2.1 Cell Lines and Maintenance

Huh 7 cells (Human hepatoma, JCRB Cell Bank) were cultured in standard Delbecco's Minimal Eagle's medium supplemented with 10% foetal calf serum (HyClone Laboratories) and antibiotics (penicillin at 10 Units/ml and streptomycin at 100 µg/ml (Sigma)) and were maintained at 37°C in 5% carbon dioxide. Mammalian cells were transfected with Lipofectamine™ 2000 Reagent (Invitrogen) according to the manufacturer's protocol.

### 2.3.2.2 Cell Harvesting

Cells were harvested 24 hours post transfection. A cell scraper was used to dislodge the attached cells into culture medium, the cells were then harvested by centrifugation at 1500 rpm



for 5 minutes at 4°C. The cell pellets were washed twice with phosphate-buffered saline (PBS) before 150 µl of RIPA buffer (50 mM Tris-HCl, 150 mM NaCl, 0.5% NP-40, 0.5% deoxycholic acid, 0.005% SDS and 1 mM phenylmethylsulfonyl fluoride (PMSF)) was added. The lysates were transferred to 1.5 ml microfuge tubes and subjected to three freeze-thaw cycles. The cell lysates were centrifuged at 14000 rpm for 20 minutes at 4°C to remove cell debris. The concentration of the cell supernatant was determined for use in Western Blot analysis and co-immunoprecipitation experiments.

### **2.3.2.3 Quantitation of Mammalian Cell Lysate Protein Concentration**

Protein solution (5 µl) was added to 1 ml of Coomassie Plus Protein Assay Reagent (Pierce, USA) in a plastic cuvette. RIPA buffer was used as a reference. Optical density of the protein solution was measured at 595 nm using an Ultraspec II spectrophotometer (LKB Biochrom, England), and the protein concentration were obtained by comparison with the standard curve.

### **2.3.2.4 Co-Immunoprecipitation**

Using 1.5 ml microcentrifuge tubes, 200 µg of cell lysate was incubated for 1 hr at room temperature with 10 µl of ANTI-FLAG M2 affinity gel (Sigma) pre-washed with RIPA buffer. The protein bound agarose gel was washed 4 times with 1 ml RIPA buffer. The agarose gel was spun at 1500 rpm for 3 min between each wash. 5 X SDS loading buffer (0.3 M Tris-HCl, pH 6.8, 5% SDS, 50% glycerol, 0.1 M DTT and 0.1% bromophenol blue) was added to the washed gel. Bound proteins were eluted from the beads by boiling the samples at 100°C for 5 minutes.

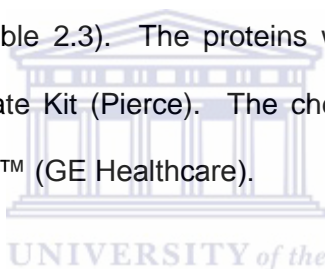
### **2.3.2.5 SDS-PAGE**

Sodium dodecyl sulfate polyacrylamide gel electrophoresis (SDS-PAGE) was used to separate denatured proteins according to their molecular weight. 5 X SDS loading buffer (0.3 M Tris-HCl pH 6.8, 5% SDS, 50% glycerol, 0.1M DTT and 0.1% bromophenol blue) were added to protein samples and boiled for 5 min at 100°C. The protein samples were resolved on 7.5 –15% SDS-

PAGE gels, using Mini-PROTEAN® 3 Cell (Bio-Rad). Electrophoresis was carried out at 20 mA per gel using a PowerPac 3000 (Bio-Rad). Protein ladders used were BenchMark™ Pretasined Ladder (Invitrogen), BenchMark™ Protein Ladder (Invitrogen) or PageRuler™ Unstained Protein Ladder (Fermentas).

### **2.3.2.6 Western Blot Analysis**

The cell lysate samples and immunoprecipitated (IP) protein samples were resolved with SDS-PAGE (see 2.3.2.5), transferred onto Hybond-C nitrocellulose membranes (GE Healthcare) and blocked with 5% non-fat milk in PBS with 0.05% Tween-20. The membranes were then incubated with an appropriate primary antibody to detect the protein, followed by the corresponding secondary antibody conjugated with horseradish peroxidase to detect the membrane bound antibodies (Table 2.3). The proteins were then visualised with the aid of SuperSignal® West Pico Substrate Kit (Pierce). The chemiluminescent protein signals were captured on Amersham Hyperfilm™ (GE Healthcare).



### **2.3.3 GST Fusion Protein Expression and Purification**

GST-DDX5 and its deletion mutants for the protein expression were transformed into the *E. coli* strain BL21-CodonPlus RIL (Stratagene, USA) and tested on a small scale of 50 ml cultures before certain clones were chosen for larger preparations of 4-7 L cultures. SDS-PAGE and Coomassie staining was used to check for the presence of fusion protein during purification.

#### **2.3.3.1 Small-Scale GST Fusion Protein Expression**

Bacteria were cultured in Terrific Broth with ampicillin (Sigma) 100 µg/ml and chloramphenicol (Fluka, USA) 20 µg/ml at 37°C. The cultures were grown to an absorbance of about 1 at 600 nm. The temperature was lowered before 0.2 mM of isopropyl-β-d-thiogalactopyranoside (Invitrogen, USA) was added to the cultures for the induction of recombinant protein production at 30°C for 3 hours (h) or 16°C for 24h. The bacterial cells were harvested by centrifugation at

4000 rpm at 4°C and the cell pellets were stored at -20°C before processing. The pellets were suspended in 10 ml lysis buffer with complete EDTA-free protease inhibitor (Roche Diagnostics, USA), according to manufacturer's instructions. The cells were lysed by sonication. Cell debris were removed by centrifugation for 1 hour at 14 000 rpm at 4°C. The soluble fractions were mixed with 100 µl of Gluthione Sepharose 4B (GSH) beads (GE Healthcare, USA), pre-washed with lysis buffer. The mixtures were allowed to bind for 3 hours at 4°C with constant mixing on a blood tube rotator. The protein bound beads were washed four times with lysis buffer to remove unbound proteins and resuspended in 1 ml lysis buffer (GST fusion protein bound on GSH beads can be used in GST pull-down assay at this stage). Elution buffer (50 mM Tris-HCl, pH 9.2 with 3 mg/ml reduced L-glutathione, Sigma) was added to the washed beads to elute bound fusion protein for 30 minutes at room temperature. The first elution was collected after spinning down the beads and a second elution was carried out overnight at 4°C. To cleave the protein from GST, C3 protease was added to the first elution and left at 4°C overnight. A small sample was taken at each step of the purification for analysis with SDS-PAGE and Coomassie Blue staining.

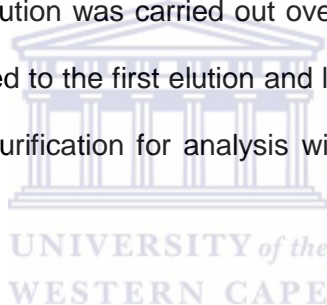


**Table 2.3: Primary and secondary antibodies used in Western blotting.**

<b>Primary Antibody</b>	<b>Type</b>	<b>Source</b>
Rabbit Anti c-Myc (A-14) (Catalogue number sc-789)	Polyclonal	Santa Cruz Biotechnology
Rabbit Anti-Flag (Catalogue number F7425)	Polyclonal	Sigma
<b>Secondary Antibody</b>		
Goat Anti-Rabbit IGG(FC) HRP (Catalogue number 31463)		Pierce

**Table 2.4: Different lysis buffers used.**


---

1.	50 mM Tris-HCl, pH 7.4, 150 mM NaCl, 1 mM MgCl <sub>2</sub> and 1 mM dithiotreitol (DTT)
2.	50 mM Tris-HCl, pH 7.4, 150 mM KCl, 1 mM MgCl <sub>2</sub> and 1 mM DTT
3.	50 mM Tris-HCl, pH 7.4, 400 mM NaCl and 0.2 mM DTT
4.	50 mM Tris-HCl, pH 7.4, 300 mM NaCl and 0.2 mM DTT
5.	50 mM Tris-HCl, pH 7.4, 300 mM NaCl, 10% glycerol, 5 mM MgCl <sub>2</sub> and 0.2 mM DTT
6.	50 mM Tris-HCl, pH 7.4, 300 mM NaCl, 10% glycerol, 5 mM MgCl <sub>2</sub> , 1.5% sarkosyl and 0.2 mM DTT

---

### 2.3.3.2 Large-Scale GST Fusion Protein Expression and Purification for Crystallisation

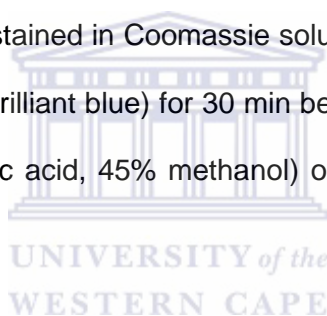
Bacteria were cultured in Terrific Broth with ampicillin (Sigma) 100 µg /ml and chloramphenicol (Fluka, USA) 20 µg /ml at 37°C. The cultures were grown to an absorbance of about 1 at 600 nm. The cultures were chilled for 30 minutes while the temperature was lowered before 0.2 mM of isopropyl-β-d-thiogalactopyranoside (Invitrogen, USA) was added to the cultures for the induction of recombinant protein production. The bacterial cells were harvested by centrifugation at 4000 rpm at 4°C and the cell pellets were stored at -20°C before processing. The pellets were later suspended in 40 ml lysis buffer with complete EDTA-free protease inhibitor (Roche Diagnostics, USA), according to manufacturer's instructions. The cells were lysed by sonication. Cell debris were removed by centrifugation for 1 hour at 14 000 rpm at 4°C. The soluble fractions were mixed with 3 ml of Gluthione Sepharose 4B (GSH) beads (GE Healthcare, USA), pre-washed with lysis buffer. The mixtures were allowed to bind for 3h at 4°C. The protein-bound beads were washed with lysis buffer to remove unbound proteins and resuspended in 40 ml lysis buffer. 3C protease was added to cleave the proteins off the beads, leaving the GST tag on the beads, overnight at 4°C. The cleaved proteins were concentrated with Amicon® Ultra-15 Centrifugal Filter Device (Millipore, USA).

The concentrated proteins were further purified through size exclusion chromatography through a Superdex-200 16/60 gel-filtration column (GE Healthcare) pre-equilibrated in gel-

filtration buffer, using an Äkta basic fast protein liquid chromatography system (GE Healthcare). 65 fractions of 2 ml were eluted. Peak fractions were analysed with SDS-PAGE and visualised through Coomassie staining to assess protein purity. The purified protein fractions were concentrated with Amicon® Ultra-15 Centrifugal Filter Device (Millipore, USA). The protein concentrations were determined by spectrometry using the molar extinction coefficient at 280 nm. The molar extinction coefficients were determined from the protein sequences of the proteins using the ProtParam tool. As a consequence of cleavage, 5 amino acids (GPLGS) remained fused to the N-terminus of the purified proteins. Aliquots of the concentrated protein were flash-frozen in liquid nitrogen and stored at  $-80^{\circ}\text{C}$ .

### **2.3.3.3 Coomassie Blue Staining**

Resolved SDS-PAGE gels were stained in Coomassie solution (10% acetic acid, 45% methanol and 0.25% Bio-Rad Coomassie brilliant blue) for 30 min before destaining with several changes of destaining solution (10% acetic acid, 45% methanol) over 2 hours or overnight to visualise protein bands.



### **2.3.3.4 Direct Spectrophotometric Protein Concentration Determination**

The concentration of purified DDX5 1-305 and DDX5 1-480 were determined by direct spectrophotometric analysis at a wavelength of 280 nm. The molar extinction coefficient ( $78090 \text{ M}^{-1}\cdot\text{cm}^{-1}$ ) and was calculated based on the amino acid sequence using the PROTPARAM tool available on the ExPASyProteomics Server of the Swiss Institute of Bioinformatics (<http://www.expasy.ch/tools/protparam.html>).

### **2.3.4 Protein Crystallisation Screens**

Purified proteins were used to set up crystallisation screens. Screening kits used were Crystal Screen™, Crystal Screen 2™, Crystal Screen Lite™, Grid Screen PEG/LiCl™, MembFac™, Natrix™, PEG/Ion Screen™ and PEG/Ion 2 Screen™ from Hamton Research, USA.

### **2.3.4.1 Sitting Drop**

Crychem™ 24-well plates (Hampton Research, USA) were used for the initial screening of crystallisation conditions. Different crystallisation reagents (0.5 ml) were first pipetted into the reservoir of each well. Protein sample (0.5 µl) was pipetted into the post of the reservoir before 0.5 µl of reagent from the reservoir was added to the drop of protein. The plate was then sealed with Crystal Clear Sealing Tape (Hampton Research, USA).

### **2.3.4.2 Hanging Drop**

EasyXtal Tool (Qiagen, USA) 24-well plates were used for refining crystallisation conditions. Crystallisation reagents (1 ml) were pipetted into each well. Protein (1 µl) was pipetted onto the bottom side of a screw cap before 1 µl of reagent from a well was added to it. The cap was then screwed onto the well with a drop of protein mixture hanging above the reservoir of reagent. The samples were resolved on 10% SDS-PAGE. The resolved gel was soaked in a fixing solution of 45% methanol and 10% acetic acid for 30 minutes and then placed in NAP100 Amplify™ (GE Healthcare) solution for 30 minutes. The gel was then placed on a piece of filter paper, covered with cling wrap and dried for 1 hour at 80°C in a Bio-Rad gel drier. The radiolabelled signals were captured on Amersham Hyperfilm™ (GE Healthcare).

## **2.4 Results and Discussion**

### **2.4.1 Mapping the Domain of Interaction of DDX5 with HCV NS5B**

A panel of DDX5 deletion mutants and NS5B cloned into pXJ40 for previous studies were used. They were co-transfected into Huh-7 cells for protein expression and interaction studies using co-immunoprecipitation and western blot techniques.

### 2.4.1.1 HCV NS5B Interacted with DDX5 and DDX5 Deletion Mutants

The top panel of Figure 2.1 shows flag-tagged HCV NS5B co-immunoprecipitated with myc-tagged DDX5 and DDX5 deletion mutants 1-348, 1-507, 206-614, 387-614 and 206-507 in lanes 1 to 6, but not the negative control (myc-GST) in lane 7. The middle panel indicates the expression of flag-NS5B and the bottom panel the expression of myc-tagged proteins. It was noted that myc-DDX5 206-507 in lane 6 of the bottom panel was larger than its expected size of about 33 kDa. Sequence analysis of the clone revealed that the stop codon was missing and the expressed myc-DDX5 206-507 contained some vector protein. The vector protein is, however, not expected to affect the outcome of the co-immunoprecipitation result with NS5B.

### 2.4.1.2 NS5B Interacted Independently with Two Sites on DDX5

Figure 2.2 is an alignment map of myc-DDX5 and its deletion mutants which shows positive interaction with flag-NS5B. From the map, it can be seen that myc-DDX5 1-384 and myc-DDX5 387-614, which represents two exclusive regions of DDX5, co-immunoprecipitated with flag-NS5B. The results indicate that there are two interaction sites in DDX5 where NS5B could bind.

### 2.4.2 Cloning of DDX5 Plasmids for GST Fusion Protein Expression in *E. coli*

DDX5 and a new panel of deletion mutants spanning DDX5 were cloned for GST pull-down interaction studies with NS5B to locate the binding sites identified in clones DDX5 1-384 and DDX5 387-614 (Figure 2.3). DDX5 was amplified from a spleen cDNA expression library and cloned into pGEX6p1, an expression plasmid with an amino-terminal glutathione S-transferase (GST) fusion partner for protein expression in bacterial cells.

## 2.4.3 Expression and Purification of Fusion Protein in a Bacterial System

### 2.4.3.1 Expression of GST-DDX5 61-434, GST-DDX5 163-411 GST-DDX5 204-319 and GST-DDX5132-434 at 30°C Induction

Expression of deletion mutants GST-DDX561-434, GST-DDX5 163-411, GST-DDX5 204-319, and GST-DDX5132-434 were first tested with cell pellets harvested from 50 ml *E. coli* cultures grown to OD of about 1 at 37°C, after chilling, it was induced at 30°C for 3h. They were lysed by sonication in 10 ml of lysis buffer (50 mM Tris pH 7.4, 150 mM NaCl, 1 mM MgCl<sub>2</sub> and 1 mM DTT). The supernatant of the lysed cells were mixed with 30 µl of GSH Sepharose 4B and left to bind for 3h at 4°C. In Figure 2.4A, lane 3, some GST-DDX5 61-434 fusion protein was detected at 70 kDa and a co-purified protein at 60 kDa was also bound to GSH Sepharose 4B. Very little fusion protein was detected in elution 1, but the co-purified protein was clearly present (Figure 2.4A, lane 5). No cleaved fusion protein was detectable in lane 6, and the co-purified protein was not cleaved by 3C protease (Figure 2.4A). No protein was detected in elution 2. C3 protease and GST proteins (Figure 2.4A, lanes 8 and 9) were loaded as input and size references for C3 cleaved elution 1 because C3 cleaved fusion protein are detected as a smaller protein band and a GST band. More fusion protein of interest may be in the insoluble fraction at between 60 and 70 kDa (Figure 2.4A, lane 1). GST-DDX5 163-411 and GST-DDX5132-434 showed no bound fusion protein (Figure 2.4B, lane 3 and Figure 2.4D, lane 3).

### 2.4.3.2 Expression of GST-DDX5 61-434, and GST-DDX5132- 434 at 16°C Induction

To check if a lower induction temperature increases the production and solubility of the fusion proteins, GST-DDX5 61-434, and GST-DDX5132-434 were cultured again at 37°C and induced at 16°C for 24h before purification with the same lysis buffer (50 mM Tris pH 7.4, 150 mM Na Cl, 1 mM MgCl<sub>2</sub> and 1 mM DTT). In Figure 2.5A, more fusion protein of GST-DDX5 61-434 was detected in lane 3 and elution 1 in lane 4. Three major bands were observed in elution 1 in lane 4, the top band at about 70 kDa should be GST-DDX5 61-434, the band at 60 kDa was the



unknown co-purified protein that was also seen in Figure 2.1A, lane 5, while the third band at about 30 kDa may be a truncated product of GST-DDX5 61-434. In lane 4, the major band at about 70 kDa in lane 5 was cleaved by C3 protease to yield a protein band above 40 kDa just below the C3 protease and a GST band at about 26 kDa. The truncated fusion protein was also cleaved by C3. The co-purified protein remains unchanged at 60 kDa.

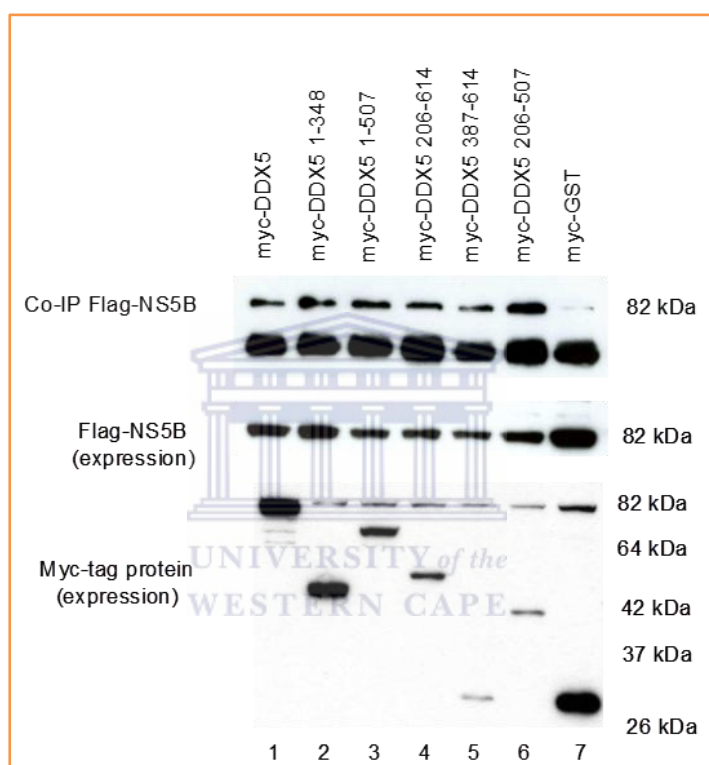


**Figure 2.1: Co-immunoprecipitation of DDX5 deletion mutants with HCV NS5B in co-transfected Huh-7 cells.** Top panel: Flag-NS5B IP with myc-p68 and myc-p68 mutants (lanes 1-6) but not with myc-GST (lane 7) detected with monoclonal anti-flag antibody. Middle panel: Flag-NS5B detected with rabbit anti-flag antibody. Bottom panel: Lane 1, myc-DDX5. Lane 2, myc-DDX5 1-348. Lane 3, myc-DDX5 1-507, lane 4, myc-DDX5 206-614. Lane 5, myc-DDX5387-614. Lane 6, myc-DDX5 206-507. Lane 7, myc-GST. Detected with rabbit anti-myc antibody.

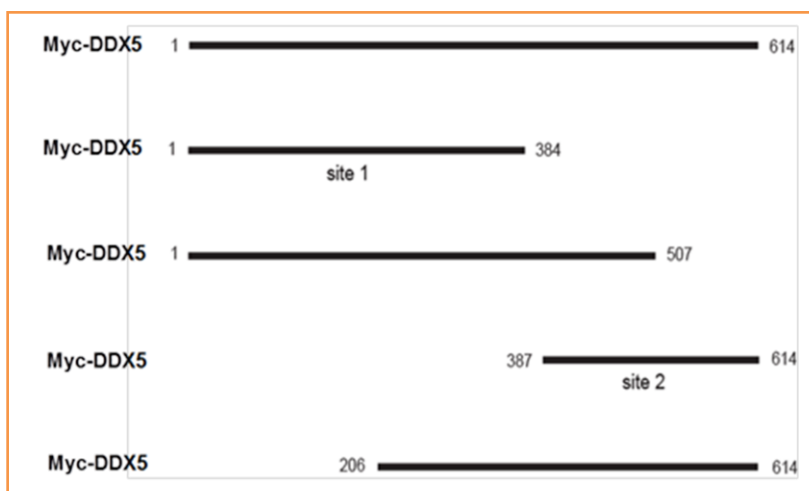


**Figure 2.2: Two exclusive DDX5 interaction sites with HCV NS5B.** Co-immunoprecipitation results identified non over-lapping regions 1-384 and 387-614 in DDX5, indicating that NS5B can interact with either one of the sites.

In Figure 2.5B, a small amount of GST-DDX5 132-434 was detected in the GSH bound fraction and in elution 1 and 2 (lanes 3, 4 and 6). The fusion protein appeared just below a co-purified protein band at 60 kDa (lane 4), and was cleaved by C3 protease in lane 5, but post cleavage product was not detected.

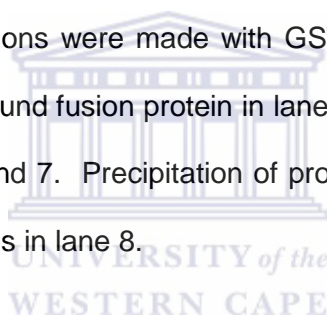
#### 2.4.3.3 Expression of GST-DDX5 43-487 and GST-DDX5 at 30° C Induction

GST-DDX5 43-487 and GST-DDX5 were cultured and induced at 30°C for 3h. A different lysis buffer (50 mM Tris-HCl pH 7.4, 150 mM KCl, 1 mM MgCl<sub>2</sub> and 1 mM DTT) was used. In Figure 2.6A, GSH bound GST-DDX5 43-487 was clearly detected in lane 3 at about 75kDa. It eluted from the GSH beads as a clean band in lane 4 and was cleaved by C3 protease to produce a protein band at about 50 kDa and a GST band at about 26 kDa. More fusion protein of interest may be in the insoluble fraction at about 75 kDa in lane 1. The expression profile of GST-DDX5 in Figure 2.6B was not very distinct, besides three protein bands observed at 60, 80 and 100

kDa, and multiple bands were present between 25-40 kDa in lane 3. The full length DDX5 may not be stable when expressed as a GST fusion protein.

#### **2.4.3.4 Expression of GST-DDX5 43-487 and GST-DDX5 at 16°C Induction**

GST-DDX5 43-487 and GST-DDX5 were cultured again and induced at 16°C for 24h to see if a lower induction temperature had any effect on their expression and solubility profiles. The harvested cells were sonicated in 10 ml lysis buffer (50 mM Tris-HCl pH 7.4, 150 mM KCl, 1 mM MgCl<sub>2</sub> and 1 mM DTT). More GST-DDX5 43-487 was detected in lane 3 of Figure 2.7A, but a few smaller protein bands were also detected. Precipitates were observed after the fusion protein was eluted from the GSH beads. Samples of the precipitates were prepared and loaded in lane 8, where a lot of the fusion protein and proteins which maybe its degradation products were detected. Similar observations were made with GST-DDX5 in Figure 2.7B, more fusion protein were obtained as GSH bound fusion protein in lane 3, and it was also present in the first and second elutions in lanes 5 and 7. Precipitation of protein occurred after elution from GSH and can be seen as multiple bands in lane 8.



#### **2.4.3.5 Expression and Purification of GST-DDX5 Deletion Mutants Induced at 18°C and Lysed in Buffer with High Salt Concentration**

Lysis buffer conditions were modified to see if a high salt buffer would help in the stability of purified GST-DDX5 and GST-DDX5 43-487. They were cultured at 37°C to OD<sub>600</sub> of about 1, chilled and induced at 18°C with 0.2 mM IPTG for 24h. The harvested bacterial cells were lysed in 10 ml of lysis buffer (50 mM Tris-HCl, pH. 7.4, 400 mM NaCl and 2 mM DTT). GST-DDX5 43-487 and GST-DDX5 purified with lysis buffer with 400 mM of NaCl did not precipitate when cleaved from GSH beads. The rest of the deletion mutants were sequentially tested under these conditions. Figure 2.8 shows the expression profile of some of the clones tested. In Figure 2.8A, GST-DDX5 61-305 in lane 3 and GST-DDX5 1-305 in lane 6 showed higher yield than GST-306-614 in lane 9.

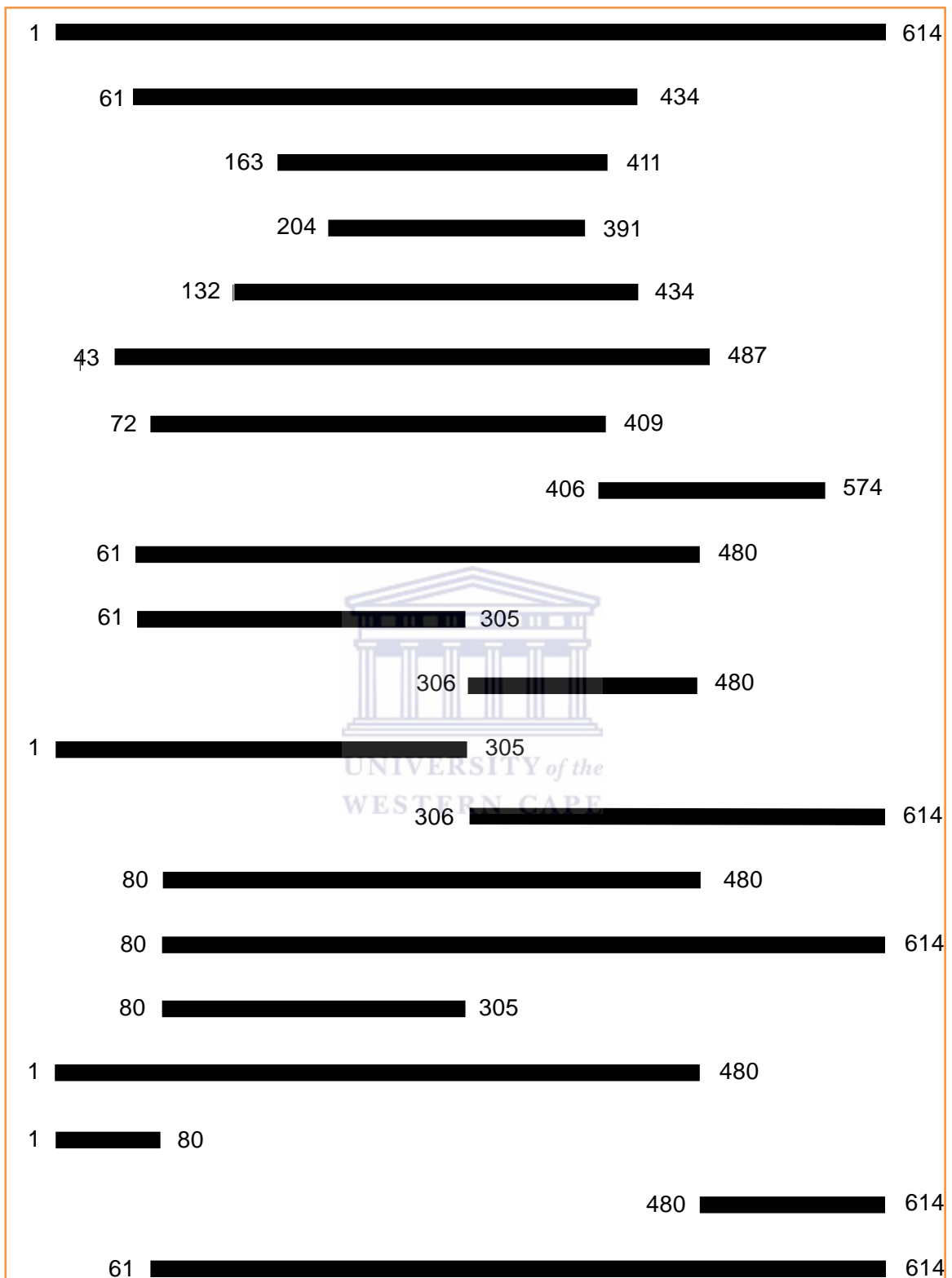


**Figure 2.3: Map of GST-DDX5 and 19 GST-DDX5 deletion mutants cloned and tested for fusion protein expression.**

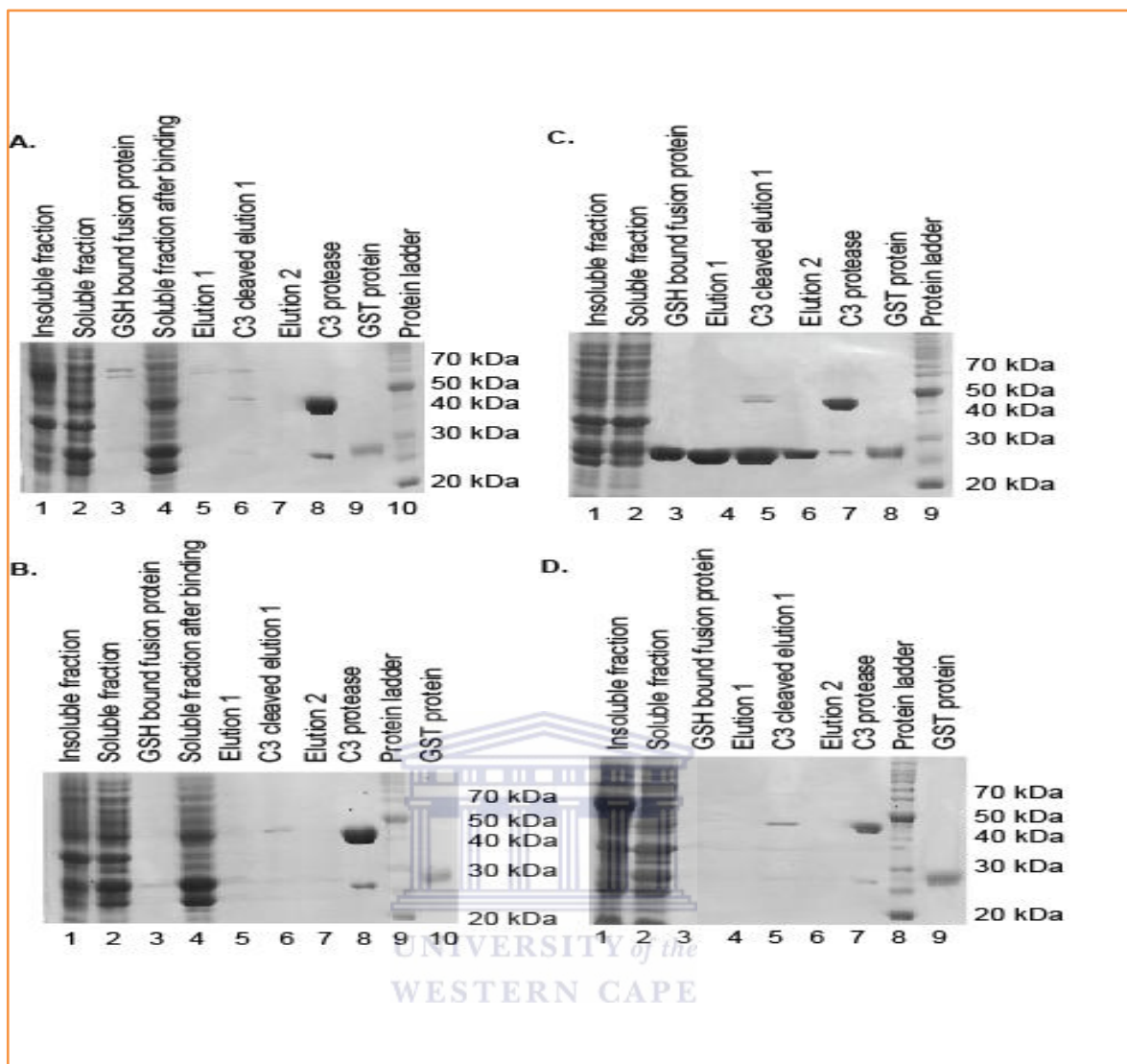
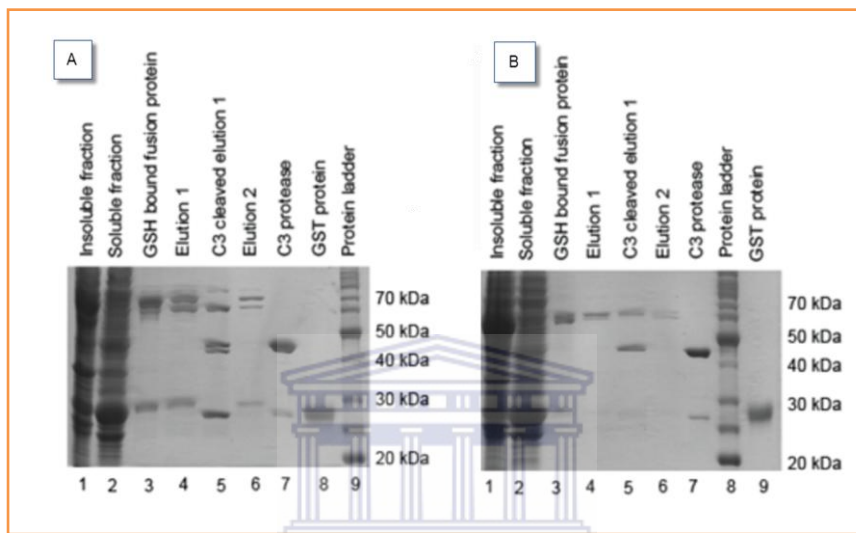


**Figure 2.4: SDS-PAGE analysis of GST-DDX5 61-434, GST-DDX5 163-411, GST-DDX5 204-319 and GST-DDX5 132-434 purification after induction at 30°C.** A. GST-DDX5 61-434. Lane 1, insoluble fraction. Lane 2, soluble fraction. Lane 3, GSH bound fusion protein. Lane 4, soluble fraction after binding with GSH. Lane 5, first elution with elution buffer. Lane 6, 3C cleaved first elution. Lane 7, second elution. Lane 8, 3C protease loaded as reference. Lane 9, GST protein loaded as reference. Lane 10, Protein molecular weight standards. B. GST-DDX5 163-411. Lane 1, insoluble fraction. Lane 2, soluble fraction. Lane 3, GSH bound fusion protein. Lane 4, soluble fraction after binding with GSH. Lane 5, first elution with elution buffer. Lane 6, 3C cleaved first elution. Lane 7, second elution. Lane 8, 3C protease. Lane 9, Protein molecular weight standards. Lane 10, GST protein. C. GST-DDX5 204-319. Lane 1, insoluble fraction. Lane 2, soluble fraction. Lane 3, GSH bound fusion protein. Lane 4, first elution with elution buffer. Lane 5, 3C cleaved first

elution. Lane 6, second elution. Lane 7, 3C protease. Lane 8, GST protein. Lane 9, Protein molecular weight standards. D. GST-DDX5132-434. Lane 1, insoluble fraction. Lane 2, soluble fraction. Lane 3, GSH bound fusion protein. Lane 4, first elution with elution buffer. Lane 5, 3C cleaved first elution. Lane 6, second elution. Lane 7, 3C protease. Lane 8, Protein molecular weight standards. Lane 9, GST protein.



UNIVERSITY of the

**Figure 2.5. SDS-PAGE of GST-DDX5 61-434, and GST-DDX5 132-434 purification after induction at 16°C.** **A.** GST-DDX5 61-434. Lane 1, insoluble fraction. Lane 2, soluble fraction. Lane 3, GSH bound fusion protein. Lane 4, first elution with elution buffer. Lane 5, 3C cleaved first elution. Lane 6, second elution. Lane 7, 3C protease. Lane 8, GST protein. Lane 9, protein molecular weight standards. **B.** GST-DDX5132-434. Lane 1, insoluble fraction. Lane 2, soluble fraction. Lane 3, GSH bound fusion protein. Lane 4, first elution with elution buffer. Lane 5, 3C cleaved first elution. Lane 6, second elution. Lane 7, 3C protease. Lane 8, protein molecular weight standards. Lane 9, GST protein.

In Figure 2.8B, GST-DDX5 80-480 and GST-DDX5 80-614 proteins appeared to be largely insoluble, as strong protein band seen at about 70 kDa in the total lysates in lanes 1 and 3, which contained the soluble and insoluble proteins, were barely visible in the supernatants in lanes 2 and 5, where only soluble proteins were left after centrifugation. GST-DDX5 80-305

was seen as a strong band at about 50 kDa in lane 10. In Figure 2.8C, GST-DDX5 61-408, GST-DDX5306-480 and GST-DDX5 1-480 can be seen in lanes 3, 6 and 9 at about 70, 50 and 80 kDa, respectively. Figure 2.8D shows that GST-DDX5 72-409 either did not express fully or may have degraded because the protein band detected at about 50 kDa in lane 3 was smaller than the expected size of about 63 kDa. GST-DDX5 406-574 was not purified in lane 9, where only multiple protein bands could be seen. C3 protease and GST proteins were seen in lanes 4 and 10 at right above 40 kDa and about 25 kDa. It was observed that some clones expressing the C-terminal of DDX5 produced purified proteins smaller than their expected molecular weight. Examples of such observations are shown in Figure 2.9, in lanes 1 and 2, GST-DDX5 480-614 and GST-DDX5 61-614 showed signs of degradation with multiple bands smaller than their expected sizes of about 40.7 kDa and 86.8 kDa respectively when analysed on SDS-PAGE.

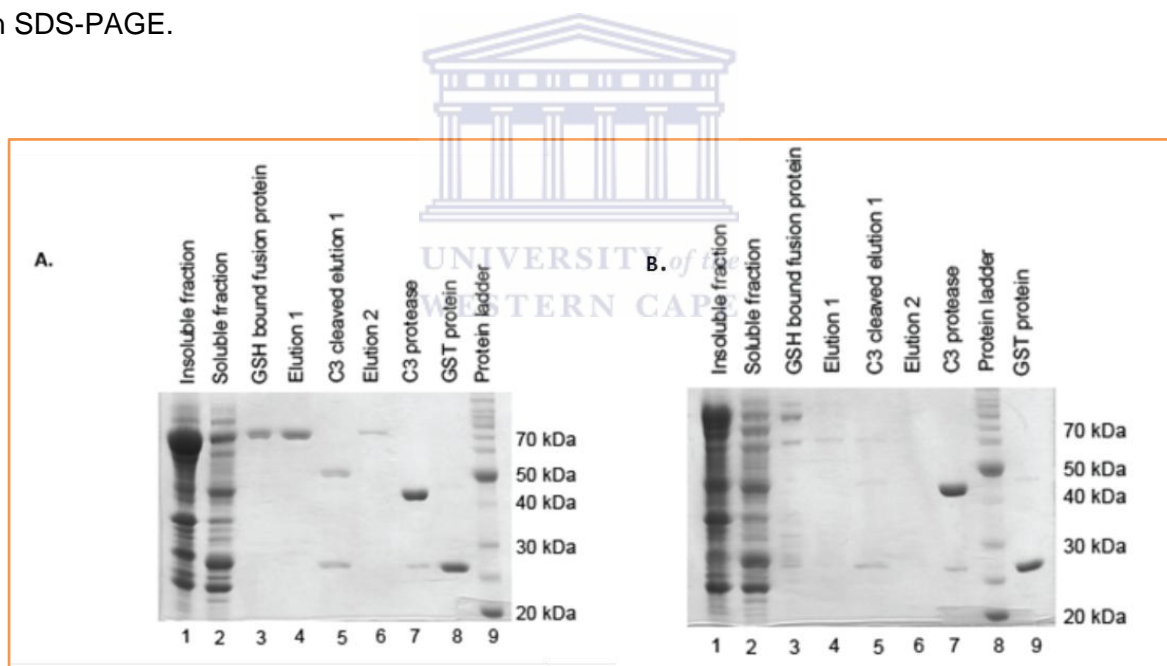


**Figure 2.6: SDS-PAGE of GST-DDX5 43-487, and GST-DDX5 purification after induction at 30° C.** **A.** GST-DDX5 43-487. Lane 1, insoluble fraction. Lane 2, soluble fraction. Lane 3, GSH bound fusion protein. Lane 4, first elution with elution buffer. Lane 5, 3C cleaved first elution. Lane 6, second elution. Lane 7, 3C protease. Lane 8, GST protein. Lane 9, protein molecular weight standards. **B.** GST-DDX5. Lane 1, insoluble fraction. Lane 2, soluble fraction. Lane 3, GSH bound fusion protein. Lane 4, first elution with elution buffer. Lane 5, 3C cleaved first elution. Lane

6, second elution. Lane 7, 3C protease. Lane 8, protein molecular weight standards. Lane 9, GST protein.

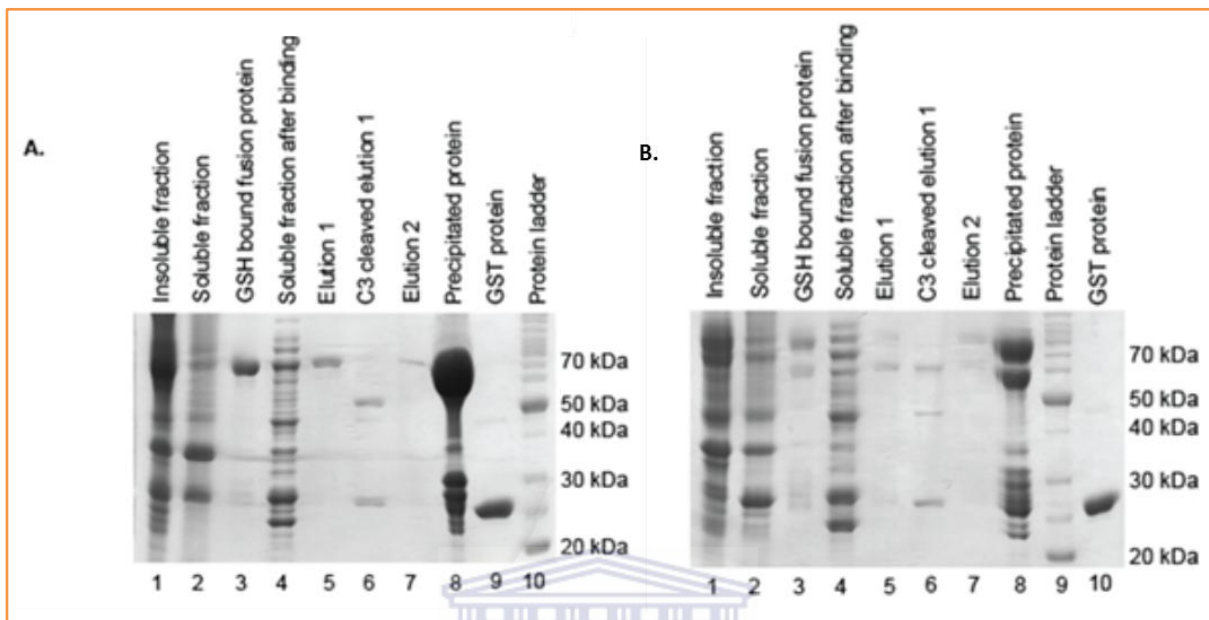


**Figure 2.7: SDS-PAGE of GST-DDX5 43-487, and GST-DDX5 purification after induction at 16° C.** A. GST-DDX5 43-487. Lane 1, insoluble fraction. Lane 2, soluble fraction. Lane 3, GSH bound fusion protein. Lane 4, soluble fraction after binding with GSH. Lane 5, first elution with elution buffer. Lane 6, 3C cleaved first elution. Lane 7, second elution. Lane 8, precipitated protein. Lane 9, GST protein. Lane 10, protein molecular weight standards. B. GST-DDX5. Lane 1, insoluble fraction. Lane 2, soluble fraction. Lane 3, GSH bound fusion protein. Lane 4, soluble fraction after binding with GSH. Lane 5, first elution with elution buffer. Lane 6, 3C cleaved first elution. Lane 7, second elution. Lane 8, precipitated protein. Lane 9, protein molecular weight standards. Lane 10, GST protein.



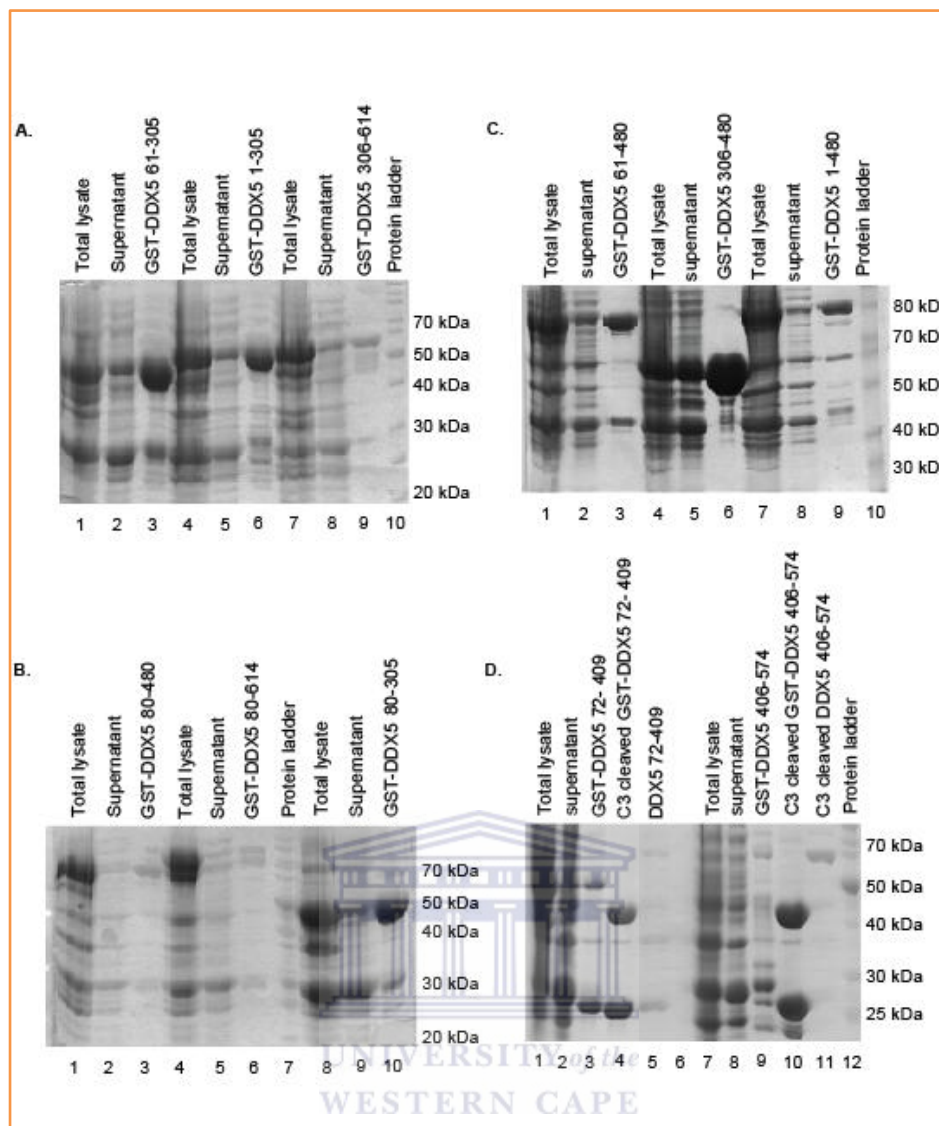


**Figure 2.8: SDS-PAGE of GST-DDX5 deletion mutants purified in high salt buffer.** A. Expression of GST-DDX5 61-305, GST-DDX5 1-305 and GST-DDX5 306-614. Lane 1, Total lysate of GST-DDX5 61-305. Lane 2, Supernatant of GST-DDX5 61-305. Lane 3, GST-DDX5 61-305. Lane 4, Total lysate of GST-DDX5 1-305. Lane 5, Supernatant of GST-DDX5 1-305. Lane 6, GST-DDX5 1-305. Lane 7, Total lysate of GST-DDX5 306-614. Lane 8, Supernatant of GST-DDX5 306-614. Lane 9, GST-DDX5 306-614. Lane 10, protein molecular weight standards. B. Expression of GST-DDX5 80-480, GST-DDX5 80-614 and GST-DDX5 80-305. Lane 1, Total lysate of GST-DDX5 80-480. Lane 2, Supernatant of GST-DDX5 80-480. Lane 3, GST-DDX5 80-480. Lane 4, Total lysate of GST-DDX5 80-614. Lane 5, Supernatant of GST-DDX5 80-614. Lane 6, GST-DDX5 80-614. Lane 7, Total lysate of GST-DDX5 80-305. Lane 8, Supernatant of GST-DDX5 80-305. Lane 9, GST-DDX5 80-305. Lane 10, protein molecular weight standards. C. Expression of GST-DDX5 61-480, GST-DDX5 306-480 and GST-DDX5 1-480. Lane 1, Total

lysate of GST-DDX5 61-480. Lane 2, Supernatant of GST-DDX5 61-480. Lane 3, GST-DDX5 61-480. Lane 4, Total lysate of GST-DDX5 306-480. Lane 5, Supernatant of GST-DDX5 306-480. Lane 6, GST-DDX5 306-480. Lane 7, Total lysate of GST-DDX5 1-480. Lane 8, Supernatant of GST-DDX5 1-480. Lane 9, GST-DDX5 1-480. Lane 10, protein molecular weight standards.

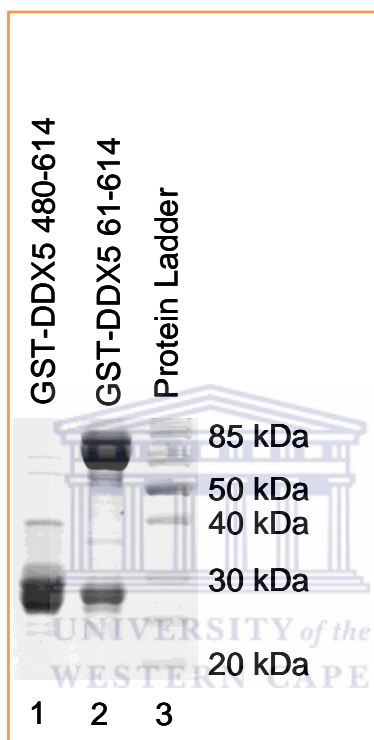


**Figure 2.9: SDS-PAGE of GST-DDX5 480-614, and GST-DDX5 61-614 showing GSH-bound proteins that were smaller than their expected molecular weight.** Lane 1, GSH bound GST-DDX5 480-614. Lane 2, GSH bound GST-DDX5 61-614. Lane 3, protein molecular weight standards.

#### **2.4.3.6 Expression and Purification of HCV GST-NS5BdelC21 and GST-NS5B 282-570**

Different expression and lysis buffer conditions were tested for expression of HCV GST-NS5B with the last 21 amino acid deleted from the C-terminal and GST-NS5B282-570. These were first induced overnight at 16°C and processed in lysis buffer with 50 mM Tris-HCl, pH 7.4, 400 mM NaCl and 2 mM DTT. As multiple bands of degradation products were seen, another lysis

buffer (50 mM Tris-HCl, pH 7.4, 300 mM NaCl, 10% glycerol 5 mM MgCl<sub>2</sub> and 2 mM DTT) was tested, followed by changes in induction temperatures and the length of induction time. Sarkosyl was also added to the lysis buffer to improve solubility of the proteins. Although the use of sarkosyl improved the yield of the proteins, it did not help with the stability of the cleaved products.

## 2.4.4 Large-Scale Protein Purification

Cultures of 4-8 liters of Clones GST-DDX5, GST-DDX5 43-487, GST-DDX5- 1-305, GST-DDX5 1-480 and GST-1-80 were grown for purification of proteins for crystal trials. HCV NS5BdelC21 and NS5B 282-570 were also purified.

### 2.4.4.1 Purification of DDX5

Induction at 16°C for 24h. Lysis buffer (50 mM Tris-HCl, pH 7.4, 400 mM NaCl, 2 mM DTT), gel-filtration buffer (10 mM Tris-HCl, pH 7.4, 400 mM NaCl, 2 mM DTT). Two major bands were observed at 35 and 50 kDa, both were smaller than the expected full length DDX5 at 68 kDa (Figure 2.10).

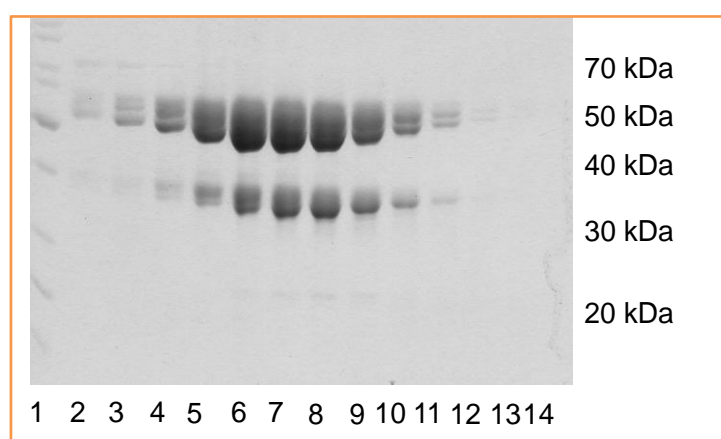


**Figure 2.10: SDS-PAGE of DDX5 purification.** Gel-filtration fractions. Lanes 1-9, gel-filtration fractions 35-44. Lane 10, protein molecular weight standards.

#### 2.4.4.2 Purification of DDX5 43-487

Induction proceeded at 16°C for 24h. Lysis buffer (50 mM Tris-HCl, pH 7.4, 400 mM NaCl, 2 mM DTT), gel-filtration buffer (10 mM Tris-HCl, pH 7.4, 400 mM NaCl, 2 mM DTT). A major protein band was observed at 50 kDa (Figure 2.11).

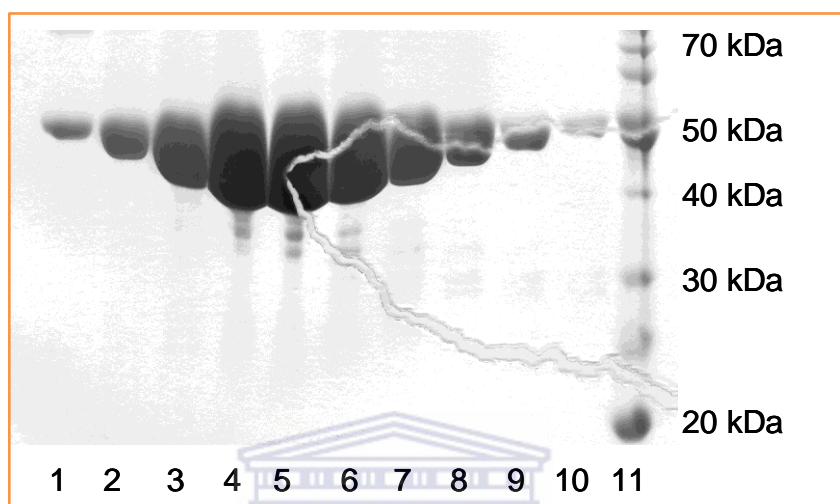


**Figure 2.11: SDS-PAGE of DDX5 43-487 purification.** Lanes 1-10, Gel-filtration fractions 35-44. Lane 11, protein molecular weight standards.

#### 2.4.4.3 Purification of DDX5 1-305

Induction was at 18°C for 24h. Lysis buffer (50 mM Tris-HCl, pH 7.4, 300 mM NaCl, 10% glycerol, 5 mM MgCl<sub>2</sub>, 2 mM DTT), gel-filtration buffer (25 mM Tris-HCl, pH 7.4, 300 mM NaCl, 10% glycerol, 5 mM MgCl<sub>2</sub>, 2 mM DTT). A major band observed at 35 kDa (Figure 2.12).

#### 2.4.4.4 Purification of DDX5 1-480

Induction occurred at 18°C for 24h. Lysis buffer (50 mM Tris-HCl, pH 7.4, 300 mM NaCl, 10% glycerol, 5 mM MgCl<sub>2</sub>, 2 mM DTT), gel-filtration buffer (25 mM Tris-HCl, pH 7.4, 300 mM NaCl, 10% glycerol, 5 mM MgCl<sub>2</sub>, 2 mM DTT). One major band was observed at 50 kDa (Figure 2.13).

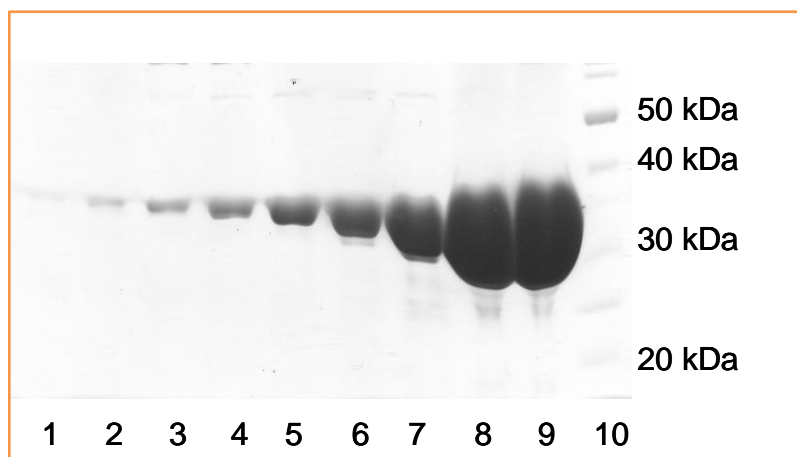


**Figure 2.12: SDS-PAGE of DDX5 1-305 purification. Gel-filtration fractions.** Lanes 1-9, Gel-filtration fractions 31-39. Lane 10, protein molecular weight standards.

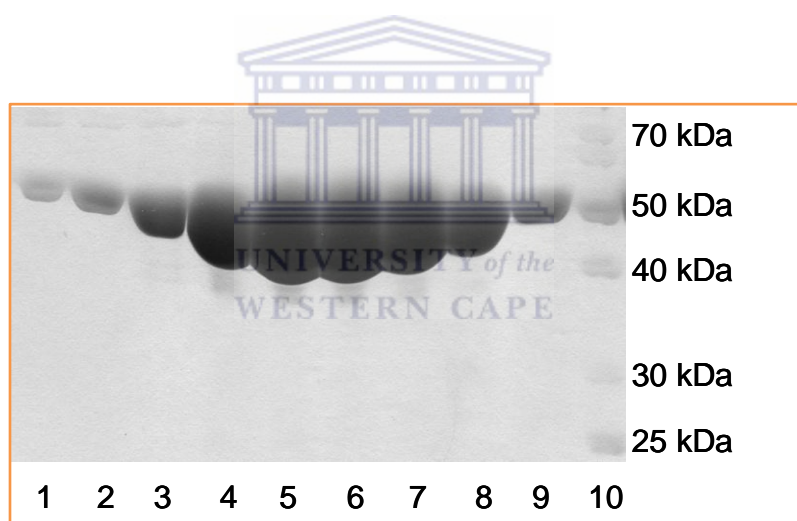


**Figure 2.13: SDS-PAGE of DDX5 1-480 purification. Gel-filtration fractions.** Lanes 1-9, Gel-filtration fractions 35-43. Lane 10, protein molecular weight standards.

#### 2.4.4.5 Purification of DDX5 1-80

Induction was at 18°C for 24h. Lysis buffer (50 mM Tris-HCl, pH 7.4, 300 mM NaCl, 5% glycerol, 5 mM MgCl<sub>2</sub>, 2 mM DTT), gel-filtration buffer (25 mM Tris-HCl, pH 7.4, 300 mM NaCl, 10% glycerol, 5 mM MgCl<sub>2</sub>, 2 mM DTT). A smeared band observed at about 10-12 kDa (Figure 2.14).

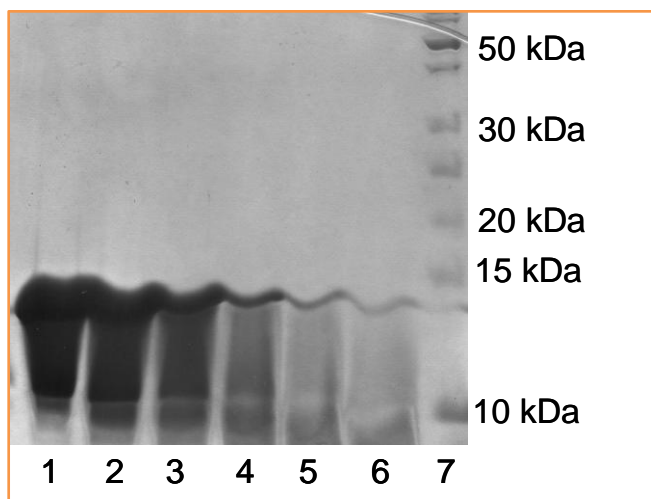


**Figure 2.14. SDS-PAGE of DDX5 1-80 purification.** Gel-filtration fractions. Lanes 1-6, gel-filtration fractions 57-62. Lane 7, protein molecular weight standards.

#### 2.4.4.6 Purification of DDX5 61-305

Induction was at 18°C for 24h. Lysis buffer (50 mM Tris-HCl, pH 7.4, 300 mM NaCl, 5% glycerol, 5 mM MgCl<sub>2</sub>, 2 mM DTT), gel-filtration buffer (25 mM Tris-HCl, pH 7.4, 300 mM NaCl, 10% glycerol, 5 mM MgCl<sub>2</sub>, 2 mM DTT) (Figure 2.15).

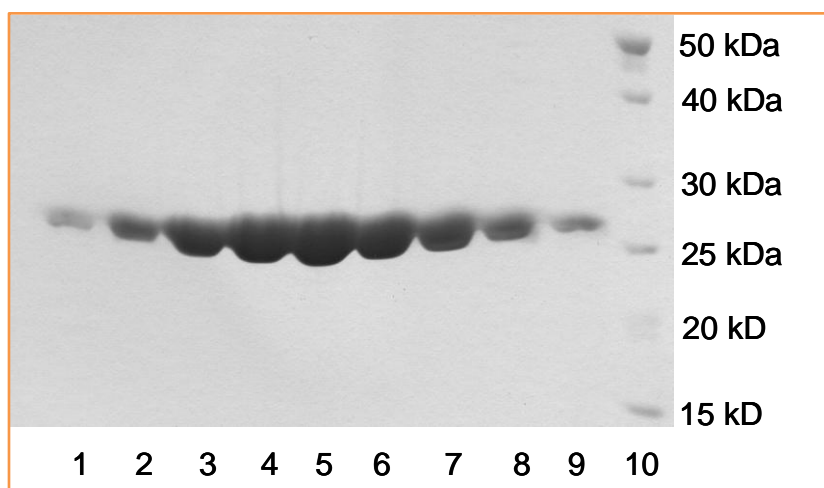


**Figure 2.15: SDS-PAGE of DDX5 61-305 purification.** Gel-filtration fractions. Lanes 1-9, gel-filtration fractions 39-47. Lane 10, protein molecular weight standards.

#### 2.4.4.7 Purification of HCV NS5BdelC21

Induction at 18° C for 24h. Lysis buffer (50 mM Tris-HCl, pH 7.4, 300 mM NaCl, 2 mM DTT), gel-filtration buffer (10 mM Tris-HCl, pH 7.4, 300 mM NaCl, 2 mM DTT). NS5BdelC21 was detected at 60 kDa (Figure 2.16).

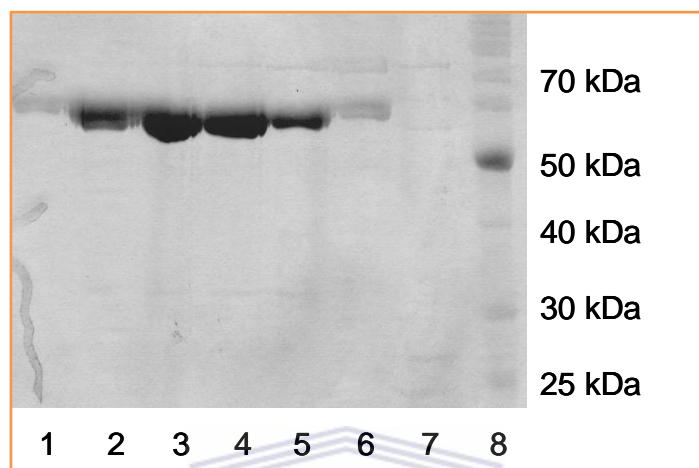


**Figure 2.16: SDS-PAGE of HCV NS5BdelC21 purification.** Gel-filtration fractions. Lanes 1-7, gel-filtration fractions 22-28. Lane 8, protein molecular weight standards.

UNIVERSITY of the  
WESTERN CAPE

#### 2.4.4.8 Purification of HCV NS5B 282-570

Induction at 16°C for 24h. Lysis buffer (50 mM Tris-HCl, pH 7.4, 300 mM NaCl, 10% glycerol, 5 mM MgCl<sub>2</sub>, 2 mM DTT), gel-filtration buffer (25 mM Tris-HCl, p. 7.4, 300 mM NaCl, 10% glycerol, 5 mM MgCl<sub>2</sub>, 2 mM DTT). NS5B 282-570 was detected as multiple bands below 30 kDa (Figure 2.17).

#### 2.4.5 Crystal Screens

Crystal trials of purified DDX5, DDX5 43-487, DDX5 1-305, DDX5 1-480 and DDX5 1-80 were set up at various concentrations with commercial crystal screening kits from Hampton Research in 24-well plates.

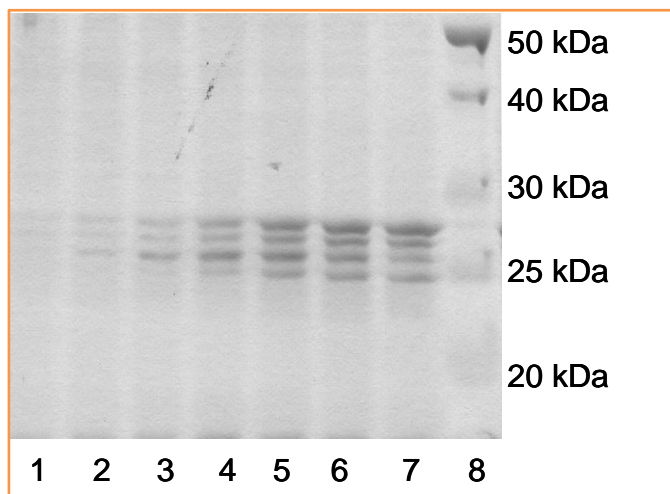


**Figure 2.17: SDS-PAGE of HCV NS5B 282-570 purification. Gel-filtration fractions.** Lanes 1-8, gel-filtration fractions 36-47. Lane 8, protein molecular weight standards.

#### 2.4.5.1 Co-Crystallisation

At a molar ratio of about 1:3, 12.86 mg/ml of NS5BdelC21 were mixed with 34.43 mg/ml of DDX5 43-487 and prepared for a co-crystallisation trial with commercial crystal screening kits from Hampton Research in 24 well plates. No crystal grew in these conditions.

#### 2.4.5.2 Refinement of Crystal Screens

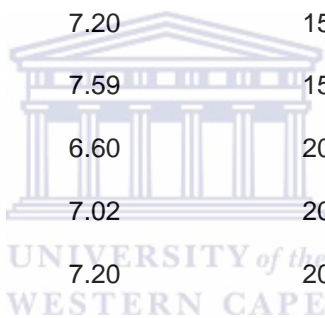
When crystal growth was observed in certain chemical conditions, new trays were set up to screen around the conditions, with a range of adjustments made to the initial growth conditions, in an effort to grow better crystals.

#### 2.4.5.3 Refinement of DDX5 Screens

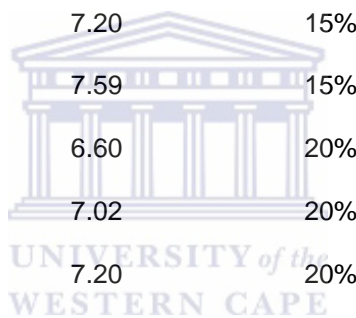
Grid screens with 30% glycerol, 0.05-0.20 M sodium formate, pH 6.60, 7.02, 7.2 7.59 and 5-30% polyethylene glycol (PEG) 3550 were set up with 9.24 mg/ml DDX5.



PEG3350	Sodium formate (M)	pH	#	PEG3350	Sodium formate (M)	pH
5%	0.05	6.60		5%	0.10	6.60
5%	0.05	7.02		5%	0.10	7.02
5%	0.05	7.20		5%	0.10	7.20
5%	0.05	7.59		5%	0.10	7.59
10%	0.05	6.60		10%	0.10	6.60
10%	0.05	7.02		10%	0.10	7.02
10%	0.05	7.20		10%	0.10	7.20
10%	0.05	7.59		10%	0.10	7.59
15%	0.05	6.60		15%	0.10	6.60
15%	0.05	7.02		15%	0.10	7.02
15%	0.05	7.20		15%	0.10	7.20
15%	0.05	7.59		15%	0.10	7.59
20%	0.05	6.60		20%	0.10	6.60
20%	0.05	7.02		20%	0.10	7.02
20%	0.05	7.20		20%	0.10	7.20
20%	0.05	7.59		20%	0.10	7.59
25%	0.05	6.60		25%	0.10	6.60
25%	0.05	7.02		25%	0.10	7.02
25%	0.05	7.20		25%	0.10	7.20
25%	0.05	7.59		25%	0.10	7.59
30%	0.05	6.60		30%	0.10	6.60
30%	0.05	7.02		30%	0.10	7.02
30%	0.05	7.20		30%	0.10	7.20
30%	0.05	7.59		30%	0.10	7.59



PEG3350	Sodium formate	pH	#	PEG3350	Sodium formate	pH
5%	0.15	6.60		5%	0.20	6.60
5%	0.15	7.02		5%	0.20	7.02
5%	0.15	7.20		5%	0.20	7.20
5%	0.15	7.59		5%	0.20	7.59
10%	0.15	6.60		10%	0.20	6.60
10%	0.15	7.02		10%	0.20	7.02
10%	0.15	7.20		10%	0.20	7.20
10%	0.15	7.59		10%	0.20	7.59
15%	0.15	6.60		15%	0.20	6.60
15%	0.15	7.02		15%	0.20	7.02
15%	0.15	7.20		15%	0.20	7.20
15%	0.15	7.59		15%	0.20	7.59
20%	0.15	6.60		20%	0.20	6.60
20%	0.15	7.02		20%	0.20	7.02
20%	0.15	7.20		20%	0.20	7.20
20%	0.15	7.59		20%	0.20	7.59
25%	0.15	6.60		25%	0.20	6.60
25%	0.15	7.02		25%	0.20	7.02
25%	0.15	7.20		25%	0.20	7.20
25%	0.15	7.59		25%	0.20	7.59
30%	0.15	6.60		30%	0.20	6.60
30%	0.15	7.02		30%	0.20	7.02
30%	0.15	7.20		30%	0.20	7.20
30%	0.15	7.59		30%	0.20	7.59



Screening conditions were further narrowed to a screen with 30% glycerol, 0.02-0.08 M sodium formate, pH 7.59 and 1-6% PEG 3550 with 9.24 mg/ml DDX5. Crystals picked from this tray diffracted poorly when tested.

PEG3350	Sodium formate (M)	pH	#	PEG3350	Sodium formate (M)	pH
1%	0.02	7.59		4%	0.02	7.59
1%	0.04	7.59		4%	0.04	7.59
1%	0.06	7.59		4%	0.06	7.59
1%	0.08	7.59		4%	0.08	7.59
2%	0.02	7.59		5%	0.02	7.59
2%	0.04	7.59		5%	0.04	7.59
2%	0.06	7.59		5%	0.06	7.59
2%	0.08	7.59		5%	0.08	7.59
3%	0.02	7.59		6%	0.02	7.59
3%	0.04	7.59		6%	0.04	7.59
3%	0.06	7.59		6%	0.06	7.59
3%	0.08	7.59		6%	0.08	7.59

#### 2.4.5.4 Refinement of DDX5 43-487 Screen

Grid screen with 0.05 M bicine pH 9.0, 0.05-0.30 M LiCl<sub>2</sub> and 5-20% PEG 6000 were set up with 10 mg/ml DDX5 43-487. No crystals were obtained using these conditions.

PEG6000	0.05 M Bicine/LiCl <sub>2</sub> (M), pH 9.0	#	PEG6000	0.05 M Bicine/LiCl <sub>2</sub> (M), pH 9.0
5%	0.05		15%	0.05
5%	0.01		15%	0.01
5%	0.15		15%	0.15
5%	0.20		15%	0.20
5%	0.25		15%	0.25
5%	0.30		15%	0.30

10%	0.05	20%	0.05
10%	0.01	20%	0.01
10%	0.15	20%	0.15
10%	0.20	20%	0.20
10%	0.25	20%	0.25
10%	0.30	20%	0.30

---

#### 2.4.5.5 Refinement of DDX5 1-305 Screen

Grid screens with 20% PEG 3350, 0.1 M Bis-Tris pH 6.5 and 1-6% Tacsimate, pH 4.00-7.00, 20% PEG MW3350 and 2-12% Tacsimate pH 7.00, and 0.2 M NaCl and 5-30% PEG 3350 were set up with 11 mg/ml of DDX5 1-305. Crystals were collected from wells with, 0.1 M Bis Tris pH 6.5, 2% Tacsimate, pH 4.0 and 20% PEG 3350. The crystals were soaked in cryosolution containing 0.1 M Bis Tris pH 6.5, 2% Tacsimate, pH 4.0, 20% PEG 3350 and 25% glycerol and flash-cooled in liquid nitrogen. Dr Sujit Datta collected native data sets using a Quantum CCD image plate on beamline13B1 at the National Synchrotron Radiation Research Center (NSRRC) in Taiwan, and solved the structure of DDX5 1-305 (Figure 2.18).



**Figure 2.18: Crystals of DDX5 1-305**


### 2.4.5.6 Refinement of DDX5 1-480 Screen

Grid screens with 20% PEG MW3350, 0.05-4% Triptone and 0.05-0.20 M HEPES pH 7.30 and two with 1% Triptone, 1-30% PEG MW3350 and 0.05-0.20 M HEPES pH 7.30 were set up with 10 mg/ml DDX5 1-480. No new crystal was obtained with these conditions.

## 2.5 Conclusion

DDX5 and its deletion mutants were cloned and expressed in *E. coli* BL21-CodonPlus RIL. DDX5 was not stable when processed in low salt buffer which led to precipitation of the protein. Even in high salt buffer conditions, efforts to purify a homogeneous full length DDX5 failed. It was noted that the C-terminal of DDX5 was prone to degradation and resulted in truncated proteins. The N-terminal of DDX5 1-305 was successfully purified to homogeneity and crystals first appeared within 2 weeks of incubation. Native data were collected from a single crystal of DDX5 1-305 grown in 0.1 M Bis-Tris pH 6.5, 2% (v/v) Tacsimate, pH 4.0 and 20% (w/v) PEG MW3350. The crystals grew to dimensions of 0.15 x 0.05 x 0.05 mm (Figure 2.18). The structural information gained from this crystal will be used in further studies on the interaction between DDX5 (the host RNA helicase) and HCV NS5B (viral RNA dependent RNA polymerase).

## CHAPTER 3<sup>1</sup>



**Structural and Functional Characterization of  
Human DDX5 and Its Interaction with NS5B of  
Hepatitis C Virus**

---

<sup>1</sup>This chapter is an expanded version of the manuscript submitted for publication as Sujit Dutta, Yook-Wah Choi, Masayo Kotaka, Burtram C. Fielding, Yee-Joo Tan. Structural and functional characterization of human DDX5 and its interaction with NS5B of hepatitis C virus.

### 3.1 Abstract

RNA helicases of the DEAD-box (Asp-Glu-Ala-Asp) family of proteins are involved in many aspects of RNA metabolism from transcription to RNA decay. They are ATPases that have many functions, including nuclear and mitochondrial splicing. They contain two conserved domains responsible for RNA binding and ATP hydrolysis. Human DEAD-box helicase DDX5 has also been implicated in a number of processes including transcription, RNA splicing and RNA decay. Previous studies show that full-length DDX5 can bind to NS5B of Hepatitis C virus (HCV). In this chapter, we report that there are two independent NS5B binding sites in DDX5, one located at the N-terminus and another at the C-terminus. The N-terminal fragment of DDX5, DDX5-1-305, was crystallized and the structure of domain I of DDX5 shows typical features found in the structures of other DEAD-box helicases. In front of domain I is the highly variable N-terminal region (NTR) of unknown function, but greatly disordered with only part of the NTR region (51-78) observable. This region forms an extensive loop and supplements the core with an additional  $\alpha$ -helix. Co-immunoprecipitation experiments revealed that the NTR of DDX5 1-305 auto-inhibits its interaction with NS5B. Interestingly, the  $\alpha$ -helix in NTR is essential for this auto-inhibition and seems to mediate the interaction between the highly flexible 1-60 residues in NTR and NS5B binding site in DDX5 1-305, presumably located within residues 79-305. Furthermore, co-immunoprecipitation experiments showed that DDX5 can also interact with other HCV proteins besides NS5B.

### 3.2 Introduction

Hepatitis C is an infectious disease affecting an estimated 150-200 million people worldwide. Infection is caused by the HCV, which can often lead to cirrhosis, steatosis, and hepatocellular carcinoma. HCV is an enveloped, single stranded positive-sense RNA virus in the family *Flaviviridae* (Rosenberg 2001). The viral genome is encoded by 3 structural proteins (core and envelope proteins, E1 and E2) and 7 non-structural proteins (p7, NS2, NS3, NS4A, NS4B, NS5A and NS5B). NS3, a serine protease and an RNA helicase, along with NS5B, an RNA-

dependent RNA polymerase (RdRP), are key enzymes required for HCV replication and therefore common targets for antiviral agents. Viral replication requires interaction between RNA, viral and host proteins (Rosenberg 2001). NS5B has been shown to interact with a growing number of host proteins, including eukaryotic initiation factor 4AII (Kyono, Miyashiro et al. 2002), cellular vesicle membrane transport protein VAP-33 (Tu, Gao et al. 1999), nucleolar phosphoprotein nucleolin (Ford, Anton et al. 1988) and the DEAD-box (Asp-Glu-Ala-Asp) RNA helicase DDX5 (Goh, Tan et al. 2004).

DDX5, also referred to as p68, is a nuclear prototypic member of the DEAD-box family of proteins. The DEAD-box family belongs to helicase superfamily II (SFII), which includes DEAH-box and Snf2 families (Gorbalenya, Koonin et al. 1989; Linder, Lasko et al. 1989; Cordin, Banroques et al. 2006; Fuller-Pace 2006; Linder 2006). DEAD-box helicases share 9 conserved motifs that are clustered in a central region and possess highly variable amino- and carboxyl-terminals. The central region of DEAD-box helicases can be organized into two domains; domain I consists of motifs Q, I (Walker A), II (Walker B, DEAD box), Ia, Ib, III and domain II consists of motifs IV, V, and VI. Motif Q, unique to DEAD-box helicases, along with motif I and II form the nucleotide binding site. Motif III has been implicated in linking ATP binding and hydrolysis with the helical activity. The remaining motifs are involved in RNA binding. The variable N- and C-terminal regions are involved in interacting with transcription factors and play an important role in transcriptional regulation.

DDX5 was first identified by its immunological cross-reactivity to a monoclonal antibody to the large T antigen of simian virus 40 (Lane and Hoeffler 1980). Co-purification of DDX5 with spliceosome initially suggested a role in RNA splicing and this was subsequently confirmed when DDX5 was shown to be an essential splicing protein acting at the U1 snRNA-5' splice site (Liu 2002). DDX5 has also been shown to be involved in RNA export, ribosome assembly, translation and RNA degradation (Rossler, Straka et al. 2001; Abdelhaleem 2005; Fuller-Pace 2006). However, there is a growing body of evidence suggesting DDX5 may have an additional role as a co-transcriptional co-activator. Current indications suggest that DDX5 is a transcriptional co-activator of estrogen receptor (Endoh, Maruyama et al. 1999), tumour



suppressor p53 (Bates, Nicol et al. 2005),  $\beta$ -catenin (Shin, Rossow et al. 2007), MyoD (Caretta, Schiltz et al. 2006) and recently androgen receptor (Clark, Coulson et al. 2008) .

DDX5 has been shown to interact with HCV NS5B suggesting it may play an important role in viral replication despite the presence of the viral helicase, NS3 (Goh, Tan et al. 2004). Overexpression of NS5B has been shown to result in the redistribution of DDX5 from the nucleus to the cytoplasm presumably to enhance HCV replication. Furthermore, depletion of endogenous DDX5 correlated with a reduction in the transcription of negative-strand HCV RNA (Goh, Tan et al. 2004). In addition, single nucleotide polymorphisms (SNPs) in the DDX5 gene have been shown to be significantly associated with increased risk of advanced fibrosis in HCV patients (Huang, Shiffman et al. 2006).

In order to gain a better understanding into the mechanism of interaction between DDX5 and NS5B, we have determined the crystal structure of domain I of DDX5 (residues 51 to 304). The contribution of residues in DDX5 to the interaction with NS5B was also evaluated by using site-directed mutagenesis and co-immunoprecipitation experiments. In addition, co-immunoprecipitation experiments were used to determine if DDX5 can interact with other HCV proteins.

### **3.3 Experimental Procedures**

#### **3.3.1 Cloning of Plasmids**

##### **3.3.1.1 Mammalian Expression Constructs**

The open reading frame encoding human DDX5 was amplified from a spleen cDNA expression library (Goh, Tan et al. 2004). DDX5 was cloned into pXJ40myc, a myc-tagged plasmid derived from pXJ40 (Xiao, Davidson et al. 1991). DDX5 deletion and substitution mutants were generated by polymerase chain reaction (PCR) (Figure 3.1) and cloned into pXJ40myc for transfection and co-immunoprecipitation study in mammalian cells. HCV proteins core 1-151, core 1-173, NS3, NS4B, NS5A and NS5B were amplified from the cDNA of HCV-S1 of

genotype 1b (Lim, Khu et al. 2001), and cloned into pXJ40flag, a flag-tagged plasmid derived from pXJ40 (Xiao, Davidson et al. 1991).

### **3.3.1.2 Glutathione S-Transferase (GST) Fusion Protein Expression Constructs**

DDX5 and its deletion mutants were cloned for fusion protein expression in *Escherichia coli* (Chapter 2, Figure 2.3). It was cloned into pGEX6p1 (GE Healthcare, USA), an expression plasmid with an amino-terminal glutathione S-transferase (GST) fusion partner. The constructs were first transformed into DH5 $\alpha$  bacterial cells before plasmid DNAs were extracted and then retransformed into BL21-CodonPlus competent cells (Stratagene) for protein expression. The sequence identity of all the plasmids cloned was confirmed by DNA sequencing (DNA Core Facility, IMCB, Singapore).

### **3.3.2 Cell Lines and Maintenance**

COS-7 cells (African green monkey kidney, ATCC) and Huh-7 cells (human hepatoma, JCRB Cell Bank) were cultured in standard Dulbecco's Minimal Eagle's medium supplemented with 10% foetal calf serum (HyClone Laboratories) and antibiotics, penicillin at 10 Units/ml and streptomycin at 100  $\mu$ g/ml (Sigma) and were maintained at 37°C in 5% carbon dioxide.

### **3.3.3 Transfection and Co-Immunoprecipitation**

Plasmids were transiently transfected into COS-7 or Huh-7 cells plated in 6-cm<sup>2</sup> tissue culture dishes using Lipofectamine (Invitrogen), according to manufacturer's instruction. The cells were harvested 24h post-transfection. A cell scraper was used to dislodge the attached cells into the medium; the cells were then harvested by centrifugation at 1500 rpm for 5 min at 4°C. The cell pellets were washed twice with phosphate-buffered saline (PBS) before 150  $\mu$ l of RIPA buffer (50 mM Tris-HCl, 150 mM NaCl, 0.5% NP-40, 0.5% deoxycholic acid, 0.005% SDS and 1 mM phenylmethylsulfonyl fluoride (PMSF)) was added. The lysates were transferred into 1.5 ml microfuge tubes and subjected to three cycles of freezing and thawing. The cell lysates were

spun down at 14000 rpm for 20 min at 4°C to remove cell debris. The concentration of the cell supernatant was determined for use in Western blot analysis and co-immunoprecipitation experiments.

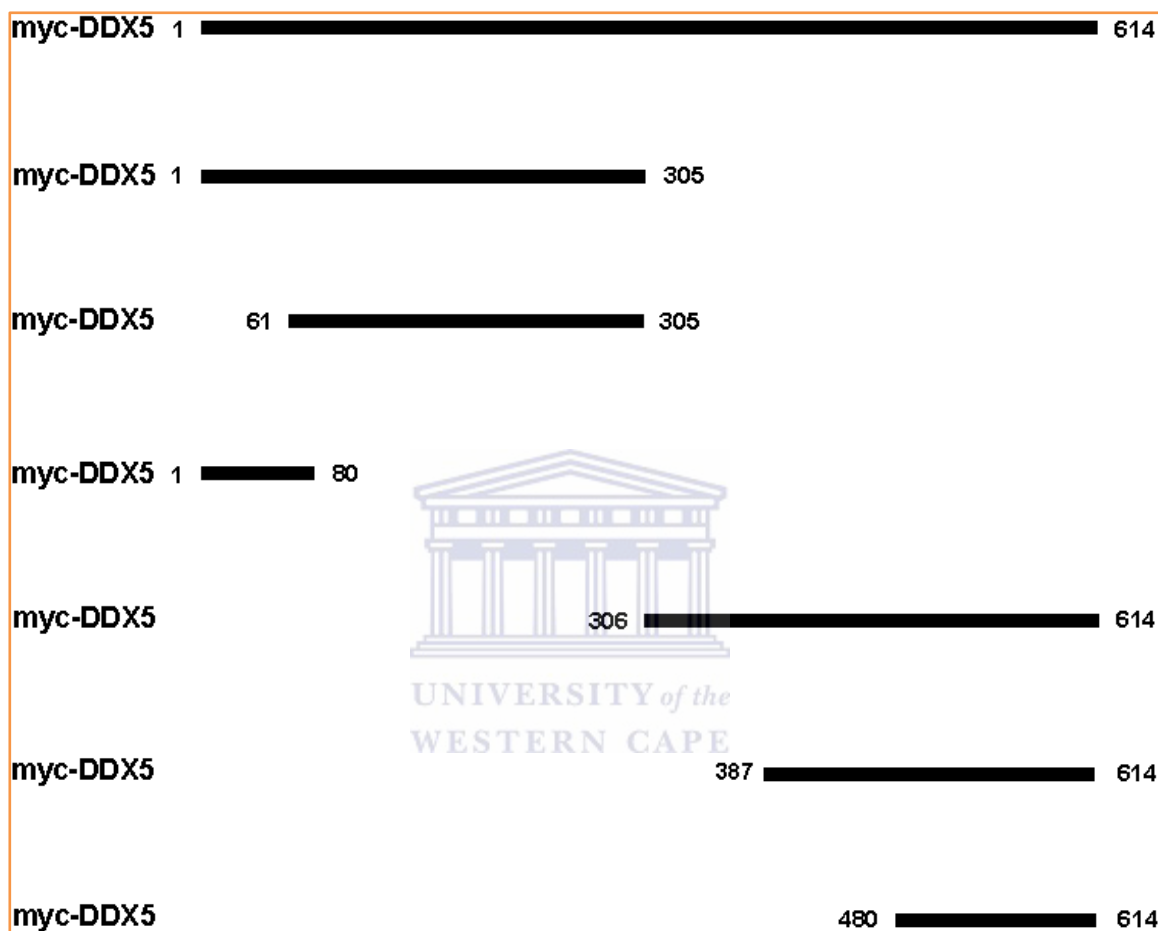


**Figure 3.1: Map of myc-DDX5 and its deletion mutants cloned for co-immunoprecipitation with NS5B.** Myc-tagged DDX5s covering the different domains of DDX5 designed for co-immunoprecipitation studies with Flag-tagged NS5B.

### 3.3.3.1 Co-Immunoprecipitation Using Unconjugated Protein A-Agarose Beads

For co-immunoprecipitation studies using Huh-7 cells and DDX5, endogenous co-immunoprecipitation studies done in COS-7 cells, 200 µg of co-transfected or singly-transfected cell lysates were first incubated with 2 µg of primary antibody for 1h at room temperature before

mixing with 20 µl pre-washed Protein A-Agarose beads (Roche). The mixtures were left to incubate overnight with agitation at 4°C. The protein-bound beads were then washed 4 times with 1 ml RIPA buffer. The agarose beads were sedimented at 1500 rpm between each wash. 5X SDS loading buffer (0.3 M Tris-HCl, pH 6.8, 5% SDS, 50% glycerol, 0.1 M dithiothreitol (DTT) and 0.1% bromophenol blue) was added to the washed beads. The bound proteins were eluted from the beads by boiling the samples at 100°C for 5 min.

### **3.3.3.2 Co-Immunoprecipitation Using Preconjugated ANTI-FLAG® M2 Affinity Gel**

For protein interaction studies using COS-7 cells, 200 µg of co-transfected cell lysates were added to 20 µl pre-washed ANTI-FLAG® M2 affinity gel (Sigma) and incubated at room temperature for 1h with agitation. The protein-bound beads were then washed 4 times with immunoprecipitation (IP) buffer. SDS-PAGE sample loading dye was added to the beads and the bound proteins were eluted from the beads by boiling at 100°C for 5 min.

### **3.3.4 Quantitation of Mammalian Cell Lysate Protein Concentration**

5 µl protein solution was added to 1 ml Coomassie Plus Protein Assay Reagent (Pierce, USA) in a plastic cuvette. RIPA buffer was used as a reference. Optical density of the protein solution was measured at 595 nm using an Ultraspec II spectrophotometer (LKB Biochrom, England), and the cell lysate protein concentration was obtained by comparison with the standard curve.

### **3.3.5 SDS-PAGE**

SDS-PAGE was used to separate denatured proteins according to their molecular weight. 5X SDS-PAGE loading buffer (0.3 M Tris-HCl, pH 6.8, 5% SDS, 50% glycerol, 0.1 M DTT and 0.1% bromophenol blue) were added to protein samples and boiled for 5 min at 100°C. The protein samples were resolved on 7.5 –15% SDS-PAGE gels, using Mini-PROTEAN® 3 Cell (Bio-Rad). Electrophoresis was carried out at 20 mA per gel using a PowerPac 3000 (Bio-Rad). Protein

ladders used were BenchMark™ Prestained Ladder (Invitrogen), BenchMark™ Protein Ladder (Invitrogen) or PageRuler™ Unstained Protein Ladder (Fermentas).

### 3.3.6 Western Blotting

SDS sample loading dye was added to transfected cell lysates and the samples were boiled at 100°C for 5 min. The cell lysate samples and IP protein samples were resolved using SDS-PAGE, transferred onto Hybond-C nitrocellulose membranes (GE Healthcare) and blocked with 5% non-fat milk in PBS with 0.05% Tween-20. The membranes were then incubated with primary antibodies to detect the protein followed by secondary antibodies conjugated with horseradish peroxidase to detect the membrane bound antibodies. The proteins were then visualised with the aid of SuperSignal® West Pico Substrate Kit (Pierce). The chemiluminescent protein signals were captured on Amersham Hyperfilm™ (GE Healthcare).

### 3.3.7 Expression and Purification for Crystallisation

The N-terminal domain of DDX5 (residues 1-305) was expressed as a glutathione-S-transferase (GST) (pGEX6p1, GE Healthcare) fusion protein. GST-DDX5 (1-305) was expressed in *Escherichia coli* BL21-CodonPlus-RIL (Stratagene). The bacterial culture was grown in Terrific Broth (TB) with ampicillin (Sigma) 100 µg/ml and chloramphenicol (Fluka) 20 µg/ml at 37°C. The cultures were grown to an absorbance of 0.8 at OD<sub>600 nm</sub>. The temperature was lowered to 16°C and 0.2 mM of isopropyl-β-d-thiogalactopyranoside (IPTG) was added to the cultures for the induction of recombinant protein production for 24h. The bacterial cells were harvested by centrifugation at 4000 rpm at 4°C and the pellet was stored at -20°C before processing. The pellet was resuspended in lysis buffer (50 mM Tris-HCl pH 7.4, 300 mM NaCl and 0.2 mM DTT) supplemented with complete EDTA-free protease inhibitor (Roche) and lysed by sonication.

Cell debris were removed by centrifugation for 1h at 14 000 rpm at 4°C. The lysate was mixed with 3 ml of Glutathione Sepharose 4B (GSH) beads (GE Healthcare), pre-washed with

lysis buffer. The mixture was allowed to batch bind for 3h at 4°C with constant rotation. The protein-bound beads were washed with lysis buffer to remove unbound material. Removal of the GST tag from the N-terminal segment of DDX5 1-305 was achieved by proteolytic cleavage using recombinant 3C protease (GE Healthcare). Cleaved protein was further purified by size-exclusion chromatography using Superdex S200 column (GE Healthcare) pre-equilibrated with elution buffer (25 mM Tris-HCl, pH 7.4, 300 mM NaCl and 0.2 mM DTT). Peak fractions analysed by SDS-PAGE were concentrated to 11 mg/ml using an Amicon Ultra-15 (Millipore) filtration device.

### 3.3.8 Crystallisation and Data Collection

Crystals of recombinant DDX5 (1-305) (11 mg/ml) were obtained at 15°C using the sitting-drop vapour diffusion method from 1:1  $\mu$ l of protein and precipitant containing 2% (v/v) Tacsimate, pH 4.0, 0.1 M BIS-TRIS pH 6.5, and 20% (w/v) polyethylene glycol (PEG) 3350. Crystals were transferred to a reservoir solution containing the precipitant with the addition of 30% glycerol, before flash-freezing in liquid nitrogen. X-ray diffraction data from a single crystal of DDX5 1-305 was collected at the National Synchrotron Radiation Research Center (NSRRC, Taiwan) on beamline 13B1. Raw data were integrated and scaled using the HKL2000 program suite (Otwinowski and Minor 1997).

### 3.3.9 Structure Determination and Refinement

The structure of DDX5 1-305 was determined by the molecular replacement method, using the structure of domain I of DDX3X (Hogbom, Collins et al. 2007) (Protein Data Bank (PDB) code 2I4I) as the search model, with the programme Molrep from CCP4 suite (1994). The model was refined with CNS (Brunger, Adams et al. 1998), and multiple rounds of manual fitting with the program O (Jones, Zou et al. 1991) using  $2F_o - F_c$  and  $F_o - F_c$  electron density maps.

### 3.3.10 GST Fusion Protein Expression and Purification for Use in GST Pull-Down Assay

GST-DDX5 deletion mutants were transformed into *Escherichia coli* BL21-CodonPlus-RIL (Stratagene). The bacterial cells were cultured in TB with ampicillin (Sigma) 100 µg/ml and chloramphenicol (Fluka) 20 µg/ml at 37°C. The cultures were grown to an absorbance of about 1 at 600 nm. The temperature was lowered to 16°C and 0.2 mM of IPTG was added to the cultures for the induction of recombinant protein production for 24h. The bacterial cells were harvested by centrifugation at 4000 rpm at 4°C and the cell pellets were stored at -20°C before processing. The pellets were later suspended in lysis buffer (50 mM Tris-HCl, pH 7.4, 400 mM NaCl and 0.2 mM DTT) supplemented with complete EDTA-free protease inhibitor (Roche). The cells were lysed by sonication. Cell debris were removed by centrifugation for 1h at 14 000 rpm at 4°C. The lysates were mixed with 100 µl of Gluthione Sepharose 4B (GSH) beads (GE Healthcare), pre-washed with lysis buffer. The mixtures were allowed to bind for 3h at 4°C with constant agitation. Protein-bound beads were washed with lysis buffer to remove unbound proteins and resuspended in 1 ml lysis buffer. GST-tagged H5N1 NS1 protein residues 1-75 and BLR, a chimeric form of the Mcl-1 protein's Bcl-2-like region (Czabotar, Lee et al. 2007), were similarly expressed after subcloning of the appropriate open reading frames into pGex6P-1 vectors (YJ Tan, unpublished results).

### 3.3.11 In Vitro Translation

pXJ40myc-DDX5(1-614), pXJ40myc-DDX5(61-614), pXJ40myc-DDX5(79-614) and pXJ40flag-NS5B plasmids were used as templates to produce the <sup>35</sup>S-labeled proteins using the TNT Reticulocyte Lysate System (Promega), according to the manufacturer's protocol.

### 3.3.12 GST Pull-Down Assay

30 µg of GST and GST fusion proteins bound on GSH beads were washed three times with IP buffer. 20 µl of <sup>35</sup>S-labeled proteins, diluted with 80 µl IP buffer (PBS with 0.5% Triton X-100, 0.5% NP40, 1 mM EDTA, 1 mM EGTA and 0.4 mM PMSF), was added to the beads and the mixtures were incubated at room temperature for 1h. The beads were then washed 4 times with IP buffer. SDS-PAGE sample loading dye was added to the beads and the bound proteins were eluted from the beads by boiling at 100°C for 5 min. The samples were resolved on a 10% SDS-polyacrylamide gel. The resolved gel was soaked in a solution of 45% methanol and 10% acetic acid for 30 min and then placed in Amplify™ solution for 30 min. The gel was placed on a piece of filter paper, covered with cling wrap and dried for 1h at 80°C in a gel drier. The radiolabelled signals were captured on Amersham Hyperfilm™ (GE Healthcare).

### 3.3.13 Antibodies

The primary and secondary antibodies used in the studies are listed in Table 3.1.

**Table 3.1: List of primary and secondary antibodies used.**

Primary Antibody	Type	Source
Rabbit anti-DDX1 (Catalogue number: BL 2421)	Polyclonal	Bethyl Laboratories, Inc.
Rabbit anti-DDX5 (Catalogue number: BL 2462)	Polyclonal	Bethyl Laboratories, Inc.
Rabbit anti-Myc	Polyclonal	Santa Cruz Biotechnology
Mouse anti-Myc	Monoclonal	Santa Cruz Biotechnology
Rabbit HA-Probe	Polyclonal	Santa Cruz Biotechnology
Mouse anti-β-Actin	Monoclonal	Sigma
Rabbit anti-Flag	Polyclonal	Sigma
Mouse anti-Flag	Monoclonal	Sigma
<b>Secondary Antibody</b>		
Goat anti-mouse HRP		Pierce
Goat anti-rabbit HRP		Pierce



## 3.4 Results and Discussion

### 3.4.1 DDX5 Contains Two Sites That Can Interact with NS5B Independently

To characterise the interaction between DDX5 and HCV NS5B and determine which domain or domains of DDX5 interact with NS5B, a panel of DDX5 deletion mutants were cloned into the pXJ40myc vector for co-immunoprecipitation studies with NS5B (Figure 3.1). Flag-tagged NS5B was expressed in Huh-7, a liver cell line that supports HCV replication, together with myc-tagged DDX5 proteins (Figure 3.2). The results showed that there are two non-overlapping binding sites in DDX5 which bound to NS5B independently. One binding site is located in the N-terminal half of DDX5 between amino acids 1 to 305 and the other in the C-terminal half of DDX5 between amino acids 306 to 614. In general, the C-terminal containing clones; myc-DDX5, myc-DDX5 1-305 and myc-DDX5 61-305 showed stronger binding with NS5B when compared to the deletion mutants that do not contain the N-terminal half of DDX5. It was observed that the deletion of the first 60 amino acids increased myc-DDX5 61-305's binding affinity to NS5B (Figure 3.2). Amongst the C-terminal clones of DDX5, myc-DDX5 306-614 bound NS5B more strongly than myc-DDX5 387-614 and myc-DDX5 480-614 (Figure 3.3). It is possible that the residues before amino acid 387 in DDX5 is involved in its binding with NS5B and their deletion weakened the interaction. Deletions of amino acids 387-479 seemed to disrupt the interaction further.

### 3.4.2 Amino Acids 61-80 in DDX5 Were Sufficient for Interaction with NS5B

Myc-DDX5 1-80 was excluded from the previous co-immunoprecipitation study with flag-NS5B because it did not express well in Huh-7 cells (data not shown). A highly transfectable cell line, 293T, was also used, but the expression level of myc-DDX5 1-80 still did not compare well with the other myc-DDX5s (data not shown). Thus, an alternative method, GST-pull down assay, was chosen to determine if the first 80 amino acids of DDX5 could interact with NS5B. Figure 3.4 shows the GST-tagged DDX5s were cloned for GST-pull down assay with in-vitro transcribed <sup>35</sup>S labeled NS5B.

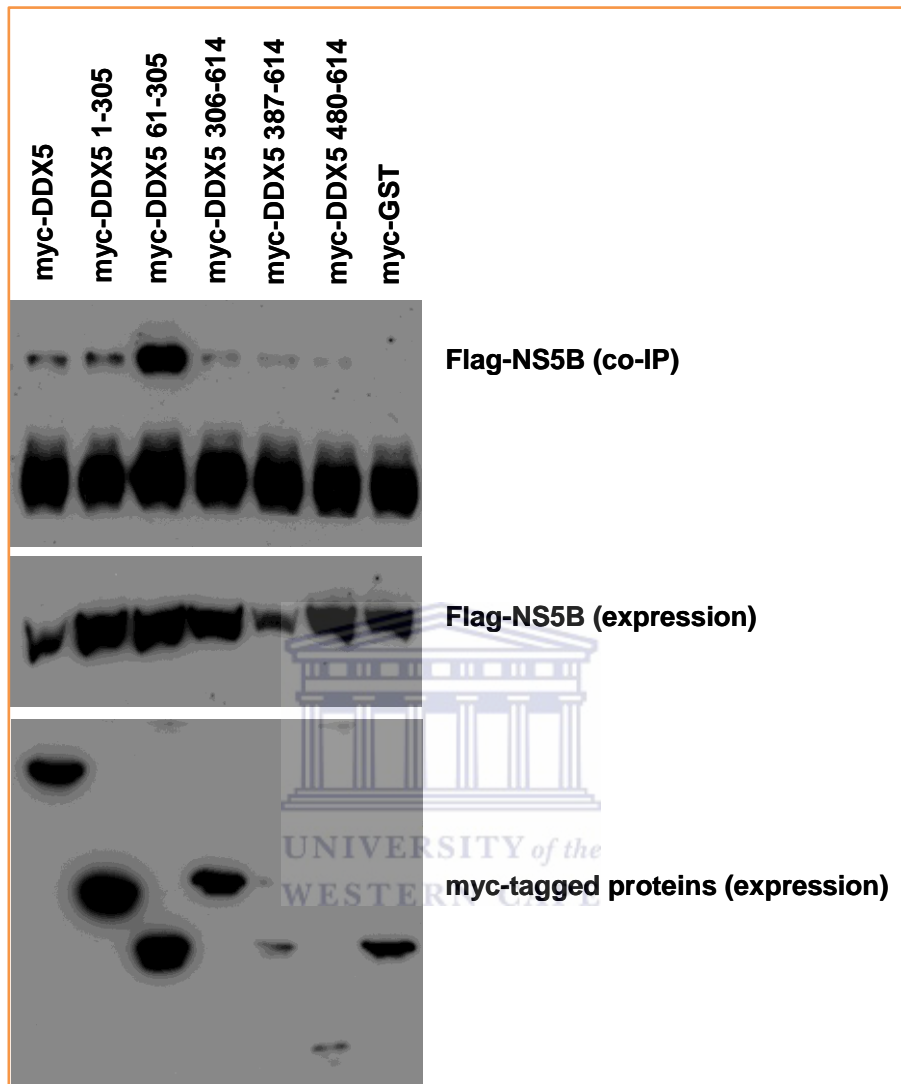


**Figure 3.2: Co-immunoprecipitation of myc-tagged DDX5s and flag- tagged-NS5B.** 200  $\mu$ g of clarified cell lysates were pre-incubated with polyclonal anti-myc antibodies before it was added to protein A-agarose beads. Co-immunoprecipitation of Flag-NS5B was detected by monoclonal anti-flag antibodies. 20  $\mu$ g of cell lysates were used to detect expressed proteins. **Top panel:** Co-immunoprecipitation of NS5B with DDX5, DDX51-305, DDX5 61-305 and DDX5 306-614, DDX5 387-614 and 480-614, but not the GST control. **Middle panel:** Expression of Flag-NS5B detected by polyclonal anti-flag antibodies. **Bottom panel:** Expression of the different myc-tagged proteins detected by polyclonal anti-myc antibodies.

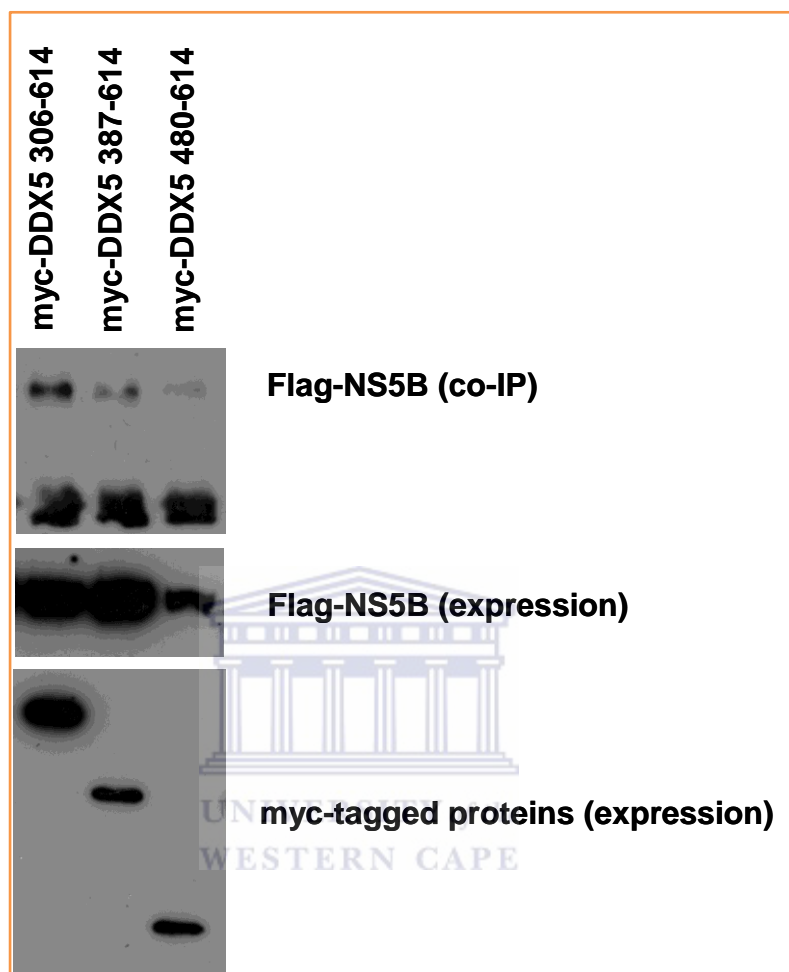


**Figure 3.3: Co-immunoprecipitation of flag-NS5B with myc-tagged C-terminal DDX5s.** 200  $\mu$ g of clarified cell lysates were pre-incubated with polyclonal anti-myc antibodies before it was added to protein A-agarose beads. Co-immunoprecipitation of Flag-NS5B was detected by monoclonal anti-flag antibodies. 20  $\mu$ g of cell lysates were used to detect expressed proteins. **Top panel:** Co-immunoprecipitation of NS5B with DDX5 306-614, DDX5 387-614 and 480-614. **Middle panel:** Expression of Flag-NS5B detected by polyclonal anti-flag antibodies. **Bottom panel:** Expression of the different C-terminal myc-tagged DDX5 proteins detected by polyclonal anti-myc antibodies.

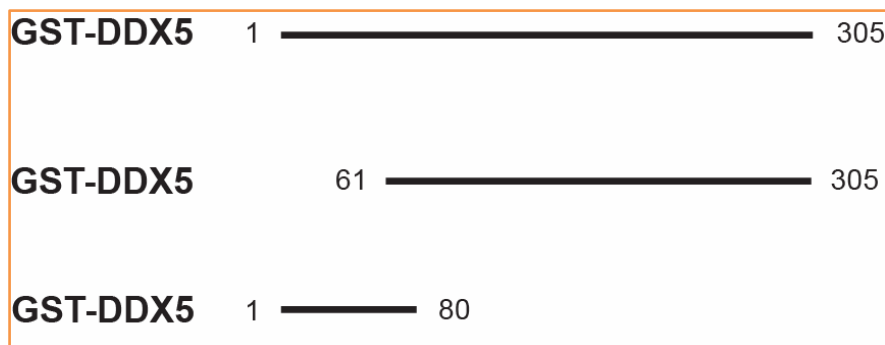


**Figure 3.4: DDX5 GST fusion proteins selected for GST pull-down assay.**

GST-tagged DDX5 1-305, 61-305 and 1-80 were successfully expressed and purified (Figure 3.5A). The results from the GST-pull-down assay showed that GST-tagged DDX5 1-305, 61-305 and 1-80 were all able to pull-down in-vitro transcribed NS5B with GST-DDX5 1-305 showing the strongest interaction with NS5B (Figure 3.5B). In contrast, no binding was observed when GST alone was used for the pull-down. The results indicated that residues 61-80 are sufficient for the interaction between NS5B and DDX5.

However, it was also observed that the GST pull-down results were inconsistent with the previous co-immunoprecipitation results where myc-DDX5 61-305 bound NS5B more strongly than myc-DDX5 1-305 (Figure 3.2). There are two possible reasons why the results from the two sets of experiments are different. One reason may be that NS5B used for GST-pull-down was expressed using rabbit reticulocyte and may lack certain co-factors that are available in the mammalian cell expression system used for co-immunoprecipitation. Another reason could be that the large GST tag of the bacterial expressed GST-DDX5 1-305 and GST-DDX5 61-305 may have affected their interaction with NS5B. This will be further explained in the latter part of this chapter.

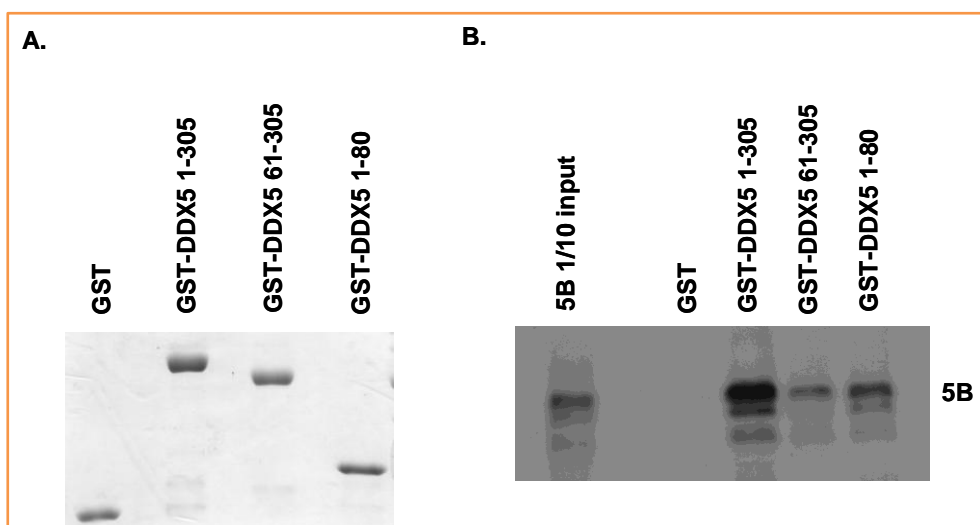


**Figure 3.5: GST pull-down of NS5B by DDX5 N-terminal fusion proteins NS5B pulled down with DDX5 fusion proteins 1-305, 61-305 and 1-80.** The assay was carried out by mixing 30  $\mu\text{g}$  of Glutathione-Sepharose bound fusion protein expressed in *E. coli* with in vitro translated  $^{35}\text{S}$ -labeled NS5B. Binding results were analysed by SDS-PAGE and autoradiography. **A.** 30  $\mu\text{g}$  of GST fusion proteins used in the pull-down assay was analyzed by SDS-PAGE followed by Coomassie blue staining to ascertain the purity of the proteins. **B.** In vitro transcribed NS5B was pulled down by N-terminal DDX5 fusion proteins DDX5 1-305, DDX5 61-305 and DDX5 1-80, but not the GST control.

### 3.4.3 Domain I of DDX5 is Similar to That of Other DEAD-Box RNA Helicases

To gain further insight into the interaction between DDX5 and NS5B, DDX5 1-305 and DDX5 306-614 were expressed as N-terminal GST fusion proteins. GST was removed with the 3C protease and as a consequence 5 amino acids (GPLGS) remained fused to the N-terminal domain. Purification of DDX5 306-614 failed as the protein underwent degradation when expressed in *E. coli* (data shown in Chapter 2). Purification of DDX5 1-305 was successful and crystallization trials were performed (data shown in Chapter 2). As shown in the GST-pull-down assay (Figure 3.5), DDX5 1-305 interacts directly with NS5B and thus represents as a suitable target for our structural studies.

DDX5 1-305 was found to crystallize in space group  $I222$  and the structure was solved by molecular replacement using the structure of domain I of DDX3X (PDB code: 2I4I) and refined to the crystallographic R-factor of 0.23 ( $R_{\text{free}}$  0.29). One molecule was identified in the asymmetric unit. Due to lack of density, residues 1-50 were not observed. DDX5 1-305 contains 8 centrally located  $\beta$ -sheets packed against 9  $\alpha$ -helices (Figure 3.6). A structure-homology search on the Dali server ([www.ebi.ac.uk/dali](http://www.ebi.ac.uk/dali)) revealed a high degree of similarity of domain I of DDX5 (residues 79-303) with the equivalent domain in human DDX3X (Hogbom, Collins et al. 2007), *Drosophila* VASA (Sengoku, Nureki et al. 2006) and eukaryotic initiation factor 4A-I (eIF4a) (Caruthers, Johnson et al. 2000; Sengoku, Nureki et al. 2006) with an rmsd of 1.4 Å, 1.7 Å and 1.9 Å, respectively.

Domain I of DDX5 contains many typical features found in the structures of other DEAD-box helicases which include the conserved motifs, Q, I (Walker A), II (Walker B, DEAD-box), Ia, Ib, and II (Figure 3.6). A sequence alignment of DDX5 with DDX3X and DDX19B also revealed high sequence identity in the conserved motifs of domain I, with the exception for the Q motif (Figure 3.7). For the Q motif, the length varies between the 3 proteins and there are only a few identical residues. The Q motif usually consists of 9 amino acids that include an essentially invariant glutamine (Tanner, Cordin et al. 2003). For DDX5, DDX3X and DDX19B, the invariant glutamine is indeed conserved (Figure 3.7). As the crystal structures of DDX3X and DDX19B have been solved, ribbon representations of these were generated using pymol. For easy comparison, only domain I is used. The three-dimensional structures showed that domain I of DDX5, DDX3X and DDX19B are structurally similar and have a core of 8  $\beta$ -strands that is surrounded by  $\alpha$ -helices (Figure 3.8).

#### **3.4.4 The ATP Binding Property of DDX5 61-305 Is Not Essential for the Interaction with NS5B**

No nucleotide is observed in the ADP/ATP binding site of the crystal structure of DDX5 61-305 indicating that the apo form of DDX5 61-305 is capable of binding NS5B in vitro (as demonstrated by GST-pull down assay in Figure 3.5). In order to determine if this is true for the

interaction between DDX5 1-305 and NS5B in Huh-7 cells, co-immunoprecipitation experiments were performed to determine the interaction of two DDX5 substitution mutants (K144N and D248N) with NS5B. A previous study has shown that the K144N substitution abolished ATP-binding while substitution within the DEAD-box did not have any effect on ATP-binding (Jalal, Uhlmann-Schiffler et al. 2007). Consistent with the results from the GST-pull-down assay, the DDX5 61-305K144N substitution mutant bound NS5B to a similar extent as DDX5 61-305 suggesting that ATP binding is not essential for the interaction (Figure 3.9). DDX5 61-305D248N substitution mutant also showed similar binding to NS5B, suggesting that the DEAD-box (ATPase activity) is also not essential for the interaction.

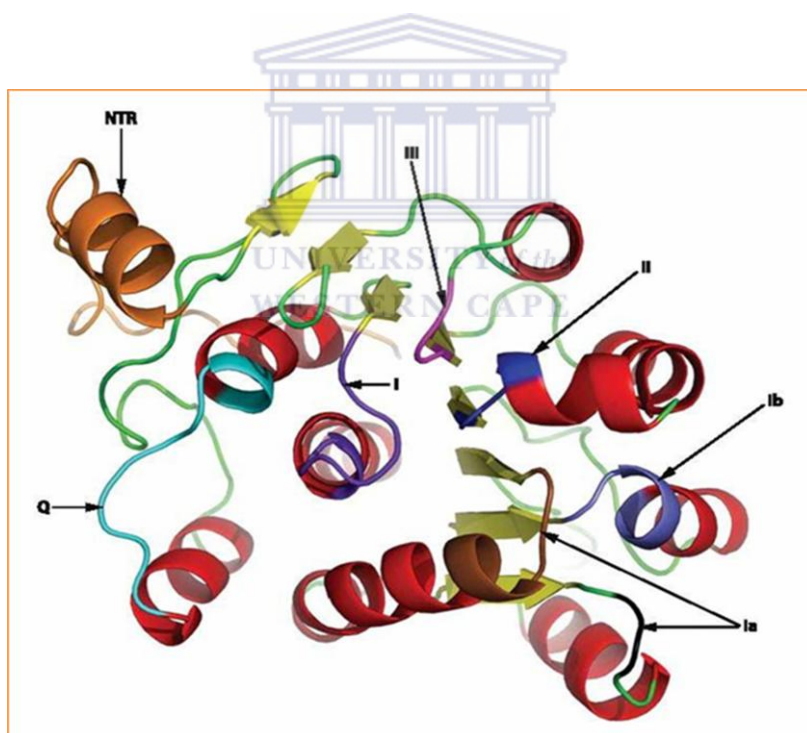


**Figure 3.6: Structure of DDX5 1-305.** The structure of DDX5-N showing a helix from the 5'-non translated region (NTR) and conserved motifs Q, I, Ia,Ib,II and III of domain 1. The structure of DDX5 1-305 was solved by Dr Sujit Dutta.

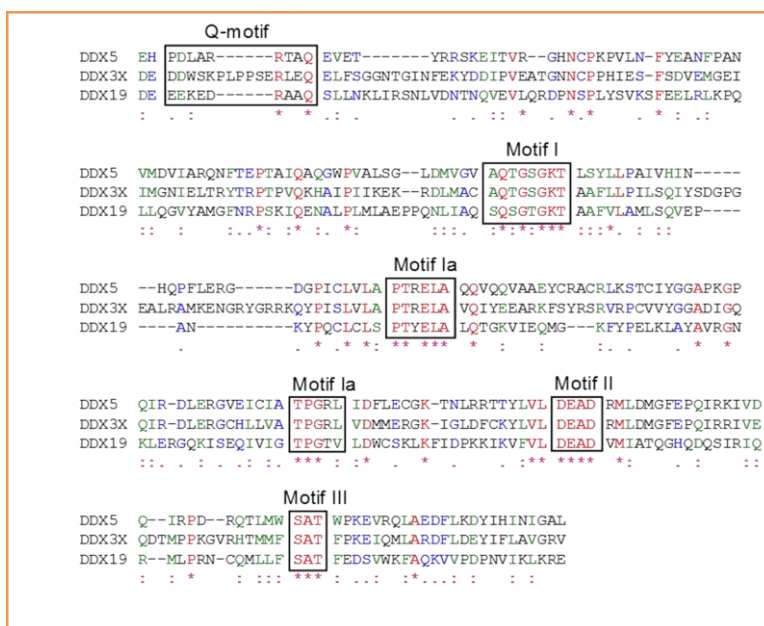


**Figure 3.7: Sequence alignment of DDX5 61-305 with DDX3X 132-420 and DDX19 49-300 showing conserved motifs of DDX5 61-305.** Sequence alignment of DDX5 61-305 (GI: 2599359) with DDX3x 132-420 (GI: 33873845) and DDX19 49-300 (GI: 3386946) showing conserved Q-motif, motif I, motif Ia, motif Ib, motif II and motif III of domain I in boxes. (\*)denotes sequence identity, (:) strongly similar and (.) weakly similar (CLUSTALW multiple alignment NPS@: Network Protein Sequence Analysis [http://npsa-pbil.ibcp.fr/cgi-bin/align\\_clustalw.pl](http://npsa-pbil.ibcp.fr/cgi-bin/align_clustalw.pl))

### 3.4.5 Flexible Region in the N-terminal of DDX5 1-305 Auto-Inhibits Its Interaction with NS5B

The highly variable N and C terminal regions of DEAD helicases play crucial roles in their regulation. To understand the mechanism of regulation, DDX5 1-305, which contains both the N-terminal flanking region (NTR) and domain I of DDX5, was crystallized and subjected to X-ray diffraction (see Chapter 2). However, due to disorder, only part of the NTR region 51-78 was observed in the electron density map. This region forms an extensive loop and supplements the core with an additional  $\alpha$ -helix (Figure 3.6).



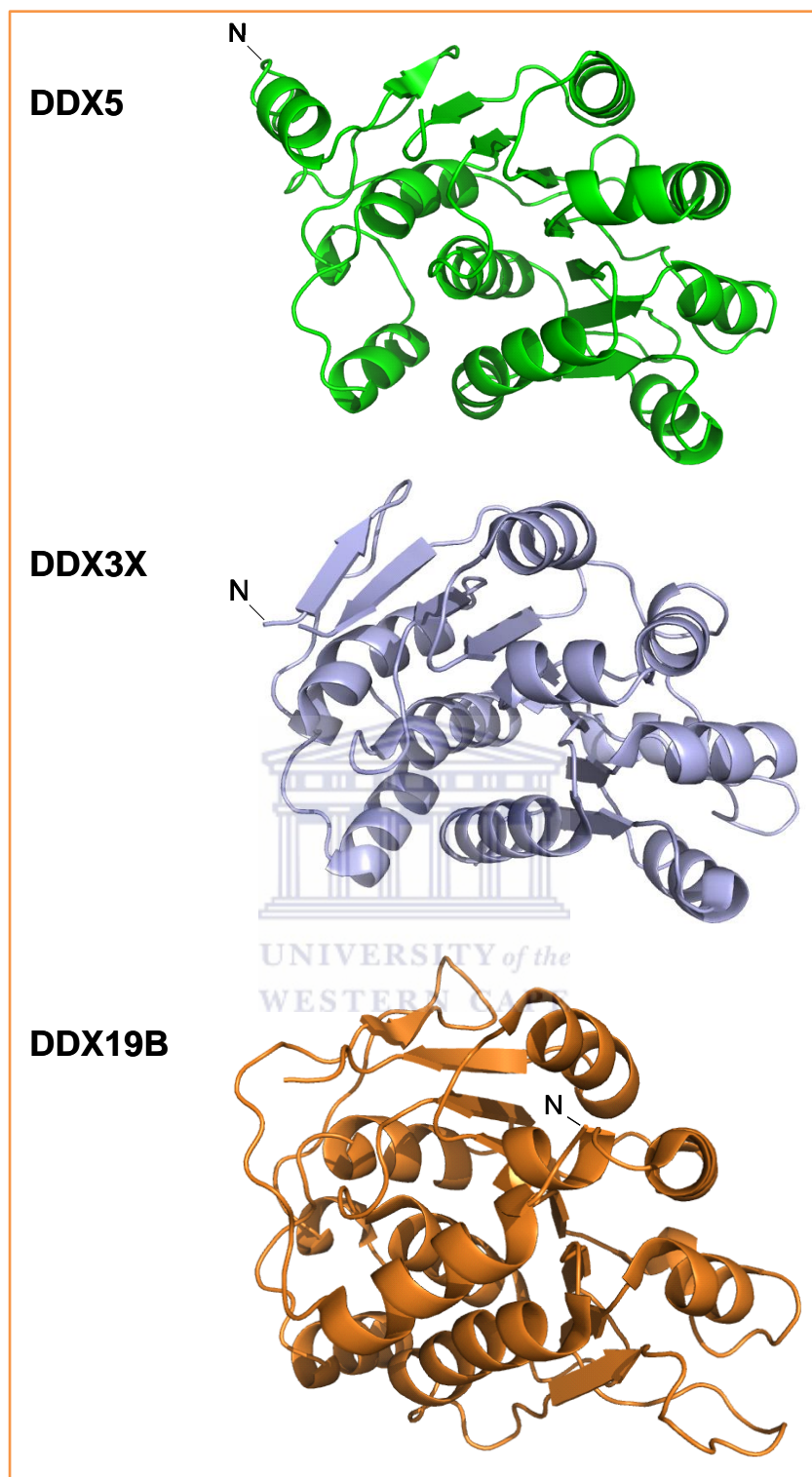


**Figure 3.8: Structure of DDX5 61-305 and the corresponding domain in DDX3X and DDX19B.**

The structures have been orientated to show the 8  $\beta$ -strands in the middle surrounded by  $\alpha$ -helices. N denotes the N terminal domain of the structure.

The co-immunoprecipitation experiments showed that DDX5 61-305 binds NS5B stronger than DDX5 1-305 (Figure 3.2), suggesting that the NTR of DDX5 1-305 can auto-inhibit its interaction with NS5B. In our crystal structure, the first 50 residues of the NTR are highly disordered while residues 51-69 form an extended loop structure and residues 70-78 form an  $\alpha$ -helix (Figure 3.10). Unfortunately, the crystal structure does not reveal any contact between the NTR and the rest of DDX5 1-305. This does not rule out that the NTR can fold back on the rest of DDX5 1-305, but rather is a reflection of the highly flexible nature of the NTR and the possibly highly dynamic nature of the interaction. Hence, to further investigate the structural elements in NTR that are involved in the auto-inhibition, more DDX5 mutants were created for co-immunoprecipitation with NS5B (Figure 3.10). The first mutant is DDX5 61-305 in which the N-terminal part of the NTR has been deleted, but the helix in the NTR remains intact. The second mutant is DDX5 79-305 where the entire NTR has been deleted. The third mutant is DDX5 1-305 $\Delta$ 70-78 where the helix in the NTR has been deleted but the flexible first 50 residues and the extended loop (residues 51 to 69) remain intact.

Consistent with the results shown in Figure 3.2, both DDX5 61-305 and DDX5 79-305 showed higher binding to NS5B than DDX5 1-305 (Figure 3.11), indicating that the auto-inhibition is abolished when part or the complete NTR is deleted. The internal deletion mutant DDX5 1-305 $\Delta$ 70-78 also binds strongly to NS5B (Figure 3.11), indicating that residues 1-69 cannot cause auto-inhibition in the absence of the helix formed by amino acids 70-78. This suggests that this helix may bring the flexible 1-69 residues of NTR close to the NS5B binding site in DDX5 1-305, presumably within residues 79-305. Overall, the results also showed that auto-inhibition involves amino acids 1-78, and the helix formed by amino acid 70-78 is necessary for the inhibition to occur (Figure 3.11). Interestingly, auto-inhibition was also observed with DDX19, another DEAD-box helicase in which the flexible N-terminal amino acid folds back and auto-inhibits ATPase activity (Collins, Karlberg et al. 2009). Based on this mode of auto-inhibition, it is possible to reconcile the fact that GST-DDX5 1-305 did not bind NS5B to a lesser extent than GST-DDX5 61-305 in the GST pull-down assay (Figure 3.5B). As the auto-

inhibition requires the NTR to be flexible, the fusion with a large protein GST at the N-terminal of NTR could have rendered it rigid and unable to fold onto the NS5B binding site.

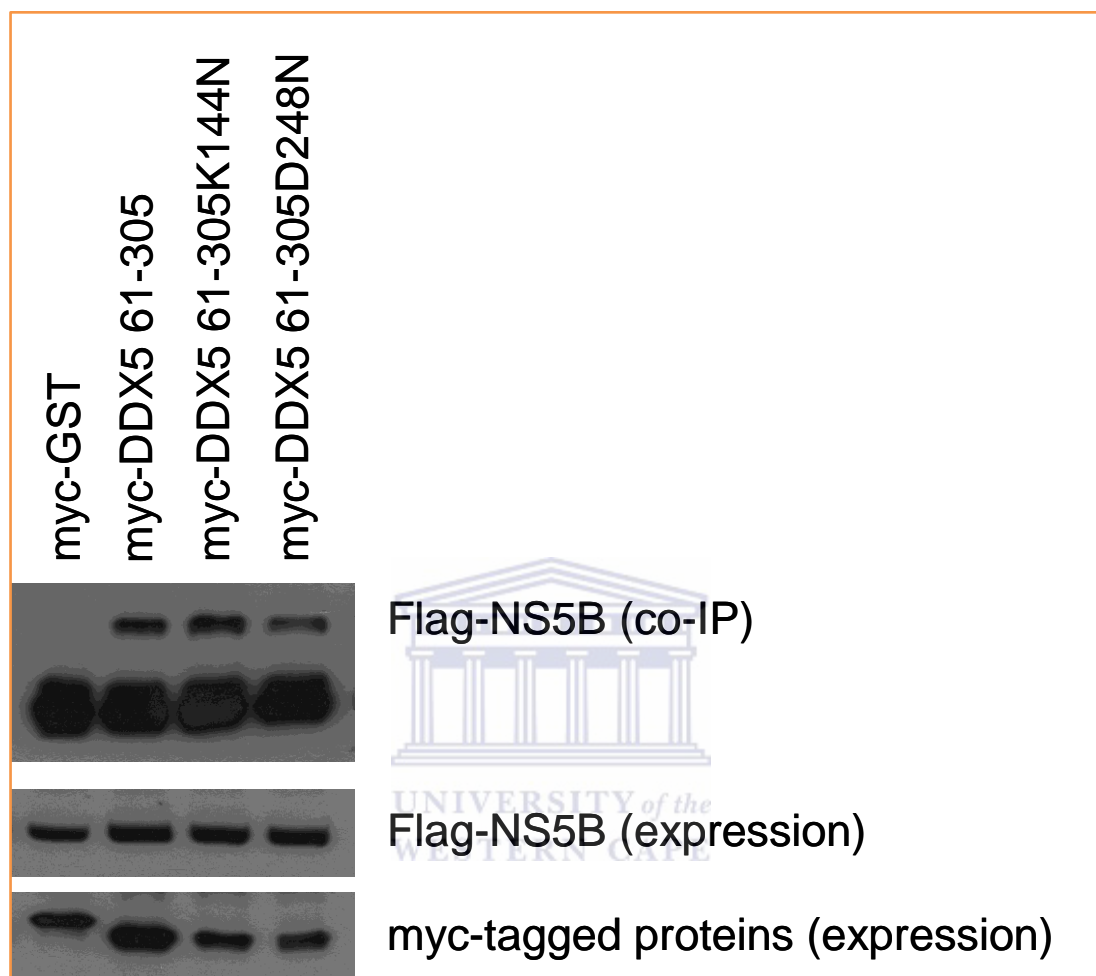


**Figure 3.9: Co-immunoprecipitation of NS5B with DDX5-N with mutated ATP binding site and ATP hydrolysis site. NS5B co-immunoprecipitated with DDX5 61-305 with a mutated ATP binding site as well as DDX5-N with a mutated ATP hydrolysis site.** 200  $\mu$ g of clarified cell lysates were pre-incubated with polyclonal anti-myc antibodies before it was added to Protein-A-agarose beads. Co-immunoprecipitation of Flag-NS5B was detected by monoclonal anti-flag antibodies. 20  $\mu$ g of cell lysates were used to detect expressed proteins. **Top panel:** Co-immunoprecipitation of NS5B with DDX5 61-305, DDX5 61-305K144N (mutated ATP binding site) and DDX5 61-305D248N (mutated ATP hydrolysis site) but not GST control. **Middle panel:** Expression of Flag-NS5B detected by polyclonal anti-flag antibodies. **Bottom panel:** Expression of the different myc-tagged proteins detected by polyclonal anti-myc antibodies.

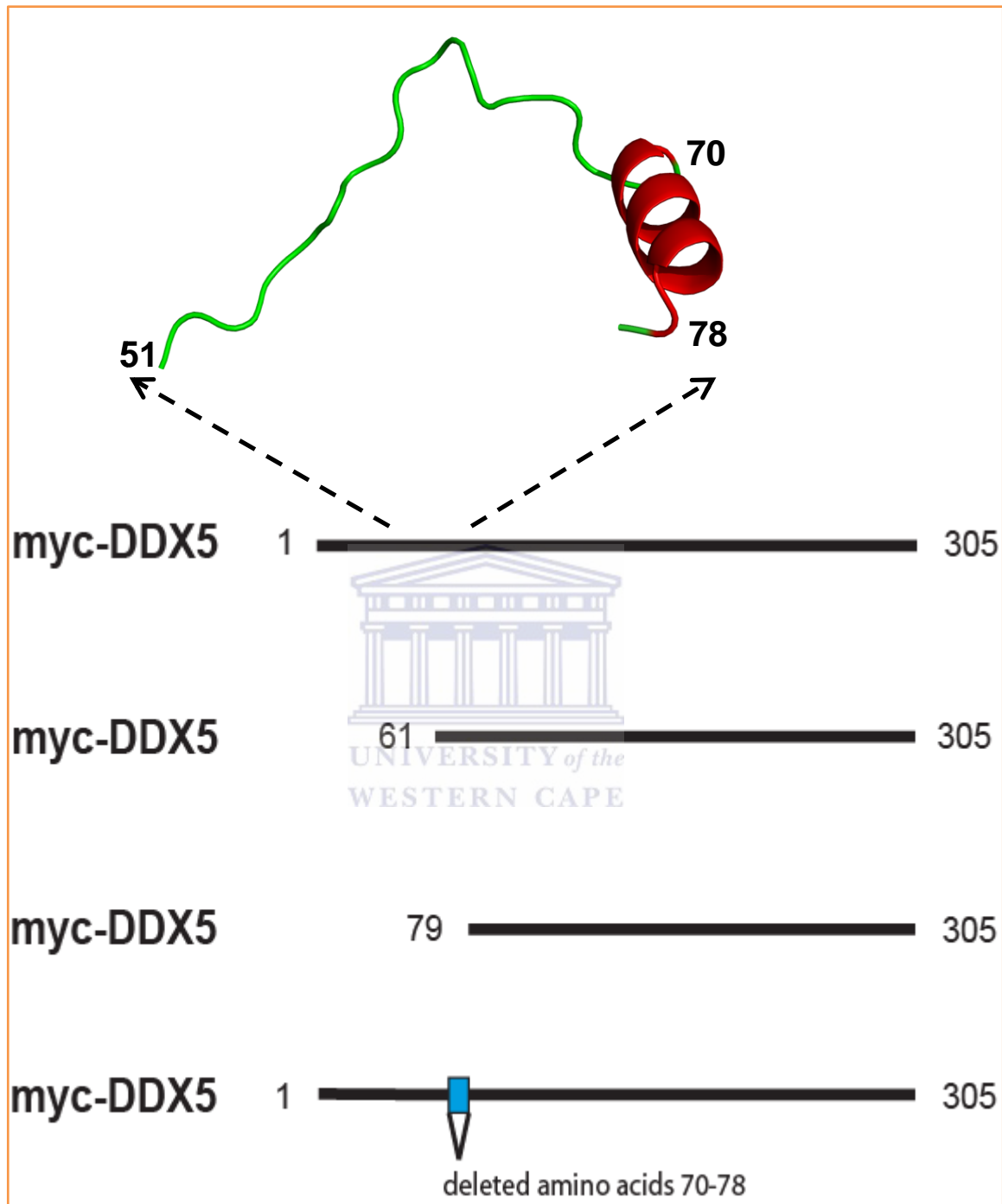


**Figure 3.10: Map of myc-DDX5 1-305 with modifications in the first 78 amino acids (NTR).** The first 50 residues of the NTR are highly disordered, followed by an extended loop structure from 51-69 and an  $\alpha$ -helix from amino acids 70-78. Deletions of the different features were made to investigate their function when DDX5 binds NS5B.

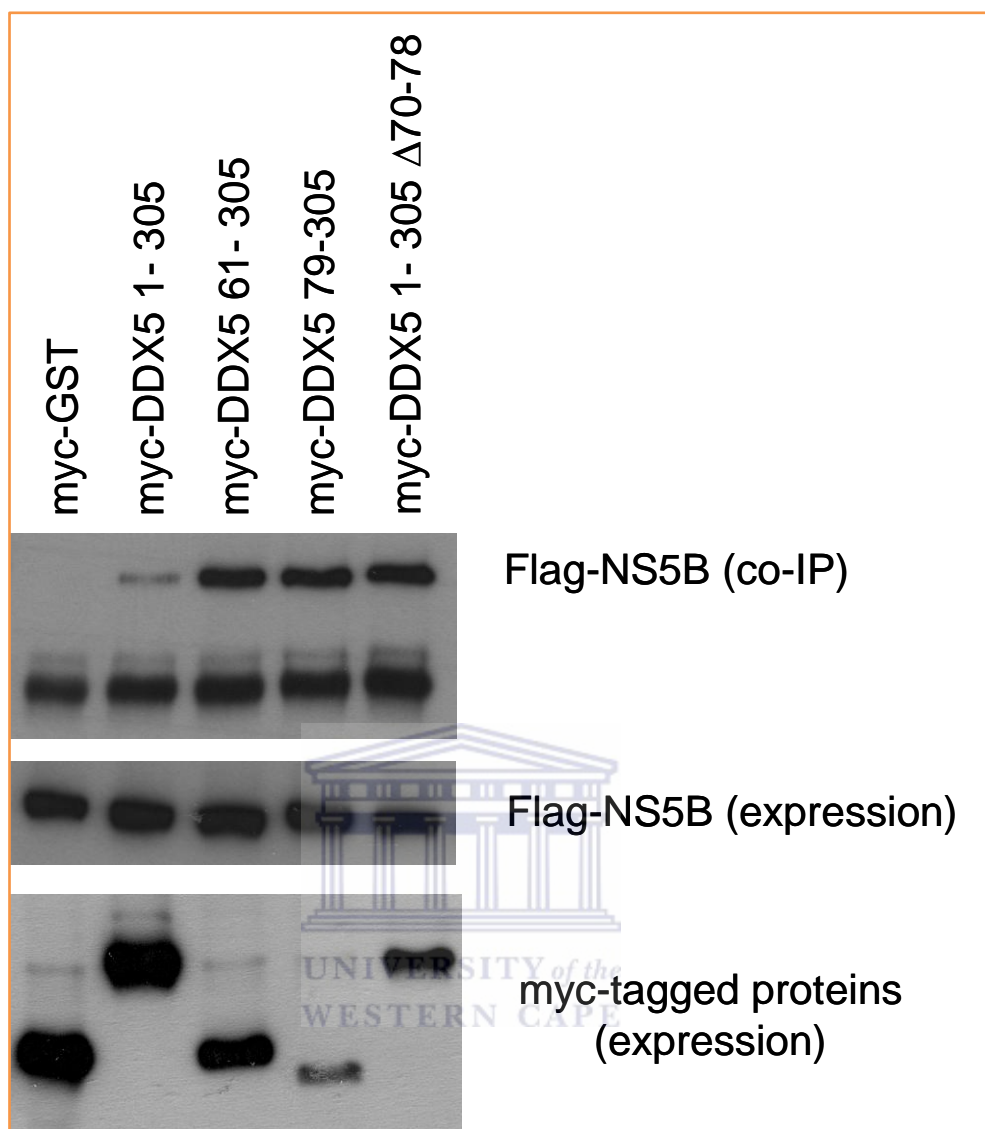


**Figure 3.11: Co-immunoprecipitation of NS5B with the N-terminal half of DDX5 with modifications in the first 78 amino acids.** 200  $\mu$ g of clarified cell lysates were pre-incubated with polyclonal anti-myc antibodies before it was added to Protein-A-agarose beads. Co-immunoprecipitation of Flag-NS5B was detected by monoclonal anti-flag antibodies. 20  $\mu$ g of cell lysates were used to detect expressed proteins. **Top panel:** Co-immunoprecipitation of NS5B with DDX5 1-305, DDX5 61-305, DDX5 79-305 and DDX5 1-305  $\Delta$ 70-78 but not GST control. **Middle panel:** Expression of Flag-NS5B detected by polyclonal anti-flag antibodies. **Bottom panel:** Expression of the different myc-tagged proteins detected by polyclonal anti-myc antibodies.

### 3.4.6 DDX5 1-80 Is Able to Interact with DDX5

In order to gather more insight into the mechanism by which the NTR of DDX5 is involved in the auto-inhibition, we sought to demonstrate a direct interaction between the NTR and the rest of DDX5 by biophysical analysis. Thus, attempts were made to express and purify DDX5 1-80. GST fusion protein of DDX5 1-80 was successfully expressed in *E. coli*, but when the 3C protease was used to cleave it from its GST tag, extensive degradation occurred as evidenced by the appearance of a smear upon separation on SDS-PAGE (Figure 3.12). Failure to obtain untagged and intact DDX5 1-80 meant that it was not possible to measure the affinity of binding between DDX5 1-80 and the rest of DDX5 via quantitative measurements like surface plasmon resonance or isothermal titration calorimetry assays. Hence, GST-DDX5 1-80 was used in a non-quantitative GST-pull-down assay as described below.

### 3.4.7 GST Pull-Down of DDX5 61-305 with GST-DDX5 1-80

Next, a GST-pull-down assay was performed by using GST-DDX5 1-80 and highly purified DDX5 61-305. The expression and purification of DDX5 61-305 were presented in Chapter 2. As shown in Figure 3.13, DDX5 61-305 bound to GST-DDX5 1-80 resulting in the appearance of an additional protein band at the molecular weight of DDX5 61-305 after the pull-down. However, it was not possible to ascertain if DDX5 61-305 also bound to GST alone because GST was similar in molecular weight to DDX5 61-305 and they could not be easily differentiated when analysed on SDS-PAGE (Figure 3.13). As it is possible that DDX5 61-305 bound to both GST-DDX5 1-80 and the GST control, the result of this experiment was inconclusive.

### 3.4.8 Unspecific Binding of DDX5 61-305 to GST-H5N1 NS1 1-75 and GST-BLR

To resolve the problem associated with size similarity of DDX5 61-305 and GST, GST tagged H5N1 NS1 protein residues 1-75 and BLR, a chimeric form of the Mcl-1 protein's Bcl-2-like region (Czabotar, Lee et al. 2007) were used as negative controls in the GST-pull-down assay of DDX5 1-80 and DDX5 61-305. It was observed that DDX5 61-305 binding was unspecific as

it bound the negative controls H5N1 NS1 1-75 and BLR as well as the intended target DDX5 1-80 (Figure 3.14).

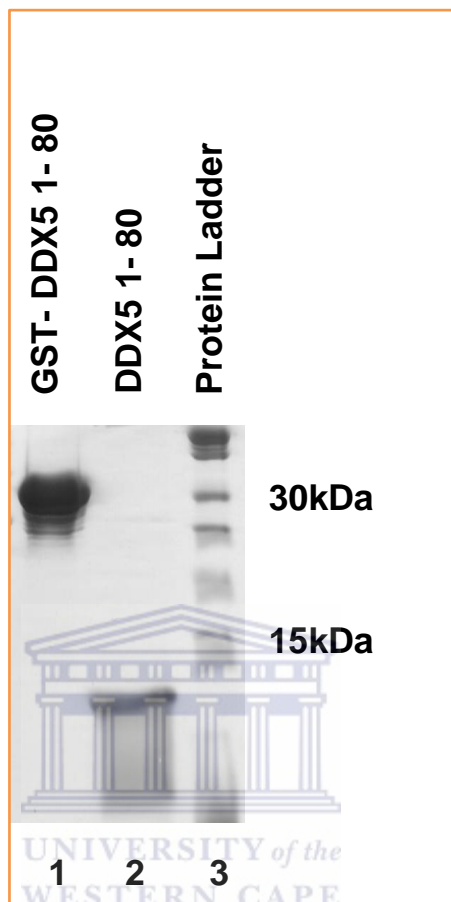


**Figure 3.12: Bacterial expression of GST-DDX5 1-80.** DDX5-1-80 was not stable when C3 protease was used to cleave it from its GST tag, a smearing of DDX5 1-80 was observed. **Lane 1:** Glutathione-Sepharose bound GST-DDX5 1-80. **Lane 2:** Purified DDX5 1-80 after C3 cleavage. **Lane 3:** Protein molecular weight standards.

### 3.4.9 Amino Acids 1-80 of DDX5 Are Able to Interact with the Rest of DDX5

The unspecific binding observed above suggests that the purified DDX5 61-305 may be misfolded and/or might have undergone self-aggregation in the buffer used in the GST-pull-down assay. To overcome this problem, the GST-pull-down assay was repeated by using rabbit reticulocytes to express the DDX5 proteins via in vitro translation. Such a cell free mammalian system has recently been reported to yield numerous proteins in the native form

(<http://www.promega.com/resources/articles/pubhub/role-of-cell-free-rabbit-reticulocyte-expression-systems-in-functional-genomics/>).

Using this system, DDX5 1-614 was successfully expressed as a single prominent band at the expected molecular weight, as observed after SDS-PAGE (Figure 3.15). DDX5 61-614 and DDX5 79-614 were also expressed although they exhibited double bands, indicating that some cleavage has occurred (Figures 3.16 and 3.17). Shorter forms of DDX5 were not successfully expressed (data not shown). GST-pull-down showed that all 3 DDX5 proteins, namely, DDX5 1-614, DDX5 61-614 and DDX5 79-614, bound to DDX5 1-80 fused to GST, but not by GST alone (Figures 3.15-3.17). Thus, it has been shown that DDX5 1-80 is capable of binding to the rest of DDX5 and this is consistent with our hypothesis that the flexible NTR of DDX5 folds back to interact with the NS5B binding site in DDX5 1-305 and causes auto-inhibition.

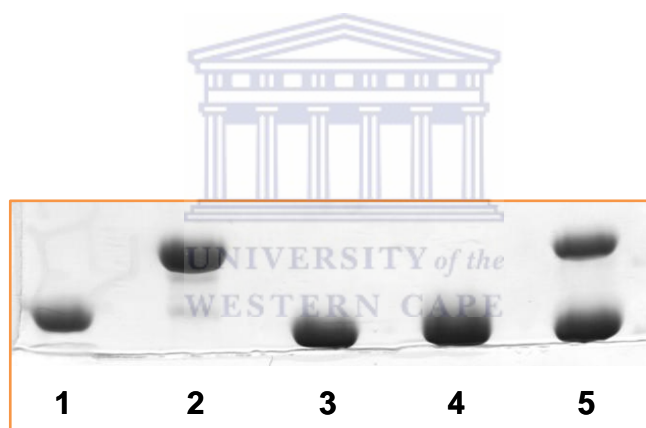


**Figure 3.13: GST-pull-down of DDX5 61-305 with GST-DDX5 1-80 with GST as control.** 20  $\mu$ g of Glutathione-Sepharose bound fusion protein expressed in *E. coli* was mixed with 200  $\mu$ g of purified DDX5 61-305. Binding results were analysed with SDS-PAGE and detected with Coomassie staining. 20  $\mu$ g of each protein used were loaded as reference. **Lane 1:** GST 20  $\mu$ g. **Lane 2:** GST-DDX5 1-80 20  $\mu$ g. **Lane 3:** DDX5 61-305 20  $\mu$ g. **Lane 4:** GST + DDX5 61-305. **Lane 5:** GST-DDX5 1-80 + DDX5 61-305.



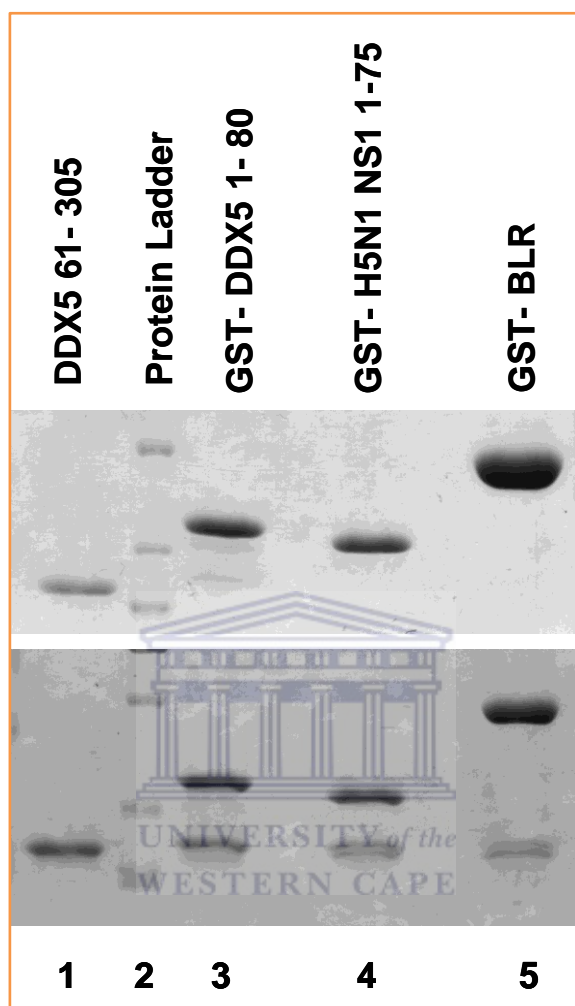


**Figure 3.14: GST pull-down of DDX5 61-305 with GST-DDX5 1-80 with NS1 and BLR as controls.** 30  $\mu$ g of Glutathione-Sepharose bound fusion protein expressed in *E. coli* was mixed with 55  $\mu$ g of purified DDX5 61-305. Binding results were analysed with SDS-PAGE and detected with Coomassie staining. **Top Panel:** 3  $\mu$ g of each protein used were loaded as reference. **Bottom panel:** Lane 1: DDX5 61-305. Lane 2: Protein molecular weight standards. Lane 3: GST-DDX5 1-80 + DDX5 61-305. Lane 4: GST-H5N1 NS1 1-75 + DDX5 61-305. Lane 5: GST-BLR + DDX5 61-305

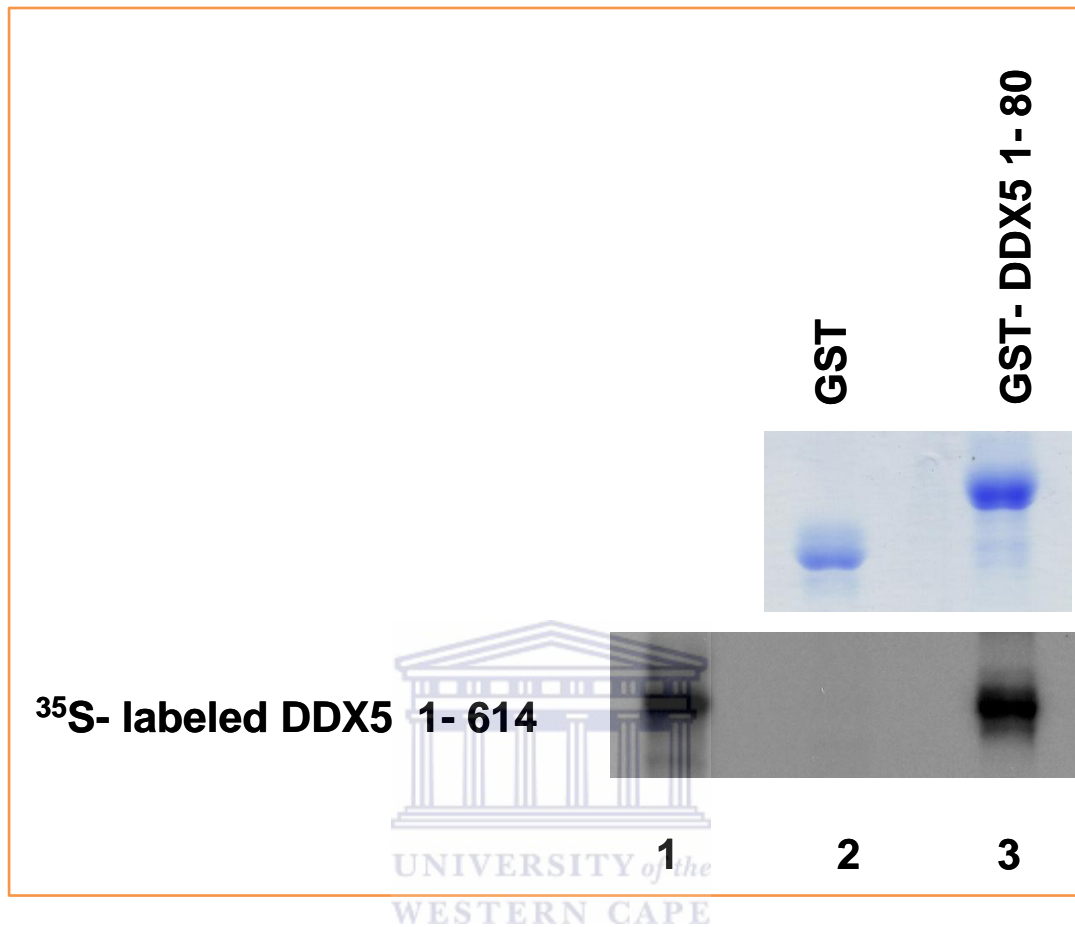


**Figure 3.15: GST pull-down of <sup>35</sup>S-labelled DDX5 1-614 by GST-DDX5 1-80.** 30 µg of Glutathione-Sepharose bound fusion protein expressed in *E. coli* was mixed with in vitro translated <sup>35</sup>S-labelled DDX5 1-614. Binding results were analysed by SDS-PAGE and autoradiography. **Upper panel:** 30 µg of Glutathione-Sepharose bound fusion proteins used in the pull-down assay was analysed by SDS-PAGE followed by Coomassie blue staining to ascertain the purity of the proteins. **Lower panel:** Lane 3 shows <sup>35</sup>S-labeled DDX5 1-614 protein bound to DDX5 1-80 but not the GST control in lane 2. One tenth of the binding input was loaded in lane 1.

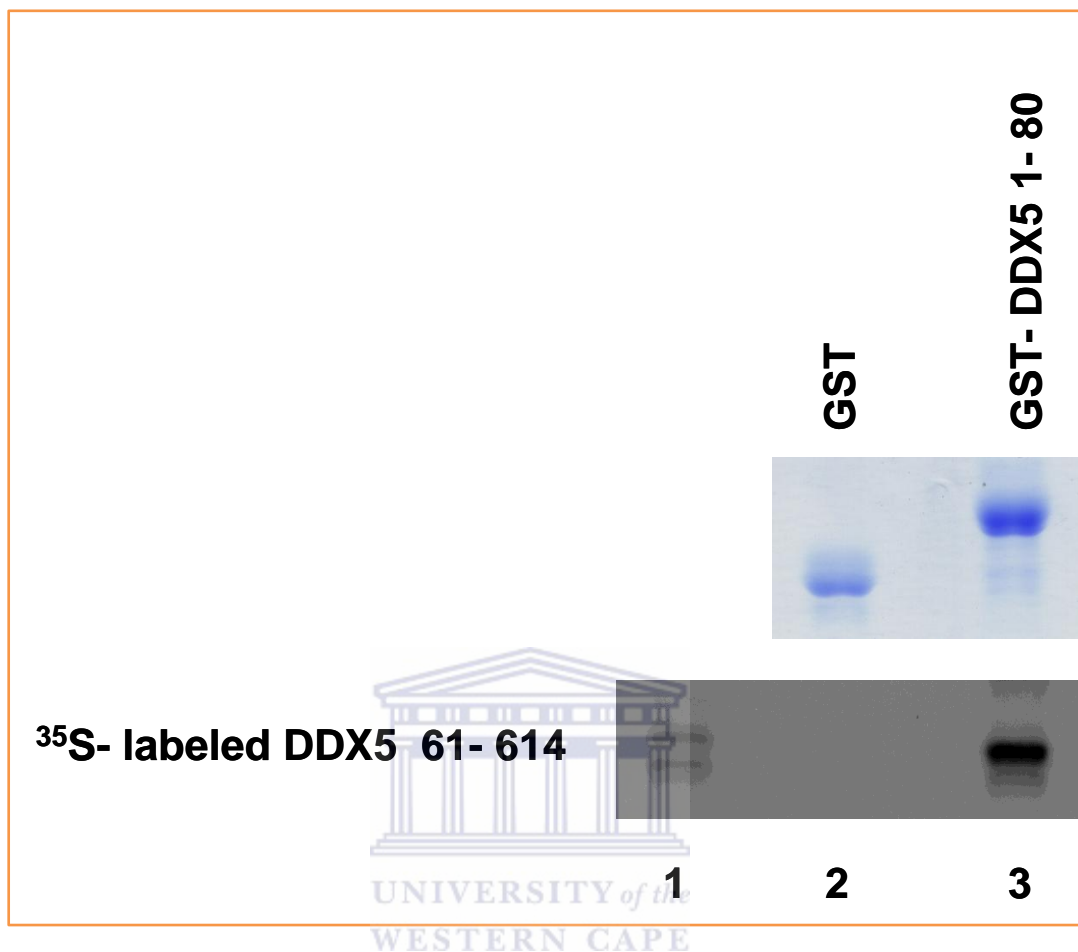


**Figure 3.16: GST-pull-down of  $^{35}\text{S}$ -labelled DDX5 61-614 by GST-DDX5 1-80.** 30  $\mu\text{g}$  of Glutathione-Sepharose bound fusion protein expressed in *E. coli* was mixed with in vitro translated  $^{35}\text{S}$ -labeled DDX5 61-614. Binding results were analysed by SDS-PAGE and autoradiography. **Upper panel:** 30  $\mu\text{g}$  of Glutathione-Sepharose bound fusion proteins used in the pull-down assay was analysed by SDS-PAGE followed by Coomassie blue staining to ascertain the purity of the proteins. **Lower panel:** Lane 3 showed  $^{35}\text{S}$ -labelled DDX5 61-614 protein bound to DDX5 1-80, but not the GST control in lane 2. One tenth of the binding input was loaded in lane 1.

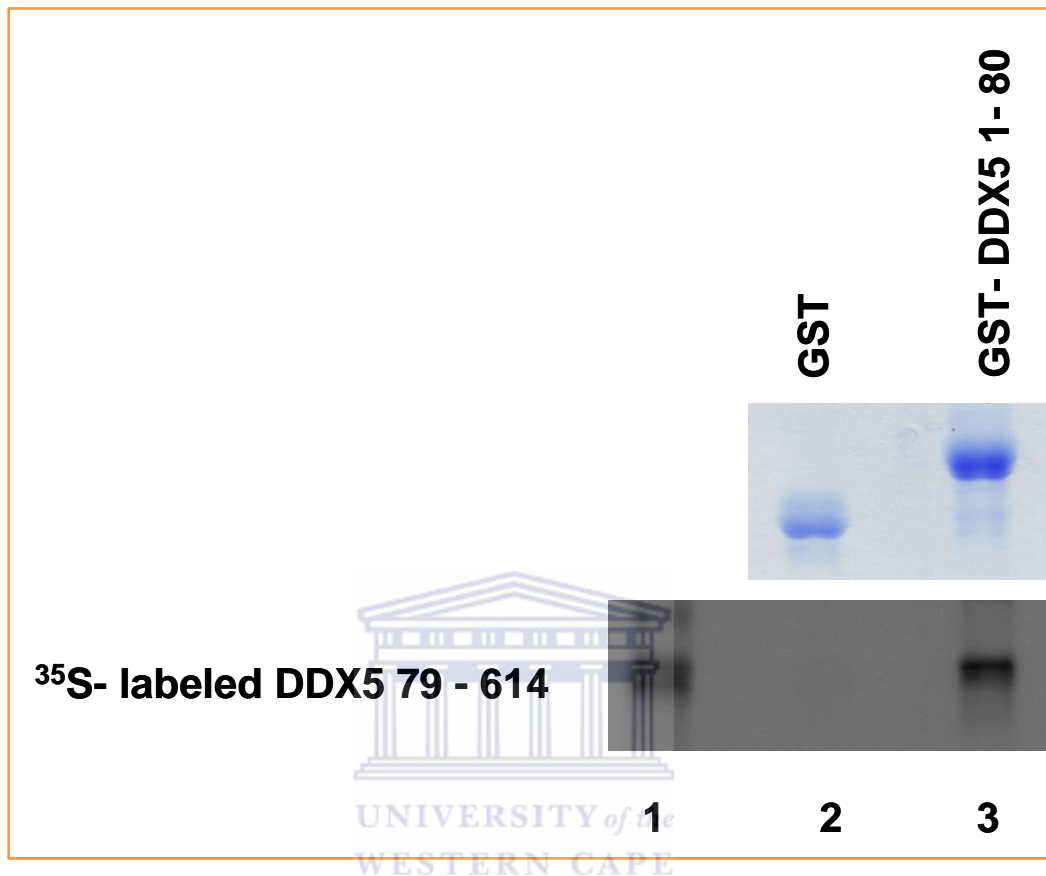


**Figure 3.17: GST pull-down of  $^{35}\text{S}$ -labelled DDX5 79-614 by GST-DDX5 1-80.** 30  $\mu\text{g}$  of Glutathione-Sepharose bound fusion protein expressed in *E. coli* was mixed with in vitro translated  $^{35}\text{S}$ -labeled DDX5 79-614. Binding results were analysed by SDS-PAGE and autoradiography. **Upper panel:** 30  $\mu\text{g}$  of Glutathione-Sepharose bound fusion proteins used in the pull-down assay was analysed by SDS-PAGE followed by Coomassie blue staining to ascertain the purity of the proteins. **Lower panel:** Lane 3 showed  $^{35}\text{S}$ -labelled DDX5 79-614 protein bound to DDX5 1-80, but not the GST control in lane 2. One tenth of the binding input was loaded in lane 1.

### 3.4.10 DDX5 Also Interacts with Core and NS3

In order to determine if DDX5 can interact with other HCV proteins, Myc-tagged DDX5 was co-transfected into COS-7 cells with Flag-tagged HCV proteins, core, NS3, NS4B, NS5A and NS5B. Flag-GST was co-transfected as a negative control in the co-immunoprecipitation experiment. The transfected cell lysates were analysed using Western blot analysis. Similar expression levels of Myc-DDX5 were detected and the expressions levels of these Flag-tagged proteins were also fairly equal (Figure 3.18). All the HCV proteins migrated to the expected molecular weight positions, except NS4B. Two bands were detected for Flag-NS4B; the bottom band at about 30 kDa corresponds to the molecular weight of the protein while the top band is probably an oligomeric form of NS4B migrating at a slower rate (Yu, Lee et al. 2006). The co-immunoprecipitation results showed that myc-DDX5 bound strongly to Flag-Core 1-173, Flag-NS3 and Flag-NS5B, and bound weakly to Flag-Core 1-151, Flag-NS4B and Flag-NS5A (Figure 18). Flag-Core 1-173 bound more strongly than Flag-Core 1-151, which suggested that the domain between amino acids 152 and 173 of core is important for its binding to DDX5. No binding was observed for Flag-GST indicating that the protein interactions observed were not due to the Myc and Flag tags.

Of all the HCV proteins, core, NS3 and NS5B show higher binding to DDX5 than NS4B and NS5A. To determine if core, NS3 and NS5B can interact with endogenous DDX5, single transfection of Flag-Core 1-173, Flag-NS3 or Flag-NS5B was carried out in COS-7 cells and co-immunoprecipitations were performed using a rabbit anti-DDX5 polyclonal antibody (Figure 3.19). Expression levels of endogenous DDX5 were similar in the samples transfected with Flag-Core 1-173, Flag-NS3 and Flag-NS5B. The Flag-tagged HCV proteins were pulled down with endogenous DDX5 when anti-DDX5 antibodies were used for the co-immunoprecipitation with Protein-A-agarose beads. None of the HCV proteins co-immunoprecipitated when an irrelevant antibody (anti-HA) was used for the co-immunoprecipitation, indicating that the interactions between endogenous DDX5 and the HCV proteins are specific. Thus, besides the interaction between DDX5 and NS5B, our results show that DDX5 can also interact specifically with core 1-173 and NS3.

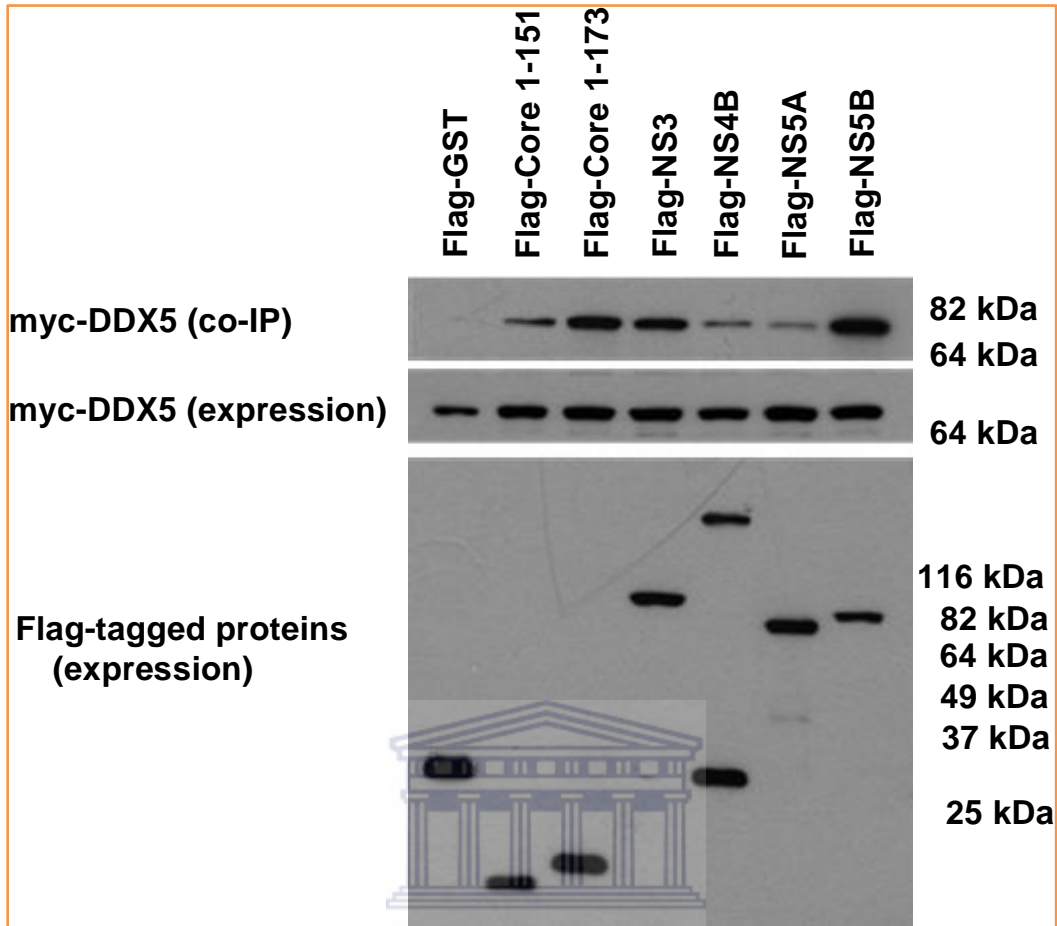


**Figure 3.18: Co-immunoprecipitation of DDX5 with HCV proteins Core 1-151, Core 1-173, NS3, NS4B, NS5A and NS5B.** 200  $\mu$ g of co-transfected cell lysates were incubated at room temperature with 20  $\mu$ l of pre-washed ANTI-FLAG® M2 affinity gel (Sigma). Co-immunoprecipitation of myc-DDX5 was detected by polyclonal anti-myc antibodies. 10  $\mu$ g of cell lysates were used to detect expressed proteins. **Top panel:** Co-immunoprecipitation of myc-DDX5 with Flag-Core 1-151, Flag-Core1-173, Flag-NS3, Flag-NS4B, Flag-NS5A or Flag-NS5B, but not GST control. **Middle panel:** Expression of myc-DDX5 detected with polyclonal anti-myc antibodies. **Bottom panel:** Expression of the different Flag-tagged proteins detected with polyclonal anti-flag antibodies.

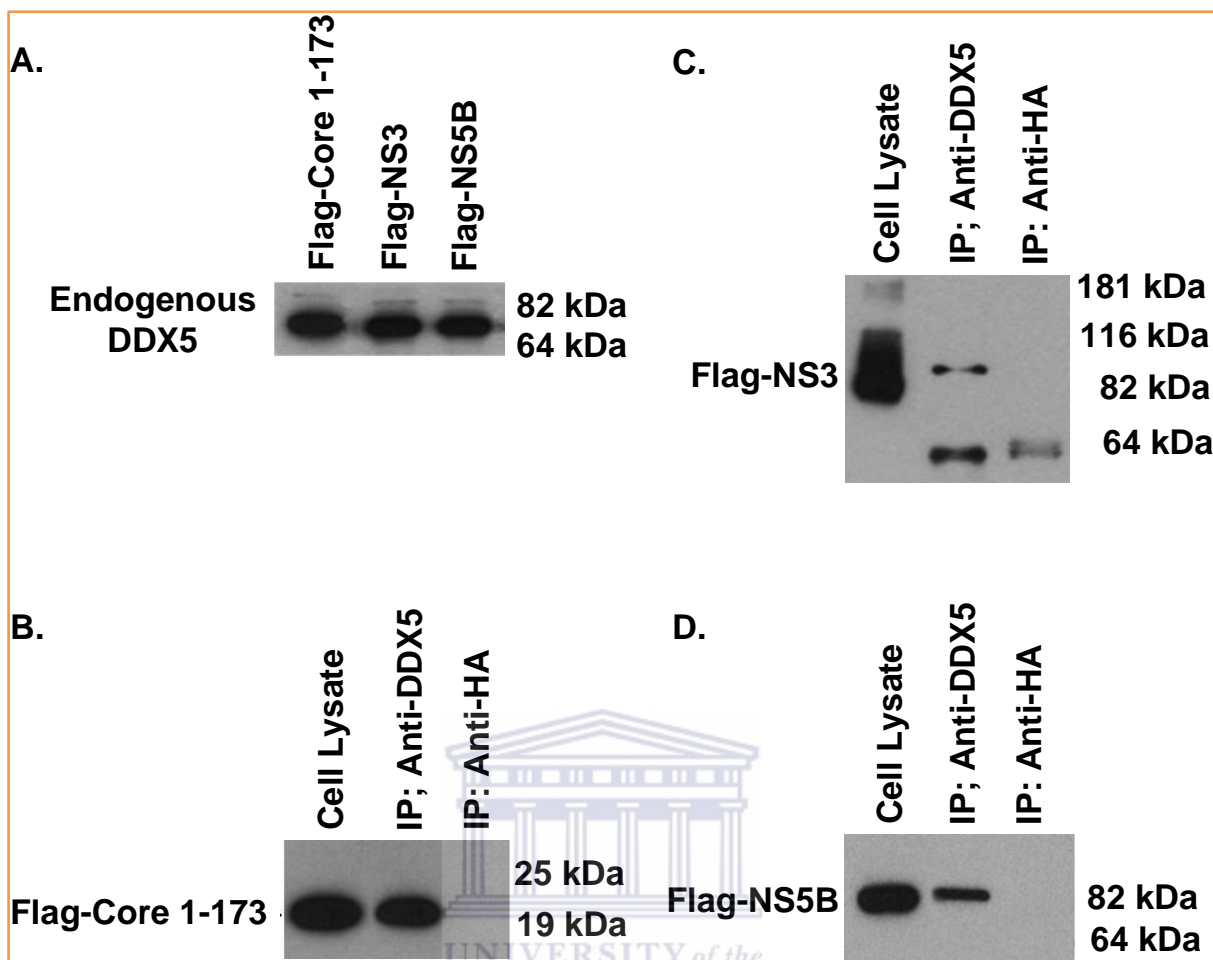


**Figure 3.19. Co-immunoprecipitation of Core 1-173, NS3, and NS5B with endogenous DDX5.**

COS-7 cells transfected with Flag-Core 1-173, Flag-NS3 or Flag-NS5B were co-immunoprecipitated with endogenous DDX5. 200  $\mu$ g of clarified cell lysates were pre-incubated with polyclonal anti-DDX5 or anti-HA antibodies before it was added to Protein-A-agarose beads. 10  $\mu$ g of cell lysates were used to detect expressed proteins. A. Expression of endogenous DDX5 in COS-7 cells transfected with Flag-Core 1-173, Flag-NS3 or Flag-NS5B detected with anti-DDX5 antibody. B, C, and D. Flag-core, NS3 and NS5B co-immunoprecipitated with endogenous DDX5 when anti-DDX5 antibodies were used for IP, but not when anti-HA antibodies were used. Co-immunoprecipitation of Flag-tagged proteins were detected by monoclonal anti-flag antibodies.

### 3.5 Conclusion

In the past decade a growing number of DEAD-box RNA helicase structures have been determined (Caruthers, Johnson et al. 2000; Carmel and Matthews 2004; Shi, Cordin et al. 2004; Sengoku, Nureki et al. 2006; Hogbom, Collins et al. 2007). They contain a central region comprising of 2 conserved domains, termed domain I and II, flanked by highly variable N- and C-terminal sequences. Comparison of known structures of domain I and II reveal they have a fold belonging to the RecA super family, where 5  $\beta$ -strands are surrounded by 5  $\alpha$ -helices (Story and Steitz 1992). We have previously shown that DDX5, a human RNA helicase belonging to a large family of DEAD-box RNA helicases, interacts with NS5B and that the C terminus of NS5B is essential for this interaction (Goh, Tan et al. 2004). Co-immunoprecipitation experiments showed there are 2 independent NS5B binding sites in DDX5, one in the N-terminal half (corresponding to residues 1 to 305 of DDX5) and the other in the C-terminal half (corresponding to residues 306 to 614 of DDX5) (Figures 2 and 3). Interestingly, DDX5 1-305 and DDX5 306-614 contain the conserved domain I and II respectively.

Using DDX5 1-305, the crystal structure of the apo form of the N-terminal half of DDX5 (residues 55-303) was solved in this study and it reveals that domain I of DDX5 contains many typical features found in the structures of other DEAD-box helicases (Figure 3.6). A sequence alignment of DDX5 with DDX3X and DDX19B also revealed high sequence identity in the conserved motifs, namely, I (Walker A), II (Walker B, DEAD-box), Ia, Ib, and II (Figure 3.7) and the three-dimensional structures showed that domain I of all three proteins are structurally similar (Figure 3.8).

The bacterially expressed and purified DDX5 1-305 is in its apo form as there is no bound ATP observed in the crystal structure as would be expected since no nucleotide supplement was added to the growth medium. This form of DDX5 1-305 is capable of binding NS5B, suggesting that the ATPase activity of DDX5 is not involved in the interaction (Figure 3.5). Consistently, co-immunoprecipitation experiments using Huh-7 cells confirmed that both



the ATP-binding and the DEAD motif in DDX5 1-305 are also not required for interaction with NS5B (Figure 3.9).

The NTRs of DEAD-box helicases are highly variable and there is limited structural information (Cordin, Banroques et al. 2006; Fuller-Pace 2006). For DDX5 1-305, no density was observed for residues 1-50 within the NTR. Analysis, using the protein disorder server RONN (Yang, Thomson et al. 2005), predicted this region to be disordered as is observed with other DEAD-box helicases. The remaining part of the NTR (residues 51 to 78) is composed of a loop and an  $\alpha$ -helix located before domain I (Figure 3.6). To our knowledge, this is only the second report of structural elements in the NTR of DEAD-box RNA helicases as most of the structures of DEAD-box RNA helicases were obtained using proteins expressed without the NTR. The first report documented an  $\alpha$ -helix in the NTR of DDX19 which inserts between domains I and II to inhibit ATP hydrolysis, unless it is displaced by RNA binding (Collins, Karlberg et al. 2009). Remarkably, our results show that the NTR of DDX5 1-305 inhibits its interaction with NS5B (Figures 3.2 and 3.11). The  $\alpha$ -helix (residues 70-78) in the NTR is essential for this auto-inhibition and seems to mediate the interaction between the highly flexible 1-70 residues in NTR and NS5B binding site in DDX5 1-305 (Figure 3.11), presumably located within residues 79-305. Furthermore, DDX5 1-80 can bind directly to full-length DDX5 as well as DDX5 with part or all of the NTR deleted (Figures 3.15-3.17), which provide further evidence that the flexible NTR of DDX5 folds back to interact with the NS5B binding site.

Our results suggest that the N-terminal (DDX5 1-305) and C-terminal (DDX5 306-614) domains of DDX5 interact with NS5B independently. The high-resolution three-dimensional structure of the apo form of DDX5 1-305 provides a basis for future studies to define the precise role of DDX5 during HCV infection. Crystallization of full-length DDX5 and the DDX5-NS5B complex is also actively being pursued. Our data also reveal that the interaction between DDX5 1-305 and NS5B is auto-inhibited by the highly flexible NTR of DDX5 1-305. It is expected that solving the structure of full-length DDX5 can help ascertain whether the  $\alpha$ -helix in the NTR of DDX5 can also insert between domains I and II like DDX19.

Recent studies revealed that the DEAD-box RNA helicases DDX3, rck/p54 and RNA helicase A are required for HCV RNA replication (Ariumi, Kuroki et al. 2007; He, Tang et al. 2008; Scheller, Mina et al. 2009). Our previous study also showed that knockdown of endogenous DDX5 by RNA interference reduces the transcription of negative-strand HCV RNA (Goh, Tan et al. 2004). It is interesting that multiple DEAD-box RNA helicases are important for HCV replication and further studies are warranted to determine if they are involved in the same step(s) of the viral life-cycle. It is also possible that these host proteins are involved in more than one viral-host interaction, for example, DDX3 not only binds the HCV core protein, but is probably associated with an HCV non-structural protein or HCV RNA itself (Owsianka and Patel 1999; Ariumi, Kuroki et al. 2007). In this study, we also showed that besides NS5B, core and NS3 can also interact with DDX5 in mammalian cells (Figures 3.18 and 3.19). Further investigations are needed to determine the mechanisms of interaction between DDX5 and NS5B, DDX5 and core, DDX5 and NS3, and the impact of these interactions on HCV replication by using the infectious clone system based on JFH-1 genotype 2a HCV (Wakita, Pietschmann et al. 2005). Since the three-dimensional structures of NS3 and NS5B have been solved, the high-resolution three-dimensional structure of DDX5 1-305 obtained in this study can also be used in computer-assisted structure-based molecular-docking to identify critical contacts between the interacting proteins.

# CHAPTER 4



Currently there is no approved vaccine for HCV prevention. Approximately 3-4 million newly HCV infected cases are added yearly to the more than 170 million existing cases world-wide. HCV is a significant healthcare burden because of its high treatment cost associated with interferon and ribavirin, and at least 10% of infected individuals may develop persistent and chronic infection which leads to cirrhosis and liver cancer (Roohvand and Kossari 2011).

In our study, we aimed to characterize the interaction between host DEAD-box RNA helicase DDX5 and NS5B, an RNA-dependent RNA polymerase of HCV, using molecular biology techniques and structural analysis.

Firstly, co-immunoprecipitation results showed that NS5B can bind to DDX5 at two independent regions. In the process of testing GST fusion protein expression of DDX5 and its panel of deletion mutants in *E.coli*, it was found that overnight induction at a lower temperature (16 or 18°C) and high salt buffer (400 mM NaCl) conditions for extraction and processing of the recombinant proteins produced a higher yield. It was also found that the C-terminal end of DDX5 was not stable when purified. Full-length DDX5 and deletion mutants which contained the C-terminal end showed signs of degradation or truncation when purified.

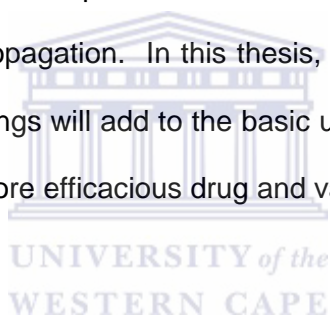
Fast protein liquid chromatography was used to purify large quantities of selected DDX5 and NS5B protein for crystallization and co-crystallization trials. Chemical conditions which showed some crystal growth were refined for improved crystallization. Crystals of DDX5 1-305 was successfully grown and collected under such refined conditions.

Native data of these crystals were collected and solved by Dr Sujit Dutta by molecular replacement using the structure of domain I of DDX3X. The solved structure of DDX5 1-305 (residues 55-303) showed high structural homology with other DEAD-box helicases and sequence alignment with DDX3X and DDX19B revealed sequence identity in the conserved motifs of Domain I. The first 50 residues of DDX5 1-305 was not observed due to low density, residues 51-69 formed an extended loop structure, residues 70-78 formed an  $\alpha$ -helix, followed by 8 centrally located  $\beta$ -sheets packed against 9  $\alpha$ -helices. Co-immunoprecipitation results showed that residues 1-78 are required for auto-inhibition of DDX5's interaction with NS5B.

GST pull-down assay of in-vitro transcribed <sup>35</sup>S-labeled NS5B showed that amino acids 61-80 of DDX5 were sufficient for interaction with NS5B. Co-immunoprecipitation results suggested that ATP binding and ATPase activity was not essential for the interaction between DDX5 and NS5B and that the flexible N-terminal flanking region of DDX5 1-305 auto-inhibited its interaction with NS5B. GSTpull-down of <sup>35</sup>S-labeled DDX5 1-614, DDX5 61-614 and DDX5 79-614 showed that GST-DDX5 1-80 was able to interact with DDX5, providing further evidence that there is auto-inhibition in the interaction between DDX5 1-305 and NS5B.

Besides NS5B, co-transfected DDX5 was found to interact with HCV's Core 1-151, Core 1-173, NS3, NS4B and NS5A. Transfected HCV Core 1-173, NS3 and NS5B proteins were found to interact specifically with endogenous DDX5.

A successful virus infection requires the evasion of host immune response and the recruitment of host factors for propagation. In this thesis, we explored the interaction between HCV NS5B and DDX5. The findings will add to the basic understanding of HCV replication and may aid future studies towards more efficacious drug and vaccine development.



## REFERENCES

- Collaborative Computational Project, Number 4. (1994). "The CCP4 suite: programs for protein crystallography." Acta Crystallogr D Biol Crystallogr 50(Pt 5): 760-3.
- Abdelhaleem, M. (2005). "RNA helicases: regulators of differentiation." Clin Biochem 38(6): 499-503.
- Abdelhaleem, M. (2010). "Helicases: an overview." Methods Mol Biol 587: 1-12.
- Ait-Goughoulte, M., C. Hourieux, et al. (2006). "Core protein cleavage by signal peptide peptidase is required for hepatitis C virus-like particle assembly." J Gen Virol 87(Pt 4): 855-60.
- Ali, S., C. Pellerin, et al. (2004). "Hepatitis C virus subgenomic replicons in the human embryonic kidney 293 cell line." J Virol 78(1): 491-501.
- Alter, H. J. and L. B. Seeff (2000). "Recovery, persistence, and sequelae in hepatitis C virus infection: a perspective on long-term outcome." Semin Liver Dis 20(1): 17-35.
- Amaratunga, M. and T. M. Lohman (1993). "Escherichia coli rep helicase unwinds DNA by an active mechanism." Biochemistry 32(27): 6815-20.
- Andersen, C. B., L. Ballut, et al. (2006). "Structure of the exon junction core complex with a trapped DEAD-box ATPase bound to RNA." Science 313(5795): 1968-72.
- Anderson, J. S. and R. P. Parker (1998). "The 3' to 5' degradation of yeast mRNAs is a general mechanism for mRNA turnover that requires the SKI2 DEVH box protein and 3' to 5' exonucleases of the exosome complex." EMBO J 17(5): 1497-506.
- Ariumi, Y., M. Kuroki, et al. (2007). "DDX3 DEAD-box RNA helicase is required for hepatitis C virus RNA replication." J Virol 81(24): 13922-6.
- Asabe, S. I., Y. Tanji, et al. (1997). "The N-terminal region of hepatitis C virus-encoded NS5A is important for NS4A-dependent phosphorylation." J Virol 71(1): 790-6.

- Banroques, J., O. Cordin, et al. (2008). "A conserved phenylalanine of motif IV in superfamily 2 helicases is required for cooperative, ATP-dependent binding of RNA substrates in DEAD-box proteins." Mol Cell Biol 28(10): 3359-71.
- Banroques, J., M. Doère, et al. (2010). "Motif III in Superfamily 2 "Helicases" Helps Convert the Binding Energy of ATP into a High-Affinity RNA Binding Site in the Yeast DEAD-Box Protein Ded1." Journal of Molecular Biology 396(4): 949-966.
- Barba, G., F. Harper, et al. (1997). "Hepatitis C virus core protein shows a cytoplasmic localization and associates to cellular lipid storage droplets." Proc Natl Acad Sci U S A 94(4): 1200-5.
- Bartenschlager, R. and V. Lohmann (2001). "Novel cell culture systems for the hepatitis C virus." Antiviral research 52(1): 1-17.
- Bates, G. J., S. M. Nicol, et al. (2005). "The DEAD box protein p68: a novel transcriptional coactivator of the p53 tumour suppressor." EMBO J 24(3): 543-53.
- Behrens, S. E., C. W. Grassmann, et al. (1998). "Characterization of an autonomous subgenomic pestivirus RNA replicon." Journal of Virology 72(3): 2364-72.
- Behrens, S. E., L. Tomei, et al. (1996). "Identification and properties of the RNA-dependent RNA polymerase of hepatitis C virus." EMBO J 15(1): 12-22.
- Benz, J., H. Trachsel, et al. (1999). "Crystal structure of the ATPase domain of translation initiation factor 4A from *Saccharomyces cerevisiae*--the prototype of the DEAD box protein family." Structure 7(6): 671-9.
- Betterton, M. D. and F. Julicher (2005). "Opening of nucleic-acid double strands by helicases: active versus passive opening." Phys Rev E Stat Nonlin Soft Matter Phys 71(1 Pt 1): 011904.
- Bleichert, F. and S. J. Baserga (2007). "The long unwinding road of RNA helicases." Mol Cell 27(3): 339-52.

- Blight, K. J., A. A. Kolykhalov, et al. (2000). "Efficient initiation of HCV RNA replication in cell culture." Science 290(5498): 1972-4.
- Blight, K. J., J. A. McKeating, et al. (2003). "Efficient replication of hepatitis C virus genotype 1a RNAs in cell culture." J Virol 77(5): 3181-90.
- Blight, K. J., J. A. McKeating, et al. (2002). "Highly permissive cell lines for subgenomic and genomic hepatitis C virus RNA replication." J Virol 76(24): 13001-14.
- Bono, F., J. Ebert, et al. (2006). "The crystal structure of the exon junction complex reveals how it maintains a stable grip on mRNA." Cell 126(4): 713-25.
- Brass, V., D. Moradpour, et al. (2007). "Hepatitis C virus infection: in vivo and in vitro models." Journal of viral hepatitis 14 Suppl 1: 64-7.
- Bressanelli, S., L. Tomei, et al. (1999). "Crystal structure of the RNA-dependent RNA polymerase of hepatitis C virus." Proc Natl Acad Sci U S A 96(23): 13034-9.
- Brunger, A. T., P. D. Adams, et al. (1998). "Crystallography & NMR system: A new software suite for macromolecular structure determination." Acta Crystallogr D Biol Crystallogr 54(Pt 5): 905-21.
- Caretta, G., R. L. Schiltz, et al. (2006). "The RNA helicases p68/p72 and the noncoding RNA SRA are coregulators of MyoD and skeletal muscle differentiation." Dev Cell 11(4): 547-60.
- Carmel, A. B. and B. W. Matthews (2004). "Crystal structure of the BstDEAD N-terminal domain: a novel DEAD protein from *Bacillus stearothermophilus*." RNA 10(1): 66-74.
- Carrera, P., O. Johnstone, et al. (2000). "VASA mediates translation through interaction with a *Drosophila* yIF2 homolog." Mol Cell 5(1): 181-7.
- Caruthers, J. M., E. R. Johnson, et al. (2000). "Crystal structure of yeast initiation factor 4A, a DEAD-box RNA helicase." Proc Natl Acad Sci U S A 97(24): 13080-5.
- Caruthers, J. M. and D. B. McKay (2002). "Helicase structure and mechanism." Curr Opin Struct Biol 12(1): 123-33.



- Chatterji, U., M. Bobardt, et al. (2009). "The isomerase active site of cyclophilin A is critical for hepatitis C virus replication." J Biol Chem 284(25): 16998-7005.
- Cheng, Z., J. Coller, et al. (2005). "Crystal structure and functional analysis of DEAD-box protein Dhh1p." RNA 11(8): 1258-70.
- Cheng, Z., D. Muhlrads, et al. (2007). "Structural and functional insights into the human Upf1 helicase core." EMBO J 26(1): 253-64.
- Choo, Q. L., G. Kuo, et al. (1989). "Isolation of a cDNA clone derived from a blood-borne non-A, non-B viral hepatitis genome." Science 244(4902): 359-62.
- Chuang, R. Y., P. L. Weaver, et al. (1997). "Requirement of the DEAD-Box protein ded1p for messenger RNA translation." Science 275(5305): 1468-71.
- Clark, E. L., A. Coulson, et al. (2008). "The RNA helicase p68 is a novel androgen receptor coactivator involved in splicing and is overexpressed in prostate cancer." Cancer Res 68(19): 7938-46.
- Collins, R., T. Karlberg, et al. (2009). "The DEXD/H-box RNA helicase DDX19 is regulated by an  $\alpha$ -helical switch." J Biol Chem 284(16): 10296-300.
- Cordin, O., J. Banroques, et al. (2006). "The DEAD-box protein family of RNA helicases." Gene 367: 17-37.
- Cordin, O., N. K. Tanner, et al. (2004). "The newly discovered Q motif of DEAD-box RNA helicases regulates RNA-binding and helicase activity." EMBO J 23(13): 2478-87.
- Czabotar, P. E., E. F. Lee, et al. (2007). "Structural insights into the degradation of Mcl-1 induced by BH3 domains." Proc Natl Acad Sci U S A 104(15): 6217-22.
- De Franceschi, L., G. Fattovich, et al. (2000). "Hemolytic anemia induced by ribavirin therapy in patients with chronic hepatitis C virus infection: role of membrane oxidative damage." Hepatology 31(4): 997-1004.
- De Francesco, R. and C. Steinkuhler (2000). "Structure and function of the hepatitis C virus NS3-NS4A serine proteinase." Curr Top Microbiol Immunol 242: 149-69.

- de la Cruz, J., D. Kressler, et al. (1999). "Unwinding RNA in *Saccharomyces cerevisiae*: DEAD-box proteins and related families." Trends Biochem Sci 24(5): 192-8.
- Dimitrova, M., I. Imbert, et al. (2003). "Protein-protein interactions between hepatitis C virus nonstructural proteins." J Virol 77(9): 5401-14.
- Dumoulin, F. L., A. von dem Bussche, et al. (2003). "Hepatitis C virus NS2 protein inhibits gene expression from different cellular and viral promoters in hepatic and nonhepatic cell lines." Virology 305(2): 260-6.
- Dustin, L. B. and C. M. Rice (2007). "Flying under the radar: the immunobiology of hepatitis C." Annual review of immunology 25: 71-99.
- Egger, D., B. Wolk, et al. (2002). "Expression of hepatitis C virus proteins induces distinct membrane alterations including a candidate viral replication complex." J Virol 76(12): 5974-84.
- Endoh, H., K. Maruyama, et al. (1999). "Purification and identification of p68 RNA helicase acting as a transcriptional coactivator specific for the activation function 1 of human estrogen receptor alpha." Mol Cell Biol 19(8): 5363-72.
- Erdtmann, L., N. Franck, et al. (2003). "The hepatitis C virus NS2 protein is an inhibitor of CIDE-B-induced apoptosis." J Biol Chem 278(20): 18256-64.
- Fang, J., S. Kubota, et al. (2004). "A DEAD box protein facilitates HIV-1 replication as a cellular co-factor of Rev." Virology 330(2): 471-80.
- Feinstone, S. M., A. Z. Kapikian, et al. (1975). "Transfusion-associated hepatitis not due to viral hepatitis type A or B." The New England journal of medicine 292(15): 767-70.
- Ford, M. J., I. A. Anton, et al. (1988). "Nuclear protein with sequence homology to translation initiation factor eIF-4A." Nature 332(6166): 736-8.
- Fuller-Pace, F. V. (2006). "DEXD/H box RNA helicases: multifunctional proteins with important roles in transcriptional regulation." Nucleic Acids Res 34(15): 4206-15.

- Fuller-Pace, F. V. and S. Ali (2008). "The DEAD box RNA helicases p68 (Ddx5) and p72 (Ddx17): novel transcriptional co-regulators." Biochem Soc Trans 36(Pt 4): 609-12.
- Ghany, M. G., D. B. Strader, et al. (2009). "Diagnosis, management, and treatment of hepatitis C: an update." Hepatology 49(4): 1335-74.
- Gillian, A. L. and J. Svaren (2004). "The Ddx20/DP103 dead box protein represses transcriptional activation by Egr2/Krox-20." J Biol Chem 279(10): 9056-63.
- Gingras, A. C., B. Raught, et al. (1999). "eIF4 initiation factors: effectors of mRNA recruitment to ribosomes and regulators of translation." Annu Rev Biochem 68: 913-63.
- Goh, P. Y., Y. J. Tan, et al. (2004). "Cellular RNA helicase p68 relocalization and interaction with the hepatitis C virus (HCV) NS5B protein and the potential role of p68 in HCV RNA replication." J Virol 78(10): 5288-98.
- Gorbalenya, A. E. and E. V. Koonin (1993). "Helicases: amino acid sequence comparisons and structure-function relationships." Current Opinion in Structural Biology 3(3): 419-429.
- Gorbalenya, A. E., E. V. Koonin, et al. (1989). "Two related superfamilies of putative helicases involved in replication, recombination, repair and expression of DNA and RNA genomes." Nucleic Acids Res 17(12): 4713-30.
- Griffin, S. D., R. Harvey, et al. (2004). "A conserved basic loop in hepatitis C virus p7 protein is required for amantadine-sensitive ion channel activity in mammalian cells but is dispensable for localization to mitochondria." J Gen Virol 85(Pt 2): 451-61.
- Hall, M. C. and S. W. Matson (1999). "Helicase motifs: the engine that powers DNA unwinding." Molecular Microbiology 34(5): 867-877.
- Hayashi, N. and T. Takehara (2006). "Antiviral therapy for chronic hepatitis C: past, present, and future." J Gastroenterol 41(1): 17-27.
- He, Q. S., H. Tang, et al. (2008). "Comparisons of RNAi approaches for validation of human RNA helicase A as an essential factor in hepatitis C virus replication." J Virol Methods 154(1-2): 216-9.

- Hogbom, M., R. Collins, et al. (2007). "Crystal structure of conserved domains 1 and 2 of the human DEAD-box helicase DDX3X in complex with the mononucleotide AMP." J Mol Biol 372(1): 150-9.
- Huang, H., M. L. Shiffman, et al. (2006). "Identification of two gene variants associated with risk of advanced fibrosis in patients with chronic hepatitis C." Gastroenterology 130(6): 1679-87.
- Hugle, T., F. Fehrmann, et al. (2001). "The hepatitis C virus nonstructural protein 4B is an integral endoplasmic reticulum membrane protein." Virology 284(1): 70-81.
- Ikeda, M., M. Yi, et al. (2002). "Selectable subgenomic and genome-length dicistronic RNAs derived from an infectious molecular clone of the HCV-N strain of hepatitis C virus replicate efficiently in cultured Huh7 cells." J Virol 76(6): 2997-3006.
- lost, I., M. Dreyfus, et al. (1999). "Ded1p, a DEAD-box protein required for translation initiation in *Saccharomyces cerevisiae*, is an RNA helicase." J Biol Chem 274(25): 17677-83.
- Jalal, C., H. Uhlmann-Schiffler, et al. (2007). "Redundant role of DEAD box proteins p68 (Ddx5) and p72/p82 (Ddx17) in ribosome biogenesis and cell proliferation." Nucleic Acids Res 35(11): 3590-601.
- Johnson, D. S., L. Bai, et al. (2007). "Single-molecule studies reveal dynamics of DNA unwinding by the ring-shaped T7 helicase." Cell 129(7): 1299-309.
- Johnson, E. R. and D. B. McKay (1999). "Crystallographic structure of the amino terminal domain of yeast initiation factor 4A, a representative DEAD-box RNA helicase." RNA 5(12): 1526-34.
- Jones, T. A., J. Y. Zou, et al. (1991). "Improved methods for building protein models in electron density maps and the location of errors in these models." Acta Crystallogr A 47 ( Pt 2): 110-9.

- Karow, A. R. and D. Klostermeier (2009). "A conformational change in the helicase core is necessary but not sufficient for RNA unwinding by the DEAD box helicase YxiN." Nucleic Acids Res 37(13): 4464-71.
- Kasai, D., T. Adachi, et al. (2009). "HCV replication suppresses cellular glucose uptake through down-regulation of cell surface expression of glucose transporters." J Hepatol 50(5): 883-94.
- Kato, T., T. Date, et al. (2003). "Efficient replication of the genotype 2a hepatitis C virus subgenomic replicon." Gastroenterology 125(6): 1808-17.
- Khromykh, A. A. and E. G. Westaway (1997). "Subgenomic replicons of the flavivirus Kunjin: construction and applications." Journal of virology 71(2): 1497-505.
- Kim, S. H. and R. J. Lin (1996). "Spliceosome activation by PRP2 ATPase prior to the first transesterification reaction of pre-mRNA splicing." Mol Cell Biol 16(12): 6810-9.
- Kyono, K., M. Miyashiro, et al. (2002). "Human eukaryotic initiation factor 4All associates with hepatitis C virus NS5B protein in vitro." Biochem Biophys Res Commun 292(3): 659-66.
- LaCava, J., J. Houseley, et al. (2005). "RNA degradation by the exosome is promoted by a nuclear polyadenylation complex." Cell 121(5): 713-24.
- Lahue, E. E. and S. W. Matson (1988). "Escherichia coli DNA helicase I catalyzes a unidirectional and highly processive unwinding reaction." J Biol Chem 263(7): 3208-15.
- Lane, D. P. and W. K. Hoeffler (1980). "SV40 large T shares an antigenic determinant with a cellular protein of molecular weight 68,000." Nature 288(5787): 167-70.
- Lanford, R. E., H. Lee, et al. (2001). "Infectious cDNA clone of the hepatitis C virus genotype 1 prototype sequence." J Gen Virol 82(Pt 6): 1291-7.
- Large, M. K., D. J. Kittlesen, et al. (1999). "Suppression of host immune response by the core protein of hepatitis C virus: possible implications for hepatitis C virus persistence." J Immunol 162(2): 931-8.

- Lechmann, M. and T. J. Liang (2000). "Vaccine development for hepatitis C." Semin Liver Dis 20(2): 211-26.
- Lee, J. H., I. Y. Nam, et al. (2006). "Nonstructural protein 5B of hepatitis C virus." Mol Cells 21(3): 330-6.
- Legrand-Abravanel, F., F. Nicot, et al. (2010). "New NS5B polymerase inhibitors for hepatitis C." Expert Opin Investig Drugs 19(8): 963-75.
- Li, X. D., L. Sun, et al. (2005). "Hepatitis C virus protease NS3/4A cleaves mitochondrial antiviral signaling protein off the mitochondria to evade innate immunity." Proc Natl Acad Sci U S A 102(49): 17717-22.
- Lim, S. P., Y. L. Khu, et al. (2001). "Identification and molecular characterisation of the complete genome of a Singapore isolate of hepatitis C virus: sequence comparison with other strains and phylogenetic analysis." Virus Genes 23(1): 89-95.
- Lin, C., L. Yang, et al. (2005). "ATPase/helicase activities of p68 RNA helicase are required for pre-mRNA splicing but not for assembly of the spliceosome." Mol Cell Biol 25(17): 7484-93.
- Lindenbach, B. D., M. J. Evans, et al. (2005). "Complete replication of hepatitis C virus in cell culture." Science 309(5734): 623-6.
- Lindenbach, B. D. and C. M. Rice (2005). "Unravelling hepatitis C virus replication from genome to function." Nature 436(7053): 933-8.
- Linder, P. (2006). "Dead-box proteins: a family affair--active and passive players in RNP-remodeling." Nucleic Acids Res 34(15): 4168-80.
- Linder, P., P. F. Lasko, et al. (1989). "Birth of the D-E-A-D box." Nature 337(6203): 121-2.
- Liu, Z. R. (2002). "p68 RNA helicase is an essential human splicing factor that acts at the U1 snRNA-5' splice site duplex." Mol Cell Biol 22(15): 5443-50.
- Lo, S. Y., F. Masiarz, et al. (1995). "Differential subcellular localization of hepatitis C virus core gene products." Virology 213(2): 455-61.

- Lohman, T. M. (1992). "Escherichia coli DNA helicases: mechanisms of DNA unwinding." Mol Microbiol 6(1): 5-14.
- Lohman, T. M. (1993). "Helicase-catalyzed DNA unwinding." J Biol Chem 268(4): 2269-72.
- Lohman, T. M. and K. P. Bjornson (1996). "Mechanisms of helicase-catalyzed DNA unwinding." Annu Rev Biochem 65: 169-214.
- Lohmann, V., F. Korner, et al. (2001). "Mutations in hepatitis C virus RNAs conferring cell culture adaptation." Journal of virology 75(3): 1437-49.
- Lohmann, V., F. Korner, et al. (1999). "Replication of subgenomic hepatitis C virus RNAs in a hepatoma cell line." Science 285(5424): 110-3.
- Macdonald, A. and M. Harris (2004). "Hepatitis C virus NS5A: tales of a promiscuous protein." J Gen Virol 85(Pt 9): 2485-502.
- Mamiya, N. and H. J. Worman (1999). "Hepatitis C virus core protein binds to a DEAD box RNA helicase." J Biol Chem 274(22): 15751-6.
- Martin, A., S. Schneider, et al. (2002). "Prp43 is an essential RNA-dependent ATPase required for release of lariat-intron from the spliceosome." J Biol Chem 277(20): 17743-50.
- Marusawa, H., M. Hijikata, et al. (1999). "Hepatitis C virus core protein inhibits Fas- and tumor necrosis factor alpha-mediated apoptosis via NF-kappaB activation." J Virol 73(6): 4713-20.
- Mercer, D. F., D. E. Schiller, et al. (2001). "Hepatitis C virus replication in mice with chimeric human livers." Nature medicine 7(8): 927-33.
- Moriya, K., H. Fujie, et al. (1998). "The core protein of hepatitis C virus induces hepatocellular carcinoma in transgenic mice." Nat Med 4(9): 1065-7.
- Mottola, G., G. Cardinali, et al. (2002). "Hepatitis C virus nonstructural proteins are localized in a modified endoplasmic reticulum of cells expressing viral subgenomic replicons." Virology 293(1): 31-43.

- Nakajima, T., C. Uchida, et al. (1997). "RNA helicase A mediates association of CBP with RNA polymerase II." Cell 90(6): 1107-12.
- Nomura-Takigawa, Y., M. Nagano-Fujii, et al. (2006). "Non-structural protein 4A of Hepatitis C virus accumulates on mitochondria and renders the cells prone to undergoing mitochondria-mediated apoptosis." J Gen Virol 87(Pt 7): 1935-45.
- Otwinowski, Z. and W. Minor (1997). "Processing of X-ray Diffraction Data Collected in Oscillation Mode." Methods Enzymol. 276: 307-326.
- Owsianka, A. M. and A. H. Patel (1999). "Hepatitis C virus core protein interacts with a human DEAD box protein DDX3." Virology 257(2): 330-40.
- Pang, P. S., E. Jankowsky, et al. (2002). "The hepatitis C viral NS3 protein is a processive DNA helicase with cofactor enhanced RNA unwinding." EMBO J 21(5): 1168-76.
- Pause, A., N. Methot, et al. (1993). "The HRIGRXXR region of the DEAD box RNA helicase eukaryotic translation initiation factor 4A is required for RNA binding and ATP hydrolysis." Mol Cell Biol 13(11): 6789-98.
- Pause, A. and N. Sonenberg (1992). "Mutational analysis of a DEAD box RNA helicase: the mammalian translation initiation factor eIF-4A." EMBO J 11(7): 2643-54.
- Pietschmann, T., A. Kaul, et al. (2006). "Construction and characterization of infectious intragenotypic and intergenotypic hepatitis C virus chimeras." Proc Natl Acad Sci U S A 103(19): 7408-13.
- Pietschmann, T., V. Lohmann, et al. (2002). "Persistent and transient replication of full-length hepatitis C virus genomes in cell culture." J Virol 76(8): 4008-21.
- Pileri, P., Y. Uematsu, et al. (1998). "Binding of hepatitis C virus to CD81." Science 282(5390): 938-41.
- Ploss, A., M. J. Evans, et al. (2009). "Human occludin is a hepatitis C virus entry factor required for infection of mouse cells." Nature 457(7231): 882-6.



- Prince, A. M., B. Brotman, et al. (1974). "Long-incubation post-transfusion hepatitis without serological evidence of exposure to hepatitis-B virus." Lancet 2(7875): 241-6.
- Ray, B. K., T. G. Lawson, et al. (1985). "ATP-dependent unwinding of messenger RNA structure by eukaryotic initiation factors." J Biol Chem 260(12): 7651-8.
- Ray, R. B., L. M. Lagging, et al. (1996). "Hepatitis C virus core protein cooperates with ras and transforms primary rat embryo fibroblasts to tumorigenic phenotype." J Virol 70(7): 4438-43.
- Ray, R. B., L. M. Lagging, et al. (1995). "Transcriptional regulation of cellular and viral promoters by the hepatitis C virus core protein." Virus Res 37(3): 209-20.
- Rocak, S. and P. Linder (2004). "DEAD-box proteins: the driving forces behind RNA metabolism." Nat Rev Mol Cell Biol 5(3): 232-41.
- Rogers, G. W., Jr., A. A. Komar, et al. (2002). "eIF4A: the godfather of the DEAD box helicases." Prog Nucleic Acid Res Mol Biol 72: 307-31.
- Roman, L. J., A. K. Eggleston, et al. (1992). "Processivity of the DNA helicase activity of Escherichia coli recBCD enzyme." J Biol Chem 267(6): 4207-14.
- Roohvand, F. and N. Kossari (2011). "Advances in hepatitis C virus vaccines, part one: advances in basic knowledge for hepatitis C virus vaccine design." Expert Opin Ther Pat.
- Rosenberg, S. (2001). "Recent advances in the molecular biology of hepatitis C virus." J Mol Biol 313(3): 451-64.
- Rossler, O. G., A. Straka, et al. (2001). "Rearrangement of structured RNA via branch migration structures catalysed by the highly related DEAD-box proteins p68 and p72." Nucleic Acids Res 29(10): 2088-96.
- Sakai, A., M. S. Claire, et al. (2003). "The p7 polypeptide of hepatitis C virus is critical for infectivity and contains functionally important genotype-specific sequences." Proc Natl Acad Sci U S A 100(20): 11646-51.

- Scheller, N., L. B. Mina, et al. (2009). "Translation and replication of hepatitis C virus genomic RNA depends on ancient cellular proteins that control mRNA fates." Proc Natl Acad Sci U S A 106(32): 13517-22.
- Schmidt-Mende, J., E. Bieck, et al. (2001). "Determinants for membrane association of the hepatitis C virus RNA-dependent RNA polymerase." J Biol Chem 276(47): 44052-63.
- Schneider, S., E. Campodonico, et al. (2004). "Motifs IV and V in the DEAH box splicing factor Prp22 are important for RNA unwinding, and helicase-defective Prp22 mutants are suppressed by Prp8." J Biol Chem 279(10): 8617-26.
- Schwer, B. (2008). "A conformational rearrangement in the spliceosome sets the stage for Prp22-dependent mRNA release." Mol Cell 30(6): 743-54.
- Schwer, B. and C. Guthrie (1991). "PRP16 is an RNA-dependent ATPase that interacts transiently with the spliceosome." Nature 349(6309): 494-9.
- Schwer, B. and T. Meszaros (2000). "RNA helicase dynamics in pre-mRNA splicing." EMBO J 19(23): 6582-91.
- Sengoku, T., O. Nureki, et al. (2006). "Structural basis for RNA unwinding by the DEAD-box protein Drosophila Vasa." Cell 125(2): 287-300.
- Shi, H., O. Cordin, et al. (2004). "Crystal structure of the human ATP-dependent splicing and export factor UAP56." Proc Natl Acad Sci U S A 101(51): 17628-33.
- Shibuya, T., T. O. Tange, et al. (2006). "Mutational analysis of human eIF4AIII identifies regions necessary for exon junction complex formation and nonsense-mediated mRNA decay." RNA 12(3): 360-74.
- Shin, S., K. L. Rossow, et al. (2007). "Involvement of RNA helicases p68 and p72 in colon cancer." Cancer Res 67(16): 7572-8.
- Sikora, B., R. L. Eoff, et al. (2006). "DNA unwinding by Escherichia coli DNA helicase I (Tral) provides evidence for a processive monomeric molecular motor." J Biol Chem 281(47): 36110-6.

- Staley, J. P. and C. Guthrie (1998). "Mechanical devices of the spliceosome: motors, clocks, springs, and things." Cell 92(3): 315-26.
- Stapleford, K. A. and B. D. Lindenbach (2011). "Hepatitis C virus NS2 coordinates virus particle assembly through physical interactions with the E1-E2 glycoprotein and NS3-NS4A enzyme complexes." J Virol 85(4): 1706-17.
- Steinmann, E., T. Whitfield, et al. (2007). "Antiviral effects of amantadine and iminosugar derivatives against hepatitis C virus." Hepatology 46(2): 330-8.
- Story, R. M., H. Li, et al. (2001). "Crystal structure of a DEAD box protein from the hyperthermophile *Methanococcus jannaschii*." Proc Natl Acad Sci U S A 98(4): 1465-70.
- Story, R. M. and T. A. Steitz (1992). "Structure of the recA protein-ADP complex." Nature 355(6358): 374-6.
- Suzuki, R., T. Suzuki, et al. (1999). "Processing and functions of Hepatitis C virus proteins." Intervirology 42(2-3): 145-52.
- Tan, S.-L. and I. National Center for Biotechnology. (2006). "Hepatitis C viruses genomes and molecular biology." from <http://www.ncbi.nlm.nih.gov/bookshelf/br.fcgi?book=hcv>.
- Tan, S. L., A. Pause, et al. (2002). "Hepatitis C therapeutics: current status and emerging strategies." Nat Rev Drug Discov 1(11): 867-81.
- Tanner, N. K. (2003). "The newly identified Q motif of DEAD box helicases is involved in adenine recognition." Cell Cycle 2(1): 18-9.
- Tanner, N. K., O. Cordin, et al. (2003). "The Q motif: a newly identified motif in DEAD box helicases may regulate ATP binding and hydrolysis." Mol Cell 11(1): 127-38.
- Tanner, N. K. and P. Linder (2001). "DExD/H box RNA helicases: from generic motors to specific dissociation functions." Mol Cell 8(2): 251-62.
- Tarn, W. Y. and T. H. Chang (2009). "The current understanding of Ded1p/DDX3 homologs from yeast to human." RNA Biol 6(1): 17-20.

- Tingting, P., F. Caiyun, et al. (2006). "Subproteomic analysis of the cellular proteins associated with the 3' untranslated region of the hepatitis C virus genome in human liver cells." Biochem Biophys Res Commun 347(3): 683-91.
- Tran, H., M. Schilling, et al. (2004). "Facilitation of mRNA deadenylation and decay by the exosome-bound, DEXH protein RHAU." Mol Cell 13(1): 101-11.
- Tseng, S. S., P. L. Weaver, et al. (1998). "Dbp5p, a cytosolic RNA helicase, is required for poly(A)+ RNA export." EMBO J 17(9): 2651-62.
- Tu, H., L. Gao, et al. (1999). "Hepatitis C virus RNA polymerase and NS5A complex with a SNARE-like protein." Virology 263(1): 30-41.
- Voisset, C. and J. Dubuisson (2004). "Functional hepatitis C virus envelope glycoproteins." Biol Cell 96(6): 413-20.
- Wakita, T., T. Pietschmann, et al. (2005). "Production of infectious hepatitis C virus in tissue culture from a cloned viral genome." Nat Med 11(7): 791-6.
- Walker, J. E., M. Saraste, et al. (1982). "Distantly related sequences in the alpha- and beta-subunits of ATP synthase, myosin, kinases and other ATP-requiring enzymes and a common nucleotide binding fold." EMBO J 1(8): 945-51.
- Wasley, A. and M. J. Alter (2000). "Epidemiology of hepatitis C: geographic differences and temporal trends." Semin Liver Dis 20(1): 1-16.
- Watanabe, M., J. Yanagisawa, et al. (2001). "A subfamily of RNA-binding DEAD-box proteins acts as an estrogen receptor alpha coactivator through the N-terminal activation domain (AF-1) with an RNA coactivator, SRA." EMBO J 20(6): 1341-52.
- Wilson, B. J., G. J. Bates, et al. (2004). "The p68 and p72 DEAD box RNA helicases interact with HDAC1 and repress transcription in a promoter-specific manner." BMC Mol Biol 5: 11.

- Wolk, B., D. Sansonno, et al. (2000). "Subcellular localization, stability, and trans-cleavage competence of the hepatitis C virus NS3-NS4A complex expressed in tetracycline-regulated cell lines." J Virol 74(5): 2293-304.
- Xiao, J. H., I. Davidson, et al. (1991). "Cloning, expression, and transcriptional properties of the human enhancer factor TEF-1." Cell 65(4): 551-68.
- Xie, Z. C., J. I. Riezu-Boj, et al. (1998). "Transmission of hepatitis C virus infection to tree shrews." Virology 244(2): 513-20.
- Xu, L., S. Khadijah, et al. (2010). "The cellular RNA helicase DDX1 interacts with coronavirus nonstructural protein 14 and enhances viral replication." J Virol 84(17): 8571-83.
- Xu, X., H. Chen, et al. (2007). "Efficient infection of tree shrew (*Tupaia belangeri*) with hepatitis C virus grown in cell culture or from patient plasma." The Journal of general virology 88(Pt 9): 2504-12.
- Yan, X., J. F. Mouillet, et al. (2003). "A novel domain within the DEAD-box protein DP103 is essential for transcriptional repression and helicase activity." Mol Cell Biol 23(1): 414-23.
- Yang, Z. R., R. Thomson, et al. (2005). "RONN: the bio-basis function neural network technique applied to the detection of natively disordered regions in proteins." Bioinformatics 21(16): 3369-76.
- Yasui, K., T. Wakita, et al. (1998). "The native form and maturation process of hepatitis C virus core protein." J Virol 72(7): 6048-55.
- Yedavalli, V. S., C. Neuveut, et al. (2004). "Requirement of DDX3 DEAD box RNA helicase for HIV-1 Rev-RRE export function." Cell 119(3): 381-92.
- Yi, M., R. A. Villanueva, et al. (2006). "Production of infectious genotype 1a hepatitis C virus (Hutchinson strain) in cultured human hepatoma cells." Proc Natl Acad Sci U S A 103(7): 2310-5.
- Yu, G. Y., K. J. Lee, et al. (2006). "Palmitoylation and polymerization of hepatitis C virus NS4B protein." J Virol 80(12): 6013-23.

- Yu, J., T. Ha, et al. (2007). "How directional translocation is regulated in a DNA helicase motor." Biophys J 93(11): 3783-97.
- Zhao, R., J. Shen, et al. (2004). "Crystal structure of UAP56, a DExD/H-box protein involved in pre-mRNA splicing and mRNA export." Structure 12(8): 1373-81.
- Zhu, Q., J. T. Guo, et al. (2003). "Replication of hepatitis C virus subgenomes in nonhepatic epithelial and mouse hepatoma cells." J Virol 77(17): 9204-10.



## APPENDIX 1

### List of Primers Used in the Generation of DDX5 Constructs

Primers	Primer sequence 5'- 3'	AT* (°C)
DDX5-1F	CGGGATCCATGTCGGGTTATTTCGAGTGACCGAGAC	79.85
DDX5-43F	CGGGATCCAAAAAGAAGTGGAAATCTTGATGAGCTG	75.44
DDX5-61F <sup>#</sup>	CGGGATCCAAGGAAATTACAGTTAGAGGTCACAAC	72.01
DDX5-72F	CGGGATCCGAGGTGGAAACATACAGAAGAAGC	74.80
DDX5-80F	CGGGATCCGAGCACCCCTGATTTGGCTAGGCGCACA	85.03
DDX5-132F	CGGGATCCTTGATATGGTTGGAGTGGCACAGACT	78.40
DDX5-163F	CGGGATCCGAGAGAGGCGATGGGCCTATTTGTTTG	80.89
DDX5-204F	CGGGATCCGGTGGTGCTCCTAAGGGACCACAAATA	80.04
DDX5-306F	CGGGATCCGAACTGAGTGCAAACCACAACATTCTT	77.72
DDX5-406F	CGGGATCCGATGTGGAAGATGTGAAATTTGTCATC	76.70
DDX5-80R	CCGCTCGAGTTACTTGCTTCTTCTGTATGTTTCCA	73.30
DDX5-305R <sup>#</sup>	CCGCTCGAGTTAAAGTGCACCAATGTTTATATGAA	71.95
DDX5-391R	CCGCTCGAGTTATTTTCCATGTTTGAATTCATTTA	71.10
DDX5-409R	CCGCTCGAGTTAATCTTCGACCAACTGAAGCAACT	75.29
DDX5-411R	CCGCTCGAGTTATTTACATCTTCCACATCTAGCC	74.18
DDX5-434R	CCGCTCGAGTTAGCGAGCAGTTCTTCCAATTTCGAT	77.59
DDX5-480R	CCGCTCGAGTTATGAACCTCTGTCTTCGACCAACT	75.57
DDX5-574R	CCGCTCGAGTTAGCTATCATAACCATTCTGGTAAG	70.64
DDX5-614R	CCGCTCGAGTTATTGGGAATATCCTGTTGGCATTG	76.59
DDX5-del70-78-F	GCACAGCAAGCAAGGAAATTACAGTTAG	64.85
DDX5-del70-78-F2	GGCGCACAGCAAGCAAGGAAATTACAGTTAG	72.02
DDX5-79F	CGGGATCCAGCAAGGAAATTACAGTTAGAGG	70.53
DDX5-del70-78-R	TCCTTGCTTGCTGTGCGCCTAGCCAAATC	75.94
DDX5-K114N-F	GGGAACACATTGTCTTATTTGCTTCC	63.64
DDX5-K114N-R	CAATGTGTTCCAGATCCAGTCTGTG	66.60

\*AT, annealing temperature; <sup>#</sup>mycDDX5-(61-305)D248N was generated using pFG384, pSG-myc-p68 (D248N) (Goh, Tan et al. 2004) as a template with forward and reverse primers DDX5-61F and DDX5-305R.